Master's thesis

NTNU
Norwegian University of Science and Technology
Faculty of Engineering
Department of Civil and Environmental Engineering

Are Berstad

Numerical Analysis of a Soil Tunnel with Jet Grouting

Master's thesis in Geotechnical Engineering
Supervisor: Gustav Grimstad
June 2022

NTNU
Norwegian University of Science and Technology

Norconsult

Are Berstad

Numerical Analysis of a Soil Tunnel with Jet Grouting

Master's thesis in Geotechnical Engineering
Supervisor: Gustav Grimstad
June 2022

Norwegian University of Science and Technology
Faculty of Engineering
Department of Civil and Environmental Engineering

NTNU
Norwegian University of
Science and Technology

Abstract

Soil tunnelling is a complex civil engineering problem, which can prove challenging to understand and design. Urbanization in Norway, where major cities often are located on soil deposits and marine clay, leads to an increased demand in underground construction works such as soil tunnels. In this thesis, a literature review is conducted on soil tunnelling and a case study is analysed in Plaxis 2D and 3D. The case study features an approx. 290 m urban shallow railway tunnel in cohesionless soil. To enable safe excavation and complete groundwater control, a jet grout ring is installed from the terrain surface prior to excavation.

Design criteria for the case study states that the jet grout ring and the primary sprayed concrete lining is neglected in long-term design. The goal of the thesis is to find the effect of the temporary supports on the permanent structure. The thesis features a preliminary 3D analysis used to calibrate a 2D analysis to find realistic deformations and stress distributions in the linings. Modelled degradation of temporary supports in long-term is performed. In addition, membrane interaction from a traditional sheet membrane and a potential use of sprayed membrane between primary and secondary lining is investigated.

Calibration of the 2D analysis show similar results as the preliminary 3D analysis in terms of crown displacements and axial forces in the primary lining. Application of an efficient preliminary 3D analysis can provide the engineer with a suitable method to calibrate a 2D analysis.

Results from the thesis show that the capacity of the jet grout ring in short-term have a sufficient theoretical capacity to withstand the full overburden pressure. Complete degradation of the jet grout is not realistic according to available literature. The analysis with partial degradation of jet grout showed a reduction in internal forces on the secondary lining compared to a theoretical full degradation. Three different approaches to model the degradation was performed, all of which showed different rates of stress transfer. If the structural capabilities of jet grout used in soil tunnelling can be verified, design with full- or partial capacity can offer reduction in designed thickness of the secondary lining. This could lower the cost and emission from soil tunnelling with jet grout supports.

Results from the analysis did not yield beneficial internal forces for the potential sprayed membrane compared to the sheet membrane. Extensions for further work is suggested and discussed. The analysis features several simplifications to find appropriate results.

Sammendrag

Løsmassetunneler er et komplekst ingeniørproblem, og kan være utfordrende både å forstå og designe. Økt urbanisering i Norge, kombinert med at mange store byer er lokalisert ved løsmasseavsetninger og marin leire, medfører behov for løsninger som ikke berører eksisterende bebyggelse og teknisk infrastruktur, som for eksempel løsmassetunneler. Denne masteroppgaven starter med en litteraturstudie om tunneler i løsmasser, og en case-studie analysert i Plaxis 2D og 3D. Case-studien består blant annet av en 290 meter lang urban jernbanetunnel i kohesjonsløs morene med liten overdekning. En jetpelring installeres fra overflaten langs hele tunnelen før driving for å gi minst mulig ulemper for nærmiljøet, samt sikre drivingen uten å påvirke grunnvannet i området.

Teknisk designbasis for prosjektet setter krav om at midlertidige sikringer, dvs. jetpelring og arbeidssikring med sprøyebetong, ikke skal inngå som en del av den permanente konstruksjonen. Det er utført en innledende 3D analyse, som skal kalibrere den videre 2D analysen, for å finne realistiske deformasjoner og spenningsfordelinger i betongkonstruksjonene. En teoretisk nedbryting av midlertidige sikringer over levetiden er modellert. I tillegg er kontaktflaten mellom betongkonstruksjonene undersøkt, som følge av en tradisjonell plastmembran og en potensiell bruk av sprøytemembran for vanntetting.

Den kalibrerte 2D analysen viser lignende resultater for deformasjoner i henget og trykkrefter i sprøytebetongen som den innledende 3D analysen. Bruk av en innledende 3D analyse kan gi ingeniøren en effektiv metode for å finne realistiske krefter i konstruksjonene og kalibrere en to-dimensjonal modell.

Resultater fra oppgaven viser at jetpelringen har teoretisk kapasitet til å ta full last fra overdekningen for en kortsiktig situasjon. En fullstending nedbryting av jetpelringen er ikke realistisk basert på tilgjengelig litteratur. Analysen med delvis nedbryting av jetpelringen viser en reduksjon av de indre kreftene i den støpte permanente konstruksjonen sammelignet med en teoretisk full nedbryting av jetpelringen. Tre ulike metoder for å modellere nedbryting er utført, og de viser ulik hastighet av spenningsoverføring. Dersom den strukturelle kapasiteten til jetpeler i løsmassetunneler kan verifiseres, kan beregninger med jetpelers fulle- eller delvise strukturelle bidrag medføre en reduksjon i den indre støpte betongens tykkelse. Dette vil bidra til lavere kostnader og mindre miljøutslipp for løsmassetunneler med jetpelsikring.

Resultater fra analysen viser at en potensiell bruk av sprøytemembran for vanntetting ikke ga gunstigere indre krefter sammelignet med en plastmembran i den spesifikke konfigurasjonen. Videre arbeid er foreslått og diskutert i oppgaven. Utførte analyser baserer seg på flere forenklinger for å få relevante resultater.

Preface

The work presented in this master's thesis in geotechnical engineering has been performed in collaboration with Norconsult AS and the Department of Civil and Environmental Engineering at the Norwegian University of Science and Technology (NTNU).

I would like to take this opportunity to thank everyone who has helped me in any way. I want to thank Gunhild Hennum and Ragnhild Saarem, at Norconsult, for proposing the topic of this thesis and supervising the work. I want to thank my supervisor at NTNU, Gustav Grimstad, for discussions and always being available at short notice. I want to thank Adolfo, Alberto and Pedro from TYPSA for sharing their soil tunnelling expertise with me. I want to thank Gunstein Mork at Bane NOR for information about the project and providing access to documents. Special thanks to Veidekke, Trevi and ILF for allowing access to their reports.

Finally, I want to thank my dog, Andy, for sticking with me and forcing me to take breaks during long days of studying and writing.

Are Berstad

June 2022

Table of contents

Figures

Tables

Abbreviations

NTNU	Norwegian University of Science and Technology
NGI	Norwegian Geotechnical Institute
NATM	New Austrian Tunnelling Method
SEM	Sequential Excavation Method
SCL	Sprayed Concrete Linings
TBM	Tunnel Boring Machine
SM	Slurry Mode
EPBM	Earth Pressure Balance Machine
Adeco-RS	Analysis of Controlled Deformation in Rocks and Soils
NITM	New Italian Tunnelling Method
NMT	Norwegian Method of Tunnelling
SAWM	Spray-on Waterproofing Membranes
PCSL	Permanent Sprayed Concrete Lining
SSL	Single Shell Lining
DSL	Double Shell Lining
CSL	Composite Shell Lining

1 Introduction

1.1 Background

The geology of Norway has led to construction of many rock tunnels and expertise in rock tunnelling. However, the growing cities increase the demand for underground construction in soil deposits. Soil tunnelling is an example of construction in such deposits.

Bane NOR, with their contractor Veidekke, is building a soil tunnel for a future railway in Strømsåsen, Drammen as part of The InterCity Projects in South-Eastern Norway (BaneNOR, 2018). This project consists of a 6 km long rock tunnel, an approx. 290m soil tunnel and an approx. 540m concrete culvert to be finished in 2023. The soil tunnel is excavated using the Sequential Excavation Method and applies jet grouting as ground reinforcement prior to excavation. This is the first large scale soil tunnel using jet grouting as soil reinforcement in Norway (Backer and Hæstad, 2020).

Norconsult AS has performed an extended geotechnical control of the permanent concrete lining in the soil tunnel using Plaxis 2D. The control involves a calculation to assess the stresses in the permanent concrete lining from the overburden- and water pressure. According to the regulations set for the Intercity Projects, the control of the permanent structure was calculated without inclusion of the jet grouted columns or temporary spared concrete lining (BaneNOR, 2019). Therefore, Norconsult want to examine what effect the temporary supports could have on the permanent structure. Investigation of interfaces for lining composite behaviour and results from a 3D analysis is also of interest.

1.2 Objective

The main objective of this study is to evaluate potential relaxation due to temporary support systems on the permanent soil tunnel structure. Realistic modelling of the excavation and the supports is necessary to extract relevant internal forces. The effect of interaction between sprayed primary lining and secondary lining will be evaluated by looking into membrane properties. In addition, it will be an objective to evaluate key factors in the analysis and uncover potential 3D effects. This will be investigated using numerical modelling in Plaxis 2D and 3D. The process of simulating soil tunnelling with numerical analysis will be researched and discussed. Most soil tunnels in Norway are designed with the assistance of foreign engineering companies but could be performed solely by Norwegian engineers if more experience is gained.

To answer these objectives, the following research questions have been formed:

- Could inclusion of temporary supports, such as jet grout and sprayed concrete lining, provide significant reduction of the internal forces in the secondary lining?
- Could partial- or full contribution of temporary supports in the permanent design lead to material and cost savings?
- Is it feasible to simulate the degradation of temporary supports to find internal forces for design of the secondary lining?
- In theory, could the soil tunnel be built without the need of a secondary lining?
- Could a sprayed waterproofing membrane provide composite structural action that is beneficial for the design compared to a traditional sheet membrane?
- For preliminary design of tunnels, can a three-dimensional analysis be used to calibrate a two-dimensional analysis?

1.3 Scope

This Master's Thesis consist of 30 credits and will be performed in 21 weeks of work from 15.01.2022 till 10.06.2022.

Using numerical analysis this study will look at the effects of applying a temporary support scheme of vertical jet grout columns and sprayed concrete lining in soil tunnelling. The inclusions of three-dimensional effects for realistic internal forces will be attempted and interface solutions between linings will be compared. The analysis will use unpublished reports from a railway project. The thesis is directed towards an audience with some geotechnical or constructional understanding. The scope of the thesis is not to criticize current design of the case study, but to gain experience in soil tunnelling and investigate current design approaches and regulations.

The scope of the study will consist of:

- Literature research on soil tunnelling, case studies, design methods and numerical analysis on tunnelling with emphasize on jet grout supports and moraine conditions.
- Presenting information about the case study.
- Analysing the case study with finite element program Plaxis 2D and 3D.

1.3.1 Limitations

The numerical analysis is limited to data from the project at hand. The numerical modelling is subjectively the most suitable approach with the available data. Due to time limitation and available computer capacity, the 3D analysis will be restricted. The analysis is performed by a student with limited experience in numerical modelling and no previous experience on soil tunnelling. A large part of the thesis is focused on learning how to perform the numerical analysis. This will limit the complexity of the analysis to fit within the time frame. Simplifications will be performed to focus on the main objectives of the thesis.

1.4 Outline

This thesis is divided into 10 chapters. Chapter 2 consists of an extensive literature search on soil tunnelling. Theory used in the analyses are explained in Chapter 3. Information about the case study is presented in Chapter 4. Chapter 5 presents the modelling procedure and material models used for the analyses. Chapter 6 describes the 3D analysis in detail and presents preliminary results. Chapter 7 describes the 2D analysis in detail.

Chapter 8 presents the main results of the analyses and discusses the results consecutively. The conclusion of the thesis is summarized in Chapter 9, and further work is proposed in Chapter 10.

2 Soil tunnelling

This chapter is a literature review divided into subchapters to account for various aspects to understand and perform numerical analysis on soil tunnels with special emphasize on jet grouted support structures and moraine conditions. The chapters are in order as follows:

- Introduction to soil tunnelling
- Soil tunnelling methods
- Methods of soil stabilization
- Sprayed Concrete Linings
- Case studies on soil tunnelling
- Design methods for tunnelling
- Numerical analysis of tunnelling

The case studies are provided to argue for a future demand of experience on soil tunnelling in Norway and to evaluate the current use of jet grout structures in soil tunnelling. Literature reviews on both numerical analysis and sprayed concrete linings are important to understand the different approaches and methods in construction and design. Understanding key aspects of numerical modelling and configurations used for jet grouting and concrete linings are important to correctly analyse current solutions.

2.1 Introduction to soil tunnelling

Soil tunnelling is an old form of engineering within the tunnelling branch. In the recent years urbanization has increased substantially, and according to Ritchie and Roser (2018) over half of the world's population live in an urban environment (UN, 2019). This will likely contribute to increased traffic and forcing the construction of more tunnels for roads and railways in the future. Some of these tunnels will face difficult ground conditions and have to be designed with minimal influence to the surface and surrounding environment. Broere (2016) mentions that the benefits of using the underground should not be overlooked, and that the means to utilize the underground is present. Therefore, it is important to increase knowledge and experience on underground works, such as soil tunnelling. It is important to not only build safely, but sustainable.

Soil tunnelling can be described as tunnelling in soft ground. When tunnelling in cohesionless soils, a temporary supporting system prior to primary lining installation is required (Lignola, Flora and Manfredi, 2008). Heuer (1974) described important parameters for soil types, which can be used to evaluate underground construction techniques. He described cohesionless soil as unstable at their respective angle of repose. Due to this an unsupported excavation of granular cohesionless soil would most likely yield a cavity collapse (Heuer, 1974).

Underground works, such as soil tunnelling, involves the process of intervening with an existing equilibrium and causing disturbance of ground conditions. The ground conditions are known approximately with help of geotechnical investigations and previous knowledge. Underground structures are according to Lunardi (2008), unlike most surface constructions, subjected to the most stress in the intermediate construction stage. To prevent the collapse of an excavated cavity, stresses must be handled (Lunardi, 2008).

Basic concepts of the dynamics of soil tunnelling are established in research by Lunardi (2008). In tunnelling the term "arch effect" relates to the channelling flow of stresses around the cavity, which is naturally occurring in rock mediums. This effect must be artificially produced for cohesionless- or loose soils (Lunardi, 2008).

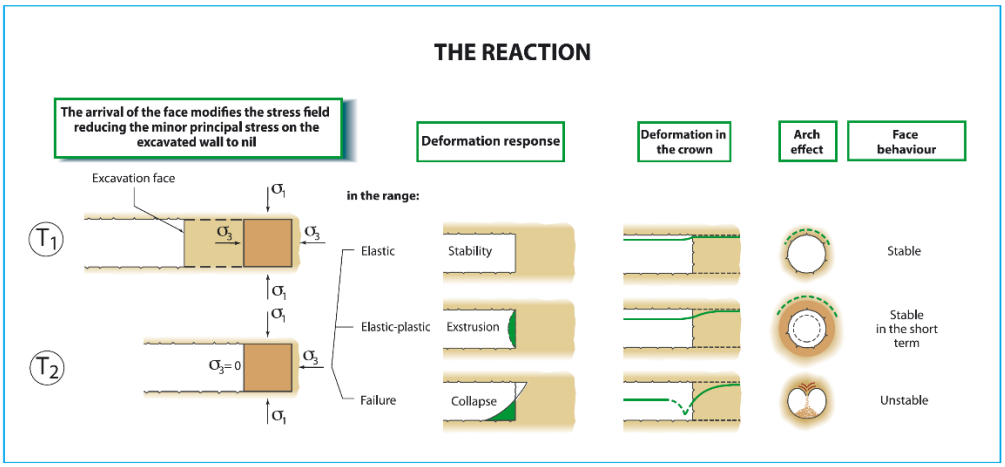

Figure 2.1: Deformation response of the medium to the action from Lunardi (2008).

Figure 2.1 displays the difference between reaction caused by excavating in different mediums. Lunardi (2008) explains that some deformation occurs ahead of the excavation face, which is a well-established phenomenon in tunnelling (Kielbassa and Duddeck, 1991; BTS, 2004). If the confinement pressure, σ_3, drops to zero the situation changes from a triaxial state to a plane stress state. If the situation is stable the medium is in an elastic range and negligible deformation occurs. Elasto-plastic behaviour caused by excavation could yield significant deformation. A failure of the medium will induce a collapse of the cavity. As shown by the Figure 2.1, if a lasting "arch effect" is achieved, the excavation face will remain stable. For shallow overburdens in urban environments, special considerations are needed (Lunardi, 2008).

2.2 Soil tunnelling methods

Several methods of soil tunnelling exist to create a stable tunnel system. This chapter will elaborate shortly on the most common ways of tunnelling in soils. Methods applied solely to rock tunnelling are excluded.

2.2.1 The New Austrian Tunnelling Method

The New Austrian Tunnelling Method (NATM) is a method of conventional tunnelling. It is also commonly referred to as the Sequential Excavation Method (SEM) and applies a sprayed concrete lining (SCL). The NATM guidelines features geotechnical design and a model for contract work. This method was developed in Austria in the 1950s. The basis of the model is to view the ground as a load-bearing element of support. During tunnel excavation the development of ground reactions will be handled by systematically adjusting the use of support elements. Therefore, monitoring is a key element in the NATM. The method can feature both drill and blast techniques and use of excavators on the face. For different geological conditions, conventional tunnelling and support methods are adapted based on the geotechnical design (Galler *et al.*, 2009).

An NATM tunnel can be performed sequentially, with a cross-section typically separated into a top-heading, support core, bench and invert. This is shown for a soft ground example in Figure 2.2. Subdividing the excavation cross-section in side- and centre drifts is also necessary in many cases. In general, soft ground tunnelling require a rigid shotcrete lining and short fixed advance rates. The shotcrete lining can both be reinforced or unreinforced. For soft soils in urban environments, it is generally required to have a closed concrete ring, which involves rapid closure of the invert. In addition, usage of supplementary supports such as jet grouting, dewatering wells, ground freezing and compressed air can provide additional safety. The concrete inner lining, or secondary lining, and amount of reinforcement is typically adjusted by the depth of overburden and surcharges (Galler *et al.*, 2009).

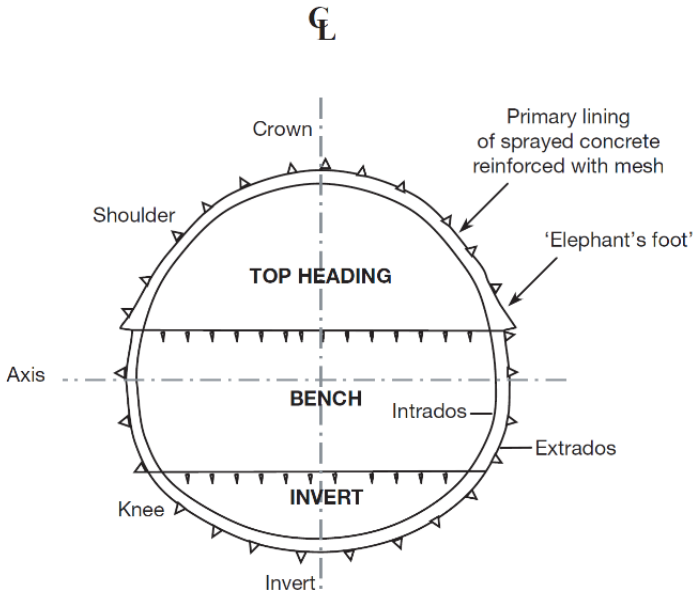

Figure 2.2: Example of an NATM excavation and primary lining from Thomas (2008).

Depending on the geotechnical design the tunnels can be drained or undrained. A drained system uses a waterproof membrane in the roof and a drainage system. An undrained system commonly features a "fully tanked" lining system. In such a system the inner lining is often designed to withstand full water pressure and all permanent loads (Galler *et al.*, 2009). The watertightness is provided by a synthetic, fabric or sprayed membrane between shotcrete lining and inner lining (Su, Bloodworth and Haig, 2013).

2.2.2 Mechanized tunnelling

The method of using a tunnel boring machine, TBM, consists of mechanized tunnel excavation of full profile using rolling cutters with different propulsion- and support systems. For soft soils there are two main operation modes that exists described by Ryan Gratias and Willis (2014). The methods are slurry mode (SM) and earth pressure balanced mode (EPBM).

The SM TBM was first developed in Japan in the 1970s and uses pressurized slurry to balance soil and water pressure on the working face. The EPBM TBM was first applied in Japan in 1974. EPBM utilizes the excavated soil to stabilize the face (Zumsteg and Langmaack, 2017). Both methods use hydraulic pistons to propel the machine forward using the concrete shield established after the excavation process. The use of additives such as polymer, bentonite or fillers allow the method to be flexible in terms of ground conditions and controlling leakage and soil abilities. A TBM can consist of both methods mentioned, which is known as the mix shields method (Ryan Gratias and Willis, 2014).

According to Jernbaneverket (2016) the TBM generally has a faster advance rate than conventional tunnelling, and has less environmental impact during excavation. Ryan Gratias and Willis (2014), from The Robbinson Company, states that the use of TBMs are the most effective tunnelling method for tunnels over 2 km in length.

2.2.3 Cut and cover

The principle of a cut and cover tunnel is a structure built using excavation from ground level. After the completion of the structure, the tunnel is covered. Due to limitations in terms of stability of the excavation, this form of construction is considered beneficial in shallow soil masses. Hung *et al.* (2009) states that cut and cover is usually more economical than bored or mined tunnels with overburdens of maximum 10-12 meters. There are two common types of cut and cover tunnels, the bottom-up and top-down method (Hung *et al.*, 2009).

The bottom-up method places temporary support walls, such as sheet piles, before excavation of the cut section. During the cut section this method has an open pit supported by structural elements. After backfilling, the supports can be removed. An alternative approach is to have an open cut with angled slopes. This does not demand the support walls and bracing, but construction requires more space (Hung *et al.*, 2009).

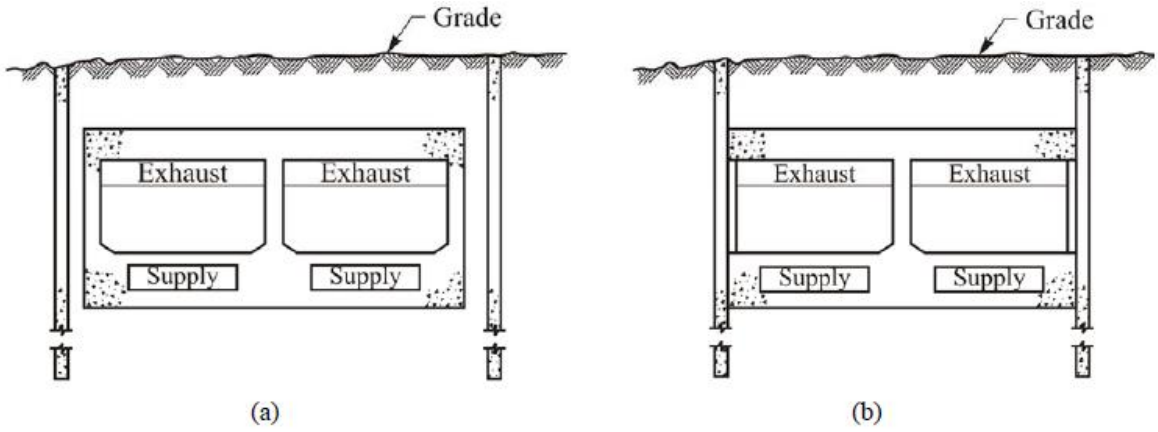

Figure 2.3: Bottom-up construction (a); Top-Down Construction (b) (Hung *et al.*, 2009).

As opposed to the open pit in the bottom-up method, the top-down method features a closed pit. Here the permanent support walls are placed first, thereafter excavation is performed down to the bottom of the future tunnel top slab. Following the completion of construction and waterproofing of the top slab, the ground is backfilled and restored. The next step is to excavate, brace and construct the inside of the structure (Hung *et al.*, 2009).

2.2.4 ADECO-RS

Adeco-RS, also commonly known as the New Italian Tunnelling Method (NITM), is a tunnelling method developed by Lunardi (2008). It is based on the concept of controlled deformation and focuses on the excavation medium, the action and reaction from excavation. "Advance core" is an important contribution to the method, which implies that deformation starts ahead of the excavation face. Therefore, having a strong advancing core is important in terms of controlling deformations. The excavation is performed full-face with mechanical or conventional tunnelling. For different scenarios many support systems are mentioned and explained (Lunardi, 2008).

2.3 Methods of soil stabilization

There exists several ways to intervene with the soil to stabilize it. Lunardi (2008) place the different interventions into three groups as seen in Figure 2.4. The three groups are:

- Preconfinement interventions.
- Confinement interventions.
- Presupport interventions.

Preconfinement interventions are defined as interventions that act ahead of the excavation face to establish an arching effect. When interventions are performed behind the face to counteract deformation, it is called confinement interventions. When support is made ahead of the excavation face, without contributing to an arching effect, it is named a presupport intervention. These interventions can either be an improvement of the ground strength or to conserve the soil strength characteristics (Lunardi, 2008). The examples covered are illustrated in Figure 2.4. The grouping system by Lunardi is used to further elaborate on the different support methods. Terminology used to describe the three groups are not universally recognised and tend to differ in literature. In this theory chapter, the terminology is adopted in convenience to describing the different methods.

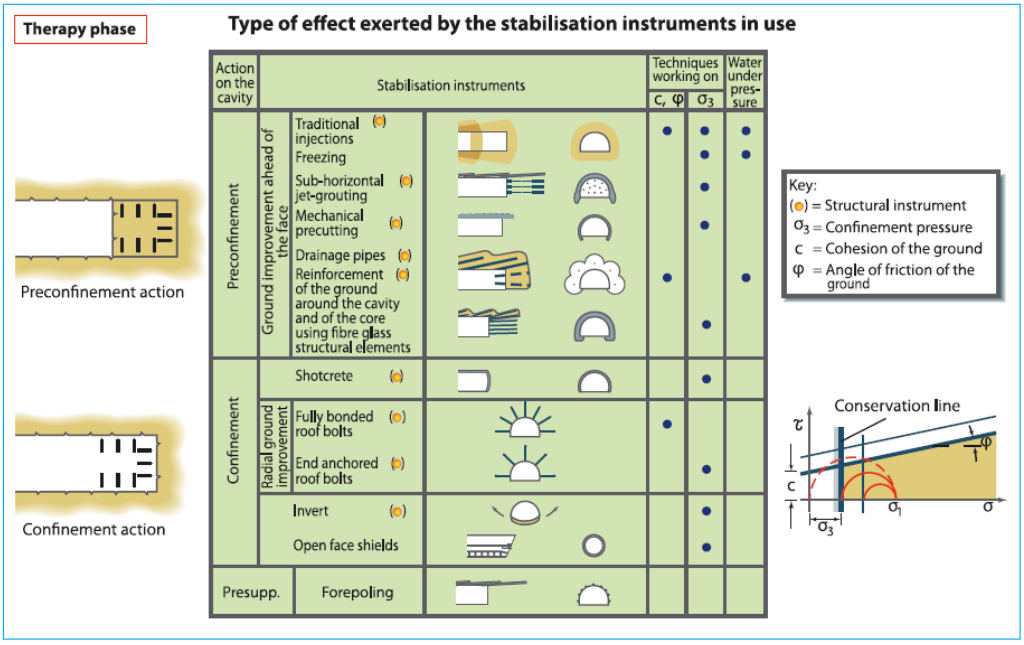

Fig. 8.2

Figure 2.4: Stabilization instruments from Lunardi (2008).

2.3.1 Preconfinement interventions

The main objective of the preconfinement interventions is to prevent a significant reduction of the principal minor stress, or confining pressure, σ_3. A stress reduction would potentially lead to radial deformation in the future tunnel (Lunardi, 2008).

Jet grouting

Jet grouting is a process where a cement-based grout mix and water is mixed into the ground with high pressures. There are several different formulas of injection material based on unique soil conditions. Jet grouting forms a lasting column in the ground that has better geotechnical properties than if the ground was left untreated (Pelizza and Peila, 1993). The most fundamental parameters of jet grouting are grout mix, jet nozzle energy, grout flow rate, grout rod rotation and withdrawal rates according to Covil and Skinner (1994). Typical construction of vertical jet grout columns is shown in Figure 2.5.

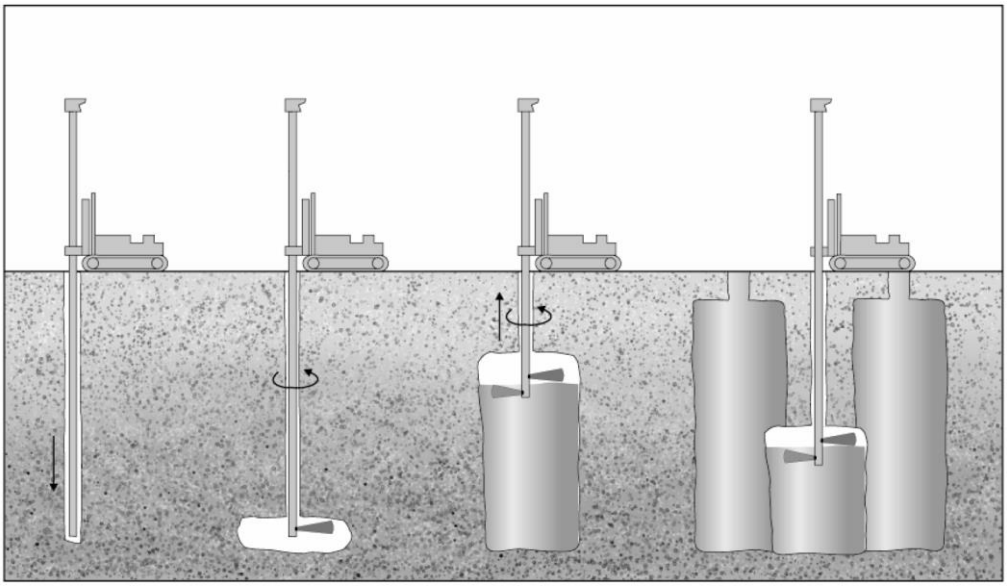

Figure 2.5: Example of construction of vertical jet grout columns from Burke (2004).

Jet-grouting technology mainly consist of the methods shown in Figure 2.6. These methods produce different results of column diameter, compressive strength and spoil return (Vegdirektoratet, 2014; Lunardi, 1997). Mono-, bi- and tri-fluid are the main methods of jet grouting. Examples of jet grouting systems are:

a) Monofluid system with cement grouting and water through a nozzle.
b) Bi-fluid system with cement grouting, and water with compressed air through a double nozzle.
c) Tri-fluid system with air and water in a double nozzle and cement grouting and water in a separate nozzle.
d) System with water and air in a double nozzle and constructional cement through a casting pipe (Vegdirektoratet, 2014).
e) Two-stage system where very high pressure water drilling precedes a second stage of grout injection to create larger diameter columns (Lunardi, 1997).

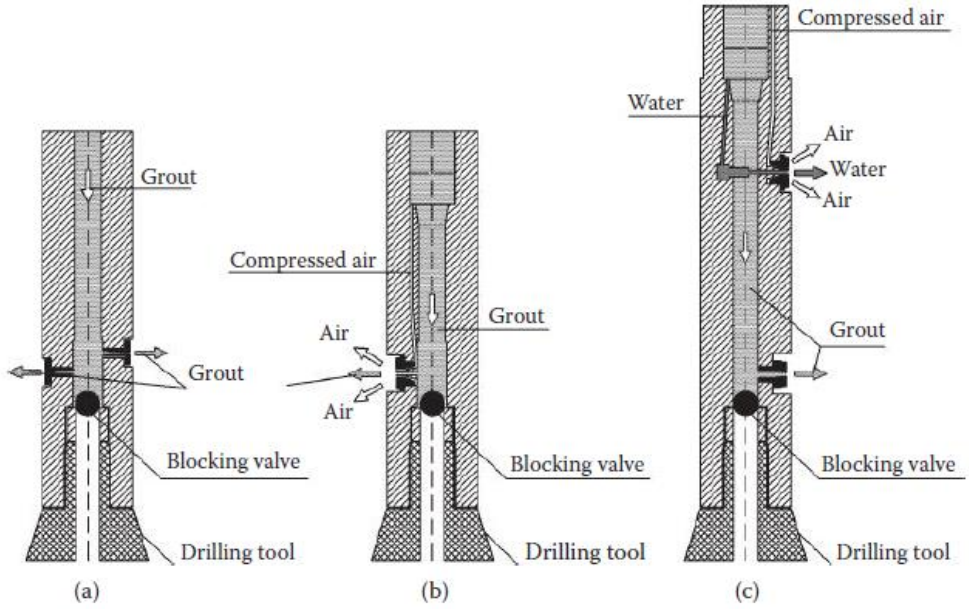

Figure 2.6: Mono- (a), bi- (b) and tri-fluid (c) systems from Croce, Flora and Modoni (2014).

Application of the jet grouting is generally considered for difficult ground and locational conditions. Prior to choosing an appropriate jet grouting system, soil investigations and preliminary field test are generally advised for proper design (Vegdirektoratet, 2014; Lunardi, 1997). Testing of variability have shown that jet grouted columns in gravelly or sandy material are generally more homogenous than in finer soils. Projects with requirements towards waterproofing, the injection of bentonite can be utilized to reduce permeability (Vegdirektoratet, 2014). Jet grouting can be applied to several different forms of underground structures. Commonly, jet grouting is used for foundations and underpinning, tunnels or hydraulic works. In hydraulic works jet grouting is especially suitable for dams due to the lowered permeability in the treated soil (Lunardi, 1997).

Conventional grouting

Conventional grouting or chemical injection is the process of injecting grout mix at lower pressures compared to jet grouting. The grout mix can be cement- or chemically based. The injection process is performed from valved tubes after drilling. Typical usage in soil tunnelling is with establishing a truncated cone injected around the cavity, performed from inside or outside the tunnel. Improved mechanical characteristics and permeability is achieved with this method. Conventional grouting is commonly performed on unstable faces, with non-cohesive behaviour. The technique can be adapted for shallow overburdens and urban environment (Lunardi, 2008). Examples of application and usage is shown in Figure 2.7. The figure shows the use of conventional injections from the excavation face, pilot tunnel and from the surface.

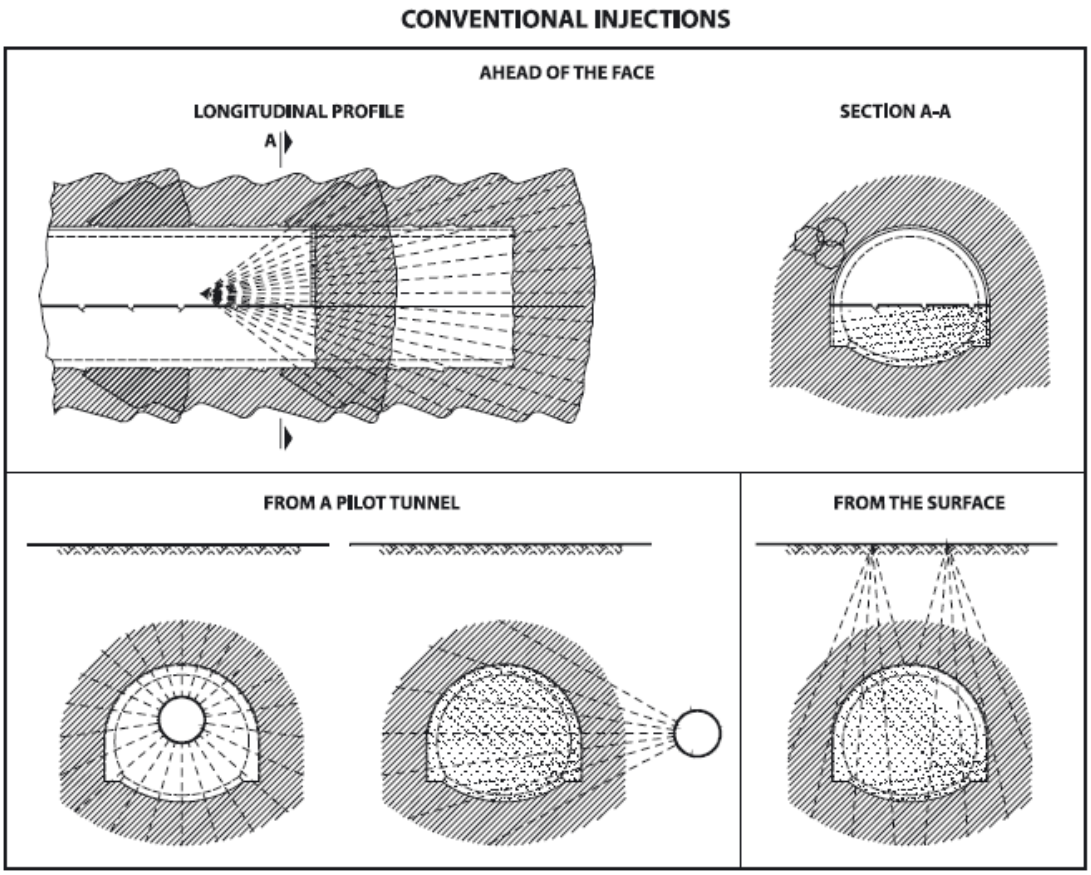

Figure 2.7: Conventional injections in soil tunnelling from Lunardi (2008).

Fibreglass reinforcement

Fibreglass reinforcements are used to stabilize the advancing core. Prior to excavation, evenly distributed holes are drilled into the tunnel face and fibreglass elements are inserted. These are later injected with a low-pressure cement mix with a controlled shrinkage. Adequate design and execution will increase strength and deformation characteristics of the ground to which the fibreglass elements are installed. Application of fibreglass is generally suitable for semi-cohesive to cohesive soil with an elasto-plastic behaviour. In combination with other methods producing an artificial arch, the treatment is also applicable to loose soils (Lunardi, 2008).

Freezing

Pre-confinement using freezing can be applied in saturated soil. The concept of the method is to excavate in frozen ground and keep it frozen until adequate supports are placed (Pelizza and Peila, 1993). Ground freezing is generally watertight and increase the soil strength (Vegdirektoratet, 2014). Muir Wood (2000) states that the method could be costly and time consuming. Liquid nitrogen is commonly used as the freezing medium. Generally, the procedure is completed from the surface, but may also be performed from the tunnel. If operated from within the tunnel, the equipment plant must be of a suitable size. Special considerations must be undertaken during design for the freezing and thawing process and suitability may vary for different ground conditions (Muir Wood, 2000). According to BaneNOR (2019), ground freezing is suitable for most ground conditions.

Mechanical pre-cutting

Mechanical pre-cutting is pre-confinement method that involves making an incision with a chain cutter along the extrados of the tunnel. Extrados refers to the outside of the specific volume and intrados refers to the inside of the specific volume. The incision has a predetermined thickness, gradient and length, which is to be immediately filled with for example fibre reinforced sprayed concrete. Incision gradient and overlapping is important to obtain adequate results. The sprayed concrete must have additives that yields rapid strength. Difficulties with cohesionless materials may be encountered with cement injection in the excavation profile (Lunardi, 2008).

Drainage

Tunnels with water as a problem can be excavated with a drained behaviour to lower the water inflow. This is often performed using drainage pipes (Pelizza and Peila, 1993). Lunardi (2008) states that during drainage, a transitory period occurs with lowered hydraulic pressure due to water filtration towards the tunnel walls. He further explains that drainage with lacking counter measures will affect the advancing core, by reducing the geomechanical strength and rigidity. Adeco-RS method suggest using an umbrella of drainage pipes, around the future tunnel, stretching three to four times the diameter length in front of the face. Lunardi specifically suggests that draining the tunnel directly from the tunnel face should be avoided (Lunardi, 2008). Draining with NATM in soft ground tunnelling, suggests using a system of external dewatering wells (Galler *et al.*, 2009).

2.3.2 Confinement interventions

Sprayed concrete

Sprayed concrete, or shotcrete, is commonly used in conventional tunnel methods such as NATM, Norwegian Method of Tunnelling (NMT) and Adeco-RS (Lunardi, 2008; Galler *et al.*, 2009). The concrete mixture is sprayed with high velocity at the tunnel walls and adheres with the surface. Due to a low cement-water ratio a high strength is developed rapidly. Sprayed concrete can be both unreinforced, fibre- and steel reinforced. It can be sprayed onto surfaces with irregularities, and additional reinforcements, such as steel ribs or steel mesh, can be applied prior to application. Use of sprayed concrete is applied to produce a confinement pressure for the cavity and if applied to the face, it will also provide face support (Lunardi, 2008). New technology, in addition to specific ground conditions, shows sprayed concrete could have a potential life-time span from 15-50 years up to 200 years (Galan *et al.*, 2019).

Early-age sprayed concrete is an important contribution to model time-dependent behaviour, especially in soil tunnelling. Eurocode EN 14487 yields a classifications of different early-age strength developments of sprayed concrete. Figure 2.8 shows a graph displaying the compressive strength increasing with time for different classes. To classify the strength, at least three measured points must fall within the area corresponding to the different classes. In the figure X is minutes, Z is hours and Y is compressive strength (MPa) (CEN, 2012).

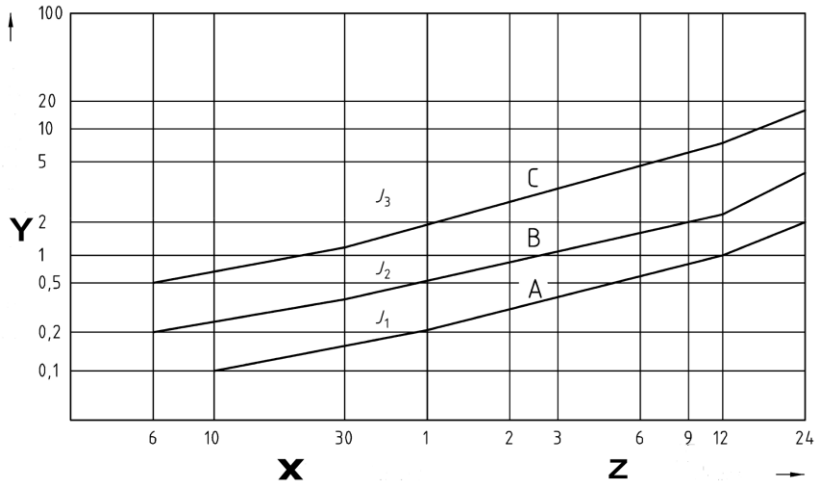

Figure 2.8: Early-age strength of sprayed concrete according to EN 14487 (CEN, 2012).

2.3.3 Pre-support interventions

Forepoling

Forepoling involves the installation of steel bars or steel sheets ahead of excavation (Lunardi, 2008). They are frequently combined with lattice girders to provide crown support. Forepoling are generally used to increase the ground support close to the excavation face. It is typically used in poor rock or soil conditions (USACE, 1997).

2.3.4 Tunnel waterproofing

Choice of waterproofing method for tunnelling is often decided by which water regime is adapted for the design. Common regimes adopted is shown in Figure 2.9. A hydrostatic regime assumes that the water table is unchanged. On the other hand, a hydrodynamic regime indicates that the ground water is lowered, due to water inflow to the cavity. Use of drainage pipes can be combined with a hydrodynamic condition to further reduce the water table (Lunardi, 2008). Soil tunnels can be excavated hydrodynamically and be designed in the long term with a hydrostatic regime, as is the case with some NATM tunnels (Lunardi, 2008; Galler *et al.*, 2009). Traditionally, the final lining is protected from potentially aggressive water using sheet membranes and geotextiles (Lunardi, 2008).

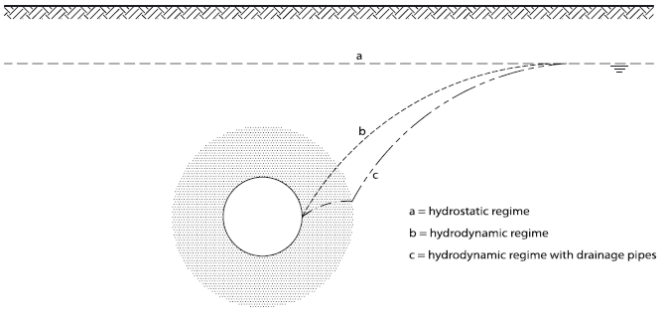

Figure 2.9: Figure describing water regimes in tunnelling from Lunardi (2008)

Compressed air

Compressed air is a temporary support method often used in shallow tunnelling to prevent water inflow during excavation. It can be used in combination with NATM, where the air loss is estimated through the excavation face and cracks in the sprayed concrete lining (Semprich, Scheid and Gattermann, 2003; Galler *et al.*, 2009). The advantage of using such a method is that the surrounding groundwater is unaffected by the excavation. Problems due to the possibility that a sudden air pressure drop could compromise tunnel stability, and the safety of workers. Required air pressure is often designed using hydrostatic water pressure combined with a safety factor. Models have been suggested to numerically simulate the air loss in the tunnel (Semprich, Scheid and Gattermann, 2003).

Waterproofing membranes

Waterproofing can typically be achieved in tunnels using sheet or spray-on membranes. Both methods have surface preparation requirements. Sheet membranes, considered frictionless in design, have no theoretical shear transfer between the primary and the secondary lining. This disables any composite behaviour between the linings. The theoretical frictionless surface due to the sheet membrane, or a separation layer, have shown to reduce the risk of cracking and reinforcement requirements (Thomas, 2008). Spray-on waterproofing membranes (SAWM) are relatively new and can be a cost-effective solution providing an easy application. Disadvantages of the spray-on membranes is the vulnerability to in-situ environmental influences and poor workmanship (Thomas, 2008). Main benefits are relatively quick and easy application, in combination with less need to work in heights. It could also potentially include lining reductions in design (Dimmock, Haig and Su, 2011).

2.4 Sprayed Concrete Linings

Sprayed concrete linings, hereby referred to as SCL, are commonly adopted in tunnelling methods such as the New Austrian Tunnelling Method as the primary lining. Typically, a secondary lining is designed to withstand the water load, and ground load for long term situation. With this assumption the sprayed lining is considered to not contribute structurally for long term. The secondary concrete lining is traditionally a cast in-situ concrete, but can also be a permanent sprayed concrete lining (PCSL) (Thomas, 2008).

Alun Thomas have specified some different lining design configurations of SCL in soft ground continuum material (Thomas, 2008; Su and Thomas, 2015; Thomas, 2021). Literature contains several different annotations to these lining configurations and therefore Table 2.1 explains typical configurations. Literature may use different terminology.

Table 2.1: Common lining configurations in SCL tunnels from Thomas (2008).

Lining configuration	Design	Comment
Single shell lining (SSL) / One pass lining	Several layers of sprayed concrete and alternatively a SAWM for water resistance.	Requires a surrounding of low permeability and special attention in joints (Thomas, 2008).
Double shell lining (DSL)	Sprayed concrete, typically sheet membrane and permanent inner lining.	Inner lining can be cast in-situ concrete or permanent sprayed concrete. In design, no tangential stress between linings is allowed.
Composite shell lining (CSL)	Sprayed concrete, SAWM and permanent inner lining.	Inner lining can be cast in-situ concrete or permanent sprayed concrete. Designed with shear, tensile and compressive stress transfer between linings.

2.4.1 Single Shell Lining

A single shell lining considers the sprayed concrete as permanent. The layering of sprayed concrete is often considered to act as a composite shell. In design, the bond strength between the layers must be sufficient to act composite. According to Thomas (2008) this is well within the bond strength of sprayed concrete. Traditionally, this approach was used for hydropower tunnels and in conditions with dry rock. In recent years, usage have extended to water-bearing soft ground tunnels (Thomas, 2008).

To increase watertightness a spray-on water membrane can be implemented in the layering of an SSL. Holter *et al.* (2014) performed tests on SSL with spray-on membranes in hard rock tunnels and concluded that the humidity level was significant for the membrane's performance. The authors emphasizes the challenge of obtaining in-situ humidity condition for testing and understanding how water migrates through sprayed concrete (Holter *et al.*, 2014). Considering watertightness, the SSL should be used in relatively impermeable ground to meet minimum criterion for railway tunnels. For example, it has been utilized successfully in London Clay with low permeability. This could however be achieved for more permeable ground using improvement techniques to improve permeability surrounding the cavity (Thomas, 2008).

2.4.2 Double Shell Lining

The double shell lining is a common solution for tunnelling. As previously mentioned, there is no bonding assumed between the linings with a sheet membrane, which can reduce the risk of cracks forming in the secondary lining. Use of a sheet membrane commonly adopts a slip interface in numerical analysis (Thomas, 2008). However, Lorenz and Galler (2015) showed a certain level of shear transfer happening between linings using a sheet membrane covered with geotextile. In situations with water pressure on a sheet membrane, a gap between the linings and membrane could occur, which would disable any shear transfer (Su and Bloodworth, 2019; Hung *et al.*, 2009). For this reason, it seems reasonable to evaluate the sheet membrane as a slip surface.

In traditional double shell lining design, the sprayed primary lining is considered degraded in long term. Thomas (2008) states that there is no evidence supporting a complete degrading of a modern sprayed concrete. An alternative is to evaluate a certain depth of the primary lining as sacrificial. Degraded sprayed concrete is commonly designed as grey rock gravel or using a degradation percentage to determine design values (Thomas, 2008). Aldrian, Thomas and Holter (2021) published an article to provide infrastructure owners and advisors with more confidence to use sprayed concrete as a permanent structure for the future. Actual experience on the Crossrail tunnels in UK with permanent sprayed concrete are discussed by the authors. In this project the PSCL was designed with a lifespan of 120 years (Aldrian, Thomas and Holter, 2021).

Galan *et al.* (2019) stated that with more available data, the sprayed concrete can be designed to last similarly to in-situ concrete. In their article, key conditions that affects the durability of sprayed concrete were reviewed. Due to the underground environment of a tunnel, the concrete is in direct contact with surrounding material and groundwater. Common issues related to sprayed concrete is leaching, sulphate attacks, freeze-thaw processes, electrochemical corrosion and sintering. In order to prevent durability issues different components can be added to prevent degrading, but some components can also lead to durability issues (Galan *et al.*, 2019).

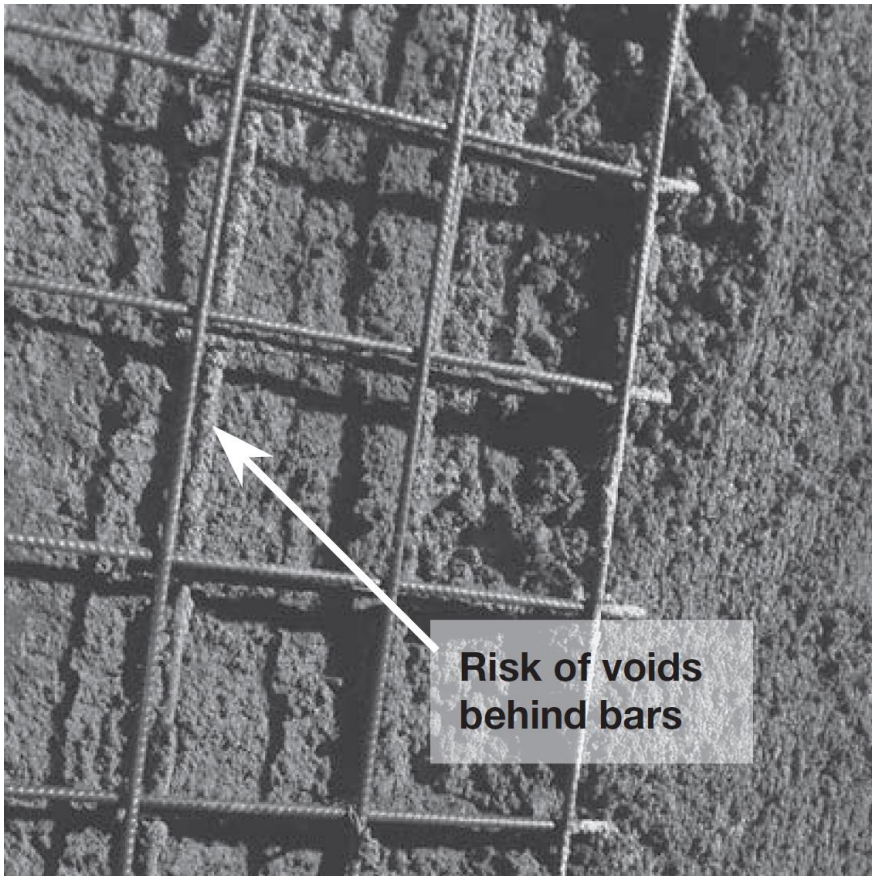

Figure 2.10: Sprayed concrete voids behind reinforcement bars from Thomas (2008).

With structural steel elements in the lining such as lattice girders and wire mesh, the sprayed lining is prone to corrosion. Due to possible cracks in the lining, a concrete cover is often not considered sufficient to counteract the corrosion. This is a reason for the current design assumption of long-term degradation of the sprayed concrete lining (Marcher, John and Ristic, 2011). Thomas (2008) discuss how the sprayed concrete will be rebounded by the steel mesh during application and potentially cause voids behind the bars, which form ideal locations for corrosion.

2.4.3 Composite Shell Lining

In a configuration with composite shell lining, the membrane is considered to produce bonding between the linings (Su and Thomas, 2015). Su and Bloodworth (2016) performed laboratory tests and parameter investigations on spray-on water membranes. Tests showed a sufficient shear strength to provide a certain degree of composite action. The study also provided interface values and specified the importance of membrane thickness and substrate roughness to achieve higher level of bonding. In a subsequent study they demonstrated the composite mechanical behaviour compared with beam tests in numerical simulations. Normal stiffness and shear stiffness parameters was used to predict a range of composite action (Su and Bloodworth, 2018).

Su and Bloodworth (2019) published a state-of-the-art review on numerically simulating composite behaviour with sprayed membranes. Modelling and design considerations was elaborated. Lining calculations in the review was performed using a thrust-moment capacity curve from Sauer, Dietmaier and Bauer (1990). General conclusions from the

review were that shear transfer between linings was only beneficial to the primary lining. The use of tensile bond strength could lead to a shared long-term water pressure which could reduce thickness of the secondary lining. An important factor of the study was the lack of data for wet membrane interface properties. Due to tensile strength in the range of 240kPa, tunnels applying composite behaviour should be limited to a water table of 20-25 meters above the invert (Su and Bloodworth, 2019).

Literature suggesting values for sprayed membranes in numerical modelling are limited. Holter reported tensile bonding strength varying from 0.5-1.2 MPa and shear bonding strengths from 1-4 MPa. Su and Bloodworth (2016) investigated interface parameters of the product TamSeal800. Suggested interface stiffness parameters for short-term are given. For long-term loading a relaxation ratio of 50% was advised. Minimum peak strengths where also suggested. Figure 2.11 show proposed parameters from the investigations (Su and Bloodworth, 2016).

Suggested ranges of interface stiffness parameters (short-term*) for composite shell lining design, assuming spray-applied waterproofing membrane (*TamSeal 800*)

Interface Type	Compression K_n GPa/m	Tension K_n GPa/m	Shear K_s GPa/m
Thin membrane, smoothed or regulated layer	10 – 16	7 – 23	0.3 – 6.7
Thin membrane, as-sprayed layer	4 – 10	7 – 23	0.9 – 9.3
Thick membrane, smoothed or regulated layer	1 – 4	2 – 22	0.3 – 3.0
Thick membrane, as-sprayed layer	1 – 8	2 – 22	0.5 – 3.3

* A suggested relaxation ratio of 50% should be applied to all stiffness values for long term loading

Interface minimum peak strengths for composite shell lining assuming spray-applied waterproofing membrane (*TamSeal 800*)

Interface Type	Compression MPa	Tension MPa	Shear MPa
Thin membrane, smoothed or regulated layer	30	0.7	2.1
Thin membrane, as-sprayed layer	11	0.7	2.0
Thick membrane, smoothed or regulated layer	10	0.7	2.0
Thick membrane, as-sprayed layer	8	0.7	1.7

Figure 2.11: Interface properties for CSL from Su and Bloodworth (2016).

Based on previous work by Holter, and Su and Bloodworth, further testing was performed by Johnson, Swallow and Psomas (2016). They suggested a shear modulus of 1 MPa, with a Poisson's ratio closer to 0.5. Pillai *et al.* (2017) published a journal article which proposed Mohr-Coulomb interface parameters based on test with the product MasterSeal 345. They presented failure values for friction angle between 10-14° and cohesion between 1.2-1.7 MPa. Shear modulus was carefully estimated to 7 MPa (Pillai *et al.*, 2017).

2.4.4 Summary

Three common lining configurations have been researched. Lining configurations are changing as new technology that can optimize the design is developed. It is important to evaluate the potential of such configurations, which may benefit future construction. Sprayed concrete can be assumed to be adhesive when sprayed on in layers. The sheet membrane between a double shell lining should, under water pressure, function as a frictionless surface when applied in design. Values for normal- and shear stiffness and strength have been presented for spray-on waterproofing membranes. Current literature does not provide sufficient data to give accurate design values for long-term and wet behaviour of sprayed membranes.

2.5 Case studies on soil tunnelling

This chapter will go through some examples of soil tunnels that have been constructed in Norway and some soil tunnels involving jet grout support systems in Europe. At the end of this chapter the level of soil tunnelling expertise in Norway has been roughly established and different excavation methods with jet grout have been researched.

2.5.1 Soil tunnels in Norway

Norwegian tunnelling is most known for rock tunnelling, since about 50% of the country is made up of exposed bedrock. The established rock tunnelling method in Norway is called the Norwegian Method of Tunnelling (NMT). According to the NMT, support mechanism is adapted in zones with weak rock (Rygh, 1992). In recent years, centralization and population growth have expanded the cities. Many major cities in Norway are situated close to the ocean and therefore the ground could contain glacial deposits from the glacier melting or marine clay due to land heave since the ice age (Jorstad, 1968). These conditions could prove challenging when constructing underground works.

Rock tunnels in Norway commonly encounter weak zones with soil material. Norwegian support methodology is generally based on the empirical Q-system. In poor rock conditions, or loose soils, the Q-system suggests pre-soundings followed by forepoling and/or pre-injections. If conditions are mostly loose soil, Norwegian road regulations state that special design is required (Vegvesen and Vegdirektoratet, 2006; Vegdirektoratet, 2015). Only a handful of designed soil tunnels have been built in Norway. Many of these are built as cut and cover tunnels. A selection of relevant soil tunnels in Norway that have been found in literature, are given in Table 2.2.

Table 2.2: Norwegian soil tunnels.

Name	Year	Ground	Excavation method	Support
Tyholttunnelen	1942	Clay	Compressed air	-
Eidsvolltunnelen	1993	Clay/silt	NATM	SSL with girders.
Jobergtunnelen	2016	Moraine mixed face	NATM	Steel pipe umbrella with DSL.
Hovengatunnelen	2018	Silty clay	Top-down C&C	Jet grout arched slab, sheet pile and top plate.

The oldest soil tunnel built in Norway that is quoted in literature, Tyholttunnelen, was built in clay conditions using compressed air. The workers accessed the tunnel face through a chamber. Due to lacking of experience and high are pressure, the workers got decompression sickness. In the 1990s a railway tunnel called Eidsvolltunnelen was built in clay/silt conditions using NATM and shotcrete roof support with steel girders (Aagaard and Gylland, 2017). In 1996 approx. 125 meters collapsed due to failure of the upper

part in the shotcrete shell. The stretch was assumingly repaired as a cut and cover (Eggestad, 1998).

The Joberg tunnel was successfully completed in 2016 through roughly 100 meters of moraine tunnelling (Langåker, 2014; Aagaard and Gylland, 2017; Aagaard, 2016). Due to the contract requiring previous experience with design of soil tunnels, an Austrian consultant was hired as subcontractor. It was excavated using NATM with pre-confinement support with the steel pipe umbrella method and a lowered groundwater table. The confinement supports were lattice girders with spacing of 1-1.5 meters with 30cm of reinforced shotcrete followed by waterproofing membrane that was enclosed by a 40-60 cm permanent inner lining. Due to mixed face excavation, no closing of invert was needed (Aagaard and Gylland, 2017). Aagaard and Gylland (2017) stated that a high ground water table in combination with the mentioned materials and the steel pipe umbrella method wouldn't be sufficient.

Ground improvement with jet grouting columns in Norway is relatively new and has recently seen increased usage. Jetgrunn is a Norwegian company, with jet grouting experience, that was part of a research program in the 1980s. They have developed methods for jet grouting that can be used in Norwegian climates, most notably the J2- and EC1 method. EC1 method is suitable in clay or enrockments. The J2 is a bi-fluid method suitable in all soils (Lier, 2017). Jetgrunn installed 450 jet grouting columns in the VA-Tunnel Örby project in Älvsjö, to create a tunnel roof through soil containing moraine, sand, silt and clay. The roof was supported with 20cm reinforced shotcrete, and where the tunnel sections were entirely above bedrock, the bench was casted with concrete. Tests of the jet grout columns showed a variation in compressive strength from 8,8-27,2 MPa. Convergence of the cavity was measured to 2,9 mm. The permeability was recorded to about 10^{-7} -10^{-8} m/s (Tyrens, 1985).

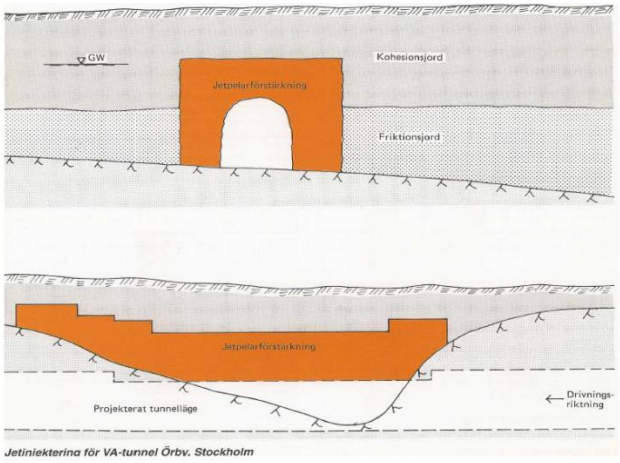

Figure 2.12: Figure of project *VA-Tunnel Örby* from Tyrens (1985).

On FV32, Gimlevegen – Augestadvegen, both methods previously mentioned were used by Jetgrunn to form a waterproof slab during a constructed soil tunnel with a top-down cut and cover solution. 2096 J2-piles were built with a required compressive strength of 7 MPa. Tests showed average compressive strength of 10.3 MPa and a characteristic compressive strength of 9.3 MPa. On another project, Skjeggestadbrua on E18, jet grouted columns were used for foundations under a bridge that had suffered ground rupture. In this project acoustics were utilized to identify contact between columns (Lier, 2017).

2.5.2 European soil tunnels with jet grout

In Europe, soil tunnelling, both mechanized and conventional, is more common than in Norway. The deciding tunnelling method, is according to Lunardi (2008) chosen by a feasibility analysis. Generally, a short tunnel length is the main reason for opting for conventional tunnelling (Lunardi, 2008). Table 2.3 lists soil tunnels with jet grout support systems excavated in soil deposits with focus on NATM tunnels.

Table 2.3: European soil tunnels with jet grouting.

Tunnel	Year	Soil	Method	Support systems
VA-Tunnel Örby	1985	Moraine,sand, silt and clay.	N/A	Jet grout roof, shotcrete.
Monte Olimpino	1989	Silty sands, gravel	NATM	Jet grout arch, sub-vertical jet grout columns and double shell-lining.
The Aeschertunnel	2009	Glacial moraine	NATM	Umbrella jet grout arch.
Fritzens Tunnel H7-1	2009 (Wallis, 2008)	Inn gravel sediments and dejection fad sediments.	NATM	Umbrella jet grout arch and compressed air. No info on linings.
Stans tunnel H4-3	2010 (Wallis, 2008)	Inn gravel sediments and dejection fad sediments.	NATM/SEM	Sub-vertical jet grout ring, DSL and compressed air.
Untersammelsdorf Tunnel	2020	Silty – fine sandy lacustrine desposits	NATM	Sub-vertical jet grout arch, wall piles and DSL configuration.
Brenner Base Tunnel – Lot Eisackquerung	NA	Gravel, soil and soft ground.	NATM/SEM	1. Sub-vertical jet grout ring. 2. Sub-horizontal jet grout arch.

Stella, Ceppi and D'Appolonia (1990) described the construction of a 750m stretch of the Monte Olimpino 2 tunnel in northern Italy in 1989. The alluvial deposits in the tunnel alignment showed silty sand and fine sands, with layers of sandy gravel. The groundwater level was characterized as 3 meters below the invert. Excavation method using jet grouting was chosen as a feasible solution, after evaluating other methods such as ground freezing, permeation- and chemical grouting. Freezing was considered expensive and time consuming. Permeation was unfeasible due to grain size and cohesionless natural of the materials. Chemical grouting was unacceptable due to water

supply pollution. The construction featured a complex order of operations with subdivision of the face and alternating excavation of sides in longitudinal direction (Stella, Ceppi and D'Appolonia, 1990).

The support design used on Monte Olimpino was a jet grout arch with temporary shotcrete with steel ribs, sheet piles for side stability and two rows of sub-vertical jet grout columns in the invert. A closed concrete secondary lining was then installed. The sub-vertical columns were designed to be retaining walls. Experience from this project suggested that the jet-grout technique was a viable alternative to other conventional techniques for soft soil tunnelling. A monitoring program also revealed that small strains and displacements was kept minimal throughout the entire construction process (Stella, Ceppi and D'Appolonia, 1990).

Coulter and Martin (2006) studied the effect of jet-grouting on surface settlements of the Aeschertunnel in Switzerland. The project consisted of two parallel shallow highway tunnels with ground conditions of Molasse bedrock, glacial moraine, and dry medium-dense silty sand. The tunnels themselves were approx. 2 km long and had a cross-section of approx. 135 m^2 (Coulter and Martin, 2006). The glacial moraine consisted of brown clayey sand and silt with some gravel and isolated boulders. It was shown to be stiff and homogenous, with no signs of instability of the face. Groundwater was perched on top of the glacial moraine according to Fries (2000).

The excavation was performed mainly using a jet grout vault, divided into a heading- and bench excavation. During excavation the moraine was observed to be dry. Support procedure for the tunnel advancement in the moraine consisted of 39 horizontal jet grout columns in an arch. Each column was 13 meters long with 2 meters overlapping in the longitudinal direction. The column diameters where 0.6 m with 0.45 m spacing to ensure overlapping. Additional support consisted of a shotcrete liner with lattice girders and welded wire mesh. The temporary liner of shotcrete was 400 mm thick in heading and bench, while the invert had 200 mm of shotcrete. The total settlements induced by the tunnelling was limited to a maximum of approx. 25mm of narrow settlement with 30% occurring ahead of the excavation face (Coulter and Martin, 2006).

The Lower Inn Valley railway line in Austria consisted of construction of multiple shallow tunnels under existing infrastructure. For the project many conventional types of constructional special works were applied, and jet grouting was utilized in difficult soil conditions. On contract H4-3 and H7-1, with tunnels submerged in groundwater, two different applications with jet grouting were used. H4-3 had a jet grout ring established from the surface around the entire perimeter, while H7-1 used jet grout pre-support in the heading (Palla and Leitner, 2009).

The ground conditions in the subsoil mainly consists of Inn gravel sediments and dejection fan sediments (Palla and Leitner, 2009). Dejection fans, or alluvial fans, is according to Bull (1977) a deposit formed as a cone where a stream leaves its source area. Permeability of the soils were measured in the range 10^{-2} and 10^{-4} m/s and the groundwater speed to 1.4m per day. To assess the suitability of jet grouting columns, a large-scale trial on vertical and inclined columns were performed (Palla and Leitner, 2009).

Fritzens Tunnel H7-1 consisted of a 430-meter-long horizontal jet grout screen. Due to groundwater existing between 0 to 2.5 meters below the tunnel crown the excavation was performed in combination with compressed air of 0.6 bar. The combination was

unique and proves that combination of support methods can give increased flexibility in tunnelling. Horizontal length of the double row jet grout screen was 15 meters with 11% inclination. A close monitoring was used and potential "jetting shadows" was filled with grout injection by steel tubes (Palla and Leitner, 2009).

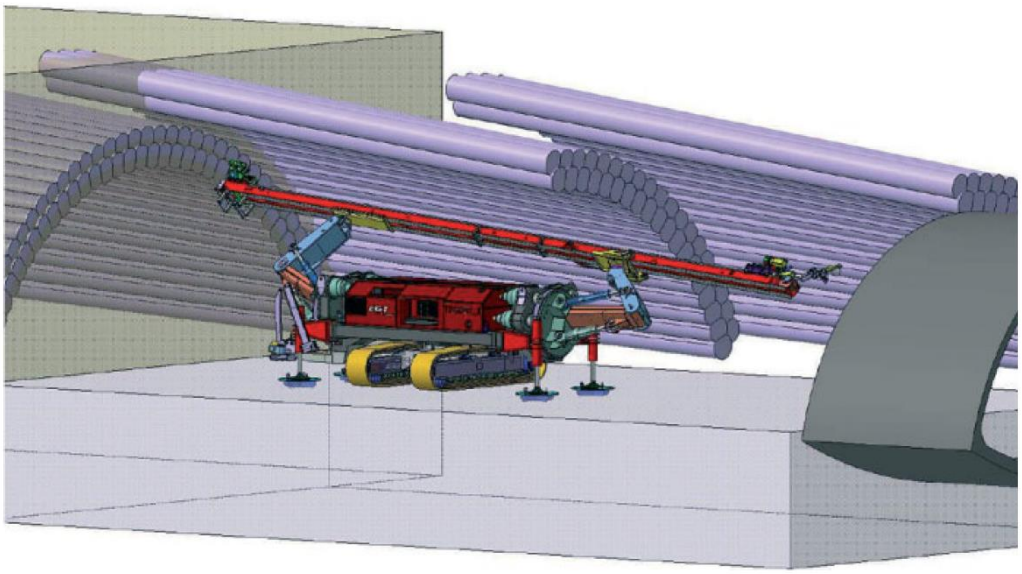

Figure 2.13: Illustration of a double jet grout screen from Fritzens Tunnel (Palla and Leitner, 2009).

The jet grout screen was drilled by uncased rotary drilling with mud flushing and the tube screen was drilled using cased hammer drills. The jet parameters were demonstrated through preliminary trials. Using this unique method Palla and Leitner (2009) states that the process can be optimised according to the in-situ ground investigations. It is also stated that a horizontal jet grouted screen can minimise deformations and induce no negative effect on the infrastructure above the tunnel if properly optimized and adapted under construction (Palla and Leitner, 2009).

The Lower Inn Valley railway also featured The Stans tunnel contract H4-3. The alignment has shallow cover and passes under critical infrastructure, such as an autobahn bridge and an existing Austrian Railway line, sensitive to settlement. This sensitivity demanded a construction method which would induce little deformation and vibration. This included that the groundwater table, which was only a few metres from the surface, should not be lowered. The contract H4-3 involves a length of approx. 750 meters. The tunnelling work was placed inside a 2-meter-thick jet grouted surround that was drilled from the surface as seen in Figure 2.14. The construction of transverse bulkheads every 20m divided the tunnel into 37 compartments. These bulkheads enabled control of the waterproofing in sections. The cross-section was 127 m^2 and the excavation was performed using compressed air (Palla and Leitner, 2009).

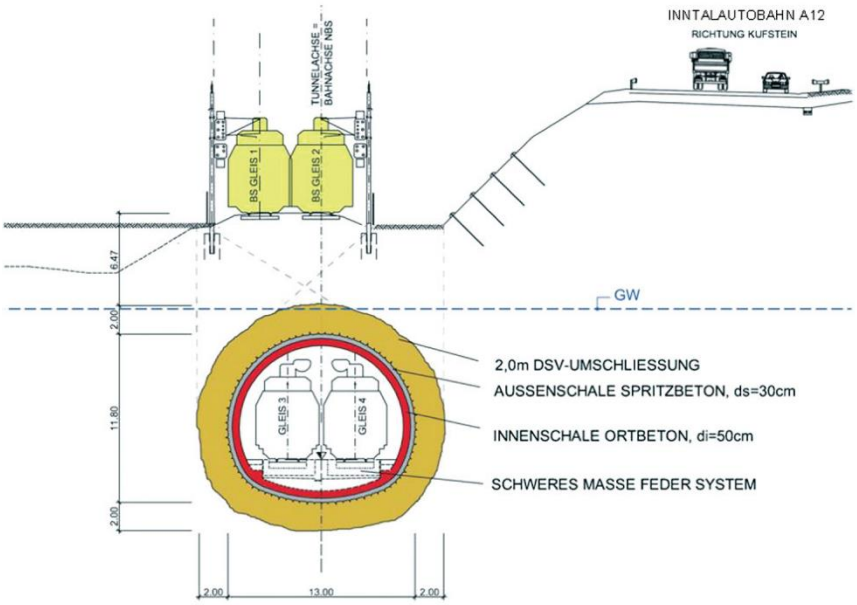

Figure 2.14: Jet grout surround at the section passing under the existing railway line (Palla and Leitner, 2009).

The contractor decided to choose a drilling pattern with overlapping of three columns with at least 10 cm. To manage this overlapping, primary, secondary, and tertiary columns were introduced as shown in Figure 2.15. The required leakage per compartment was to be 5 l/s and the minimum required compression strength set to 5 MPa, which was proven during preliminary trials. The column diameter was based on 1.9 m for vertical columns and the columns could be inclined up to 60° to deal with obstacles on the surface. Boreholes was drilled using uncased rotary drilling with mud flushing (Palla and Leitner, 2009).

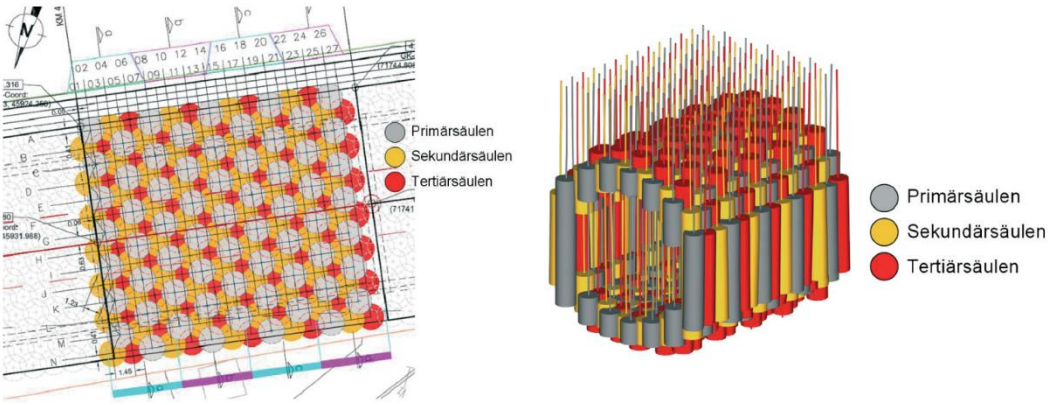

Figure 2.15: Layout and 3D-view of a typical compartment (Palla and Leitner, 2009).

A well-developed quality assurance system and standard documentation of jet grouting works was essential in the making of this successful project. Adaptive jet grouting works, in agreement between project parties, led to overcoming unusual events and observations (Palla and Leitner, 2009). In a TunnelTalk interview in 2008 with the BEG General Manager at the time, Dipl.-Ing. Johann Herdina confirmed the performance of the jet-grout ring. It was described as an expensive but highly effective solution (Wallis,

2008). The system applied in the Stans Tunnel is similar to the case study of this thesis and shows the potential of a vertical jet grout ring.

Untersammelsdorf tunnel is a 665m long double railway track with an excavation area of 133 m^2. It was set to be finished within 2020 as part of contract 60.3. This project met challenging subsoil, which mostly consisted of silty to fine sandy lacustrine deposits. In the bench, invert and below invert, some sections showed quaternary gravels and sands, glacial advance gravels, and moraine sediments. The tunnelling concept was to utilize pre-support of 2.5-3 m thick jet grouted arch with contiguous bored pile walls on both sides. Due to uncertainty of the joint strength between jet grout and the wall piles, a notch filled with primary lining was used in the wall piles to handle vertical load. Face stability was handled using dished shotcrete and jet grout columns that were placed with 2.03 m spacing in the longitudinal direction. In addition, temporary horizontal bracing was used during planning of bench and invert procedure (Höser *et al.*, 2018).

Höser *et al.* (2018) used a Monte-Carlo simulation to optimise grid patterns for the arch. Specified compressive strength for the jet grout arch was set to 3.35 MPa. However, investigations of the jet grout arch showed an average compressive strength of 7.34 MPa and a minimum of 4.81 MPa. Although up to 14 meters of defective areas due to insufficient column diameters where discovered, the structural integrity of the overall system was sufficient. The joint between jet grout body and bored piles had discontinuities but showed no measured displacement. For the notch filled with primary lining a fine shotcrete was used that after 24 hours had a strength of 23 MPa (Höser *et al.*, 2018).

The Brenner Base Tunnel has a section called *Eisackquerung*, from km 54.0-56.1. It was designed by ILF Consulting Engineers in 2008 and from 2011 to 2015. The design had to consider challenging ground conditions with groundwater and low overburden height. Two different design methods were made for the soil tunnel part. A small segment was designed with jet grouting established from the surface to form compartments, which is identical to the design showed in Figure 2.15. The rest of the soil tunnel was either cut and cover or a sub-horizontal jet grout arch with some vertical columns created from within the tunnel. The cross section was about 120m^2 and was divided into a heading, bench and an invert (ILF, 2018).

2.5.3 Summary from case studies

Norway has limited experience with soil tunnelling and assistance from foreign experience is often required to design the solutions. The current development of cities will likely lead to an increase in the demand for soil tunnelling experience. Cases presented in this chapter show that jet grout can be installed vertically ahead of the excavation and horizontally with the excavation. Key parameters for success seem to be the focus on a mixture between proper design, monitoring, feasibility and adaptability during excavation. Jet grout is suitable as an option in shallow soil and where groundwater lowering can impose surface settlements and instability. Adaptation to ensure waterproofing can be done, using for instance compressed air. The vertically installed jet grout ring as mentioned in Stans Tunnel and Brenner Base Tunnel is a relatively new concept. These cases show that the solution is feasible and gives promising results. Case studies covered shows that usage of jet grouting columns in granular and moraine soils could be a feasible solution.

2.6 Design methods for tunnelling

Designing the structural system of soil tunnelling is a complex and difficult procedure (Lunardi, 2008). Currently there are no European tunnel design standards or shared guidelines at European level. Athanasopoulo *et al.* (2019) deems it feasible to create such design standards, at least for typical configurations. As for now, current design is based on national knowledge, guidelines, experience with client/industrial standards and parts of Eurocodes (Athanasopoulo *et al.*, 2019). It is expected that a shared standard for design will be established.

2.6.1 Empirical and analytical methods

Prediction of displacements and stresses in tunnelling can be solved by either empirical-, analytical- or numerical analysis. Empirical approaches, such as by Peck (1969), are widely used. His approach was based on field observations and featured simple assumptions that neglected horizontal displacements or structural interactions. Galler *et al.* (2009) suggests that analytical and/or numerical analysis methods should be used to study failure modes and deformation. Several analytical approaches exists, such as the ones by Sagaseta (1987) and Bobet (2001). Bobet (2001) created an analytical approach that was based on an elastic model and could predict both structural interactions and horizontal displacements.

2.6.2 Closed-form solutions

Designing a tunnel lining using a closed solution based on continuum mechanics often considers the relative stiffness of the lining compared to the surrounding medium. Equations are used to simulate the impact of relative stiffness on bending moments. According to USACE (1997) the assumptions in this method are best matched if the lining is installed directly behind the excavation face. In general the loads are applied as vertical and horizontal stresses correlated by the in-situ earth pressure coefficient as seen by the example method in Figure 2.16 (USACE, 1997). These closed-form solutions are often not capable of modelling complex procedures such as pre-convergence, stress relief and an accurate representation of ground-lining interaction. According to Schutz (2010) these methods are simple, but have limitations on shallow overburdens in urban areas.

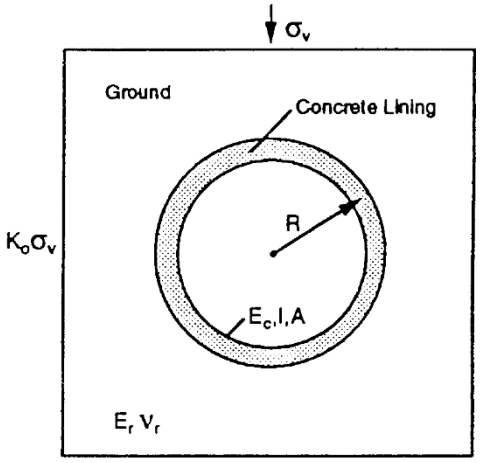

Figure 2.16: Lining in Elastic Ground, Continuum Model (USACE, 1997, p. 178)

2.6.3 Beam-spring models

Beam-spring models are commonly used in the design of tunnel linings. The method is also referred to as the hyperstatic reaction method, embedded frame, beam-spring method and 1D method *(Barpi, Barbero and Peila, 2011; Thomas, 2008; Hung et al., 2009)*. This method could feature the use of finite element computer programs with beam elements representing the lining. To simulate interaction between surrounding medium and the lining, tangential and radial springs are applied as elastic supports to the beam element nodes. In this way conditions of lining configurations, such as a full slip or no slip, can be simulated. A simple example of estimation of these springs, also called subgrade reaction modulus's, are shown for a segmental lining in equation 1 and 2. A segmental lining typically occurs with pre-cast concrete segments in TBM tunnelling (USACE, 1997). Simplified reaction modulus can be derived for non-segmental linings.

$$k_r = \frac{E_r * b * \theta}{(1 - v_r)} \tag{1}$$

and

$$k_t = \frac{k_r * G}{E_r} \tag{2}$$

where:

k_r = radial spring stiffness

k_t = tangential spring stiffness

G = the shear modulus

E_r = elastic modulus of rock properties

v_r = Poisson's ratio of the rock

θ = arc subtended by the beam element in radians

b = length of the tunnel element considered

Shallow soil tunnels are typically described with a cover-to-diameter ratio, C/D, less than 2 (Ngan Vu, Broere and Bosch, 2017). Most structural design models in literature focus on moderate to deep tunnels. Ngan Vu, Broere and Bosch (2017) stated that these models do not adequately describe the actions in shallow tunnels due to disregard of buoyancy. Duddeck and Erdmann (1985) published analytical solutions based on continuum- and a beam-spring model, that have been widely used in the industry. Duddeck (1988) proposed these models as suitable to calculate internal forces in shallow tunnels in soft soils. The models assumed plane strain conditions, active soil pressure equal to initial stresses in the ground, ground reverting to conditions prior to excavation and ground-lining interaction limited to radial and tangential springs with elastic materials (Duddeck and Erdmann, 1985).

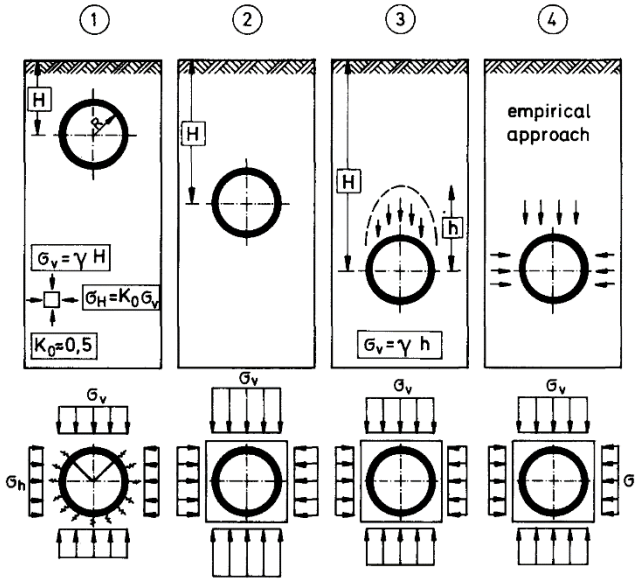

Figure 2.17: Plane-strain design models from ITA Working Groups 1988 (Duddeck, 1988).

Duddeck (1988) presented this design approach, where case 1 in Figure 2.17 is the representative model for shallow overburdens. Ngan Vu, Broere and Bosch (2017) presented an updated method following Duddeck and Erdmann. Duddeck and Erdmann used uniform loads of the overburden pressure for upper and lower parts of the tunnel and a uniform horizontal load using coefficient of horizontal effective stresses. The springs are also applied with equal value for the entire lining (Duddeck and Erdmann, 1985). The coefficient of horizontal stresses is by some guidelines assumed to be significantly reduced after a SCL construction (Marcher, John and Ristic, 2011).

As seen in Figure 2.18, the updated method applied non-uniform loads around the tunnel to account for pressure variations with depths, circular geometry and buoyancy. With this new method the springs around the tunnel are recalculated for each frame element, to further refine the beam-spring model (Ngan Vu, Broere and Bosch, 2017).

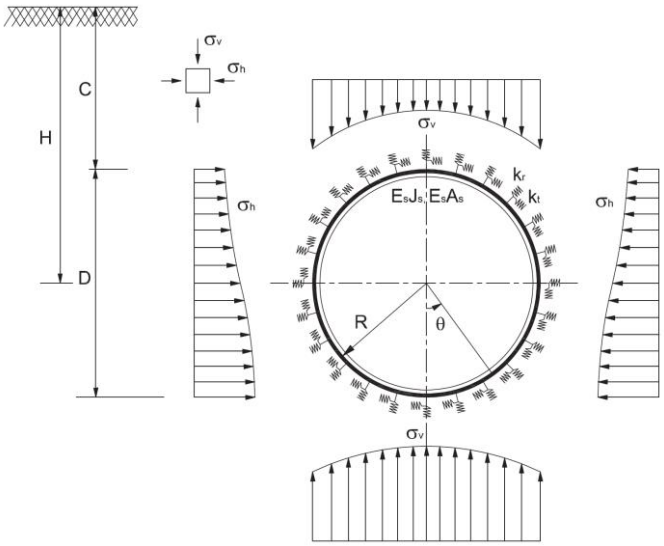

Figure 2.18: Soil pressure on the tunnel linings by updated method (Ngan Vu, Broere and Bosch, 2017).

Alun Thomas stated that beam-spring models used to simulate tunnel junctions was not suitable due to the model not being capable of a realistic stress redistribution (Thomas, 2008). The British Tunnelling Society design guide states that the beam-spring models "tend to underestimate the beneficial effects of soil-structure interaction". In addition, shear stresses acting in the ground are generally not considered (BTS, 2004). Due to limitations in describing the ground structure interaction it is advised to limit the use of this method where a support arch is important. The beam-spring models are therefore often used for modelling the final lining, applying the loads imposed on the temporary lining (Hung *et al.*, 2009).

2.6.4 Continuous finite element model

The continuous finite element model accounts for situations where finite element models have both ground and structural elements. Continuous finite element models are either two or three-dimensional models. For line structures in general, the two-dimensional model is commonly accepted. For three-dimensional stress states, such as pre-supports or intersections, three-dimensional models are recommended. Continuous finite element models can consider both ground-structure interaction and excavation sequence. Use of a two-dimensional continuous finite element model makes it possible to verify both initial support elements and the final lining (Hung *et al.*, 2009).

Hung *et al.* (2009) suggests with their guidelines that for designing sequential excavation and support systems, numerical finite methods should be used as these allow for direct ground-structure interaction. Marcher, John and Ristic (2011) suggests use of continuous finite element models to extract forces acting on the primary lining and design the final lining with a beam-spring model.

2.6.5 Degradation of temporary support

In tunnelling, the project criteria and/or aggressive groundwater could limit the initial support structures to only have short-term structural contribution (Hung *et al.*, 2009; BaneNOR, 2019). Some articles in literature describe the procedure of using a continuous finite element model to simulate a degradation process (Thomas, 2008; Usman and Galler, 2013; Ziller and Cont, 2018; Trunda and Hilar, 2020; Marcher, John and Ristic, 2011; Usman *et al.*, 2011). Thomas (2008) mentions "grey rock" procedures based on a presentation by M. John, Prague 2006. Here either 50% degradation or full degradation of lining is assumed for long-term design, with use of stiffness- and strength reduction.

Marcher, John and Ristic (2011) thoroughly presented the load-sharing effects in SCL tunnels in their article. A transition from an elastic- to elastoplastic model to simulate the degradation of the primary lining is suggested. The article states that the uneven force distribution in the primary lining due to staggered excavation, will be distributed more evenly when transferred to the secondary lining. The load distributed to the secondary lining should be dependent on the ratio of stiffness between ground and lining. In a "fully tanked" system the loads are distributed over the entire cross-section (Marcher, John and Ristic, 2011).

Usman and Galler (2013) reviewed long-term deterioration of linings with a numerical approach. Their approach featured linings with volume elements in a three-dimensional finite element program. Degradation was attempted through decreasing stiffness and strength by 10% each step. Results from this study showed a load transfer from primary

lining to secondary lining. Young's modulus was deemed a capable deterioration factor but showed slower rate of stress transfer than with a reduction of strength parameters. Deterioration with Young's modulus did, however, produce an earlier load transfer. Some stress was assumed transferred to the ground following the degradation (Usman and Galler, 2013).

Ziller and Cont (2018) suggested an approach named the damaged primary lining approach. The article compared a traditional approach, which features full load transfer between linings to the new approach. The traditional approach featured the deactivation of the primary lining modelled as a plate simultaneously with activation of the secondary lining as a volume element. The proposed damaged primary lining method applies volume elements for both linings and featured a decrease of compressive strength, cohesion and Young's modulus. The authors stated that this method was not more conservative, but rather more realistic than previous approaches. The study was performed on rock tunnelling (Ziller and Cont, 2018).

In the Crossrail tunnels in UK, many new improvements in SCL methodology were used. The project used permanent sprayed concrete, fibre reinforced concrete and spray-applied waterproofing membranes. It featured a permanent primary lining, where 75 mm of the sprayed concrete was considered sacrificial in long term design (Thomas, 2021). The design method of a sacrificial layer can be performed with increasing the layers thickness to withstand aggressive chemicals (BTS, 2004; Hung *et al.*, 2009).

2.6.6 Summary on design methods

There are currently no European standards for tunnel design, but a standardization has been requested. Empirical methods are still used, but analytical and numerical methods should be used for complex situations. The industry uses many different methods, with the beam-spring model and continuous finite element model being prominent. The beam-spring model in a finite element model is commonly applied for final lining design. With this model it is important to use realistic modelling parameters with estimated subgrade reaction modules. Continuous finite element models are also frequently used, capable of describing the full procedure and verifying the structures. Literature research have also shown that the beam-spring- and continuous FE model can be combined.

From literature it can be assumed that to study relaxation on the secondary lining, a continuous FE model is most feasible. In a continuous finite element model, it is possible to model the degradation of temporary supports to find the loads acting on the permanent structure. With this it is also possible to study the transfer of stresses to the ground for an additional arching effect. As mentioned in literature, the stress transfer should depend on relative stiffness of the ground and lining.

2.7 Numerical analysis of tunneling

Numerical analysis is capable of modelling complex situations, different soil behaviours and construction stage considerations. It also features the option to perform parameter studies, to investigate key parameters of the analysis. Limitations are supposedly based on the software- and engineering understanding of the engineer (Yahya and Abdullah, 2014). Lunardi (2008) mentions that the finite element method is indispensable for construction of very shallow overburdens or for interaction with structures.

2.7.1 Two- versus three-dimensional modelling

Swoboda (1979) showed that two-dimensional models could sufficiently determine the construction procedure, material properties and support systems in tunnelling. However, it was suggested that three-dimensional models are needed to realistically account for time dependency due to the driving face (Swoboda, 1979). Erdmann (1983) studied three-dimensional theory in plane strain models and showed that relative displacements for the tunnel crown were only 40% compared to the three-dimensional model. Analysis showed that in an unrealistic case of full transfer of primary stress, the lining would only take 55% of the stress (Erdmann, 1983). Duddeck (1988) found that for shallow tunnels in soft ground, almost 100% of the primary stress could be acting on the lining.

Kielbassa and Duddeck (1991) stated that the plane strain design model is an upper-limit model regarding stresses in the lining. Vlachopoulos and Diederichs (2014) referred to this approach as straight excavation, also stating that the method does not account for stress redistribution and deformations ahead of the excavation face. Kielbassa and Duddeck's work on stress-strain fields lead to an approach of stress release, accounting for the unsupported excavation prior to lining installation in two-dimensional analysis. The model can be seen in Figure 2.19, where the stress release is based on splitting factors derived from diagrams (Kielbassa and Duddeck, 1991).

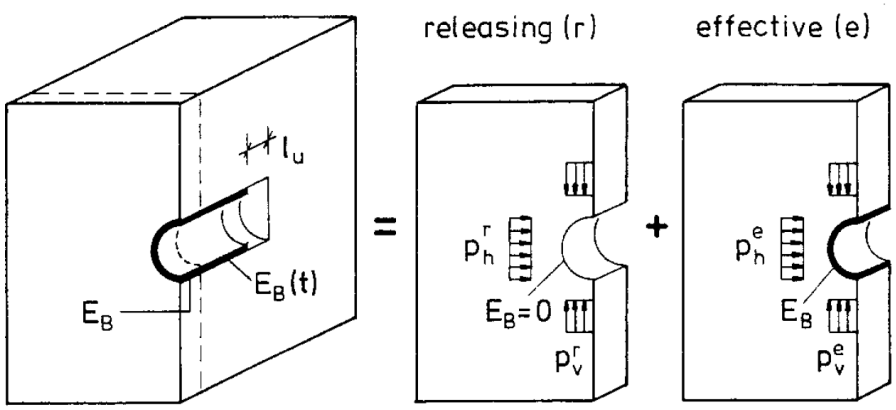

Figure 2.19: Model in 2D for covering 3D effects from Kielbassa and Duddeck (1991).

Other methods to account for the driving face and three-dimensional effects in 2D-models exist in literature, such as the convergence-confinement method (Panet *et al.*, 2001). Vlachopoulos and Diederichs (2014) have suggested practical approaches and recommendations to this approach using longitudinal displacement profiles suitable in combination with ground- and support reaction curves. Several practical solutions exist to predict the displacements prior to support installation. They stated that limitations due

to the methods being based on circular tunnel in isotropic medium must be considered. Thus, for tunnel analyses with staggered excavation, sequenced support and non-isotropic stresses they recommend using three-dimensional analyses beyond preliminary design phase (Vlachopoulos and Diederichs, 2014; Vlachopoulos and Diederichs, 2009; Oke, Vlachopoulos and Diederichs, 2018).

Galli, Grimaldi and Leonardi (2004) used a 3D model to simulate the procedure of tunnel excavation and lining. The article concluded that 3D models could automatically simulate the real construction procedure, while 2D modelling was dependent on relaxation to simulate lining and soil interaction. Thomas (2008) states that due to arching in the ground, the tunnel lining is most likely not experiencing the original in situ stress state.

2.7.2 Numerical analysis of tunnels with jet grout supports

Available literature on numerical modelling of tunnels with jet grouting is limited and most of the literature exists on the horizontal jet grouted canopies (Pichler *et al.*, 2004; Coulter and Martin, 2006; Barla and Bzowka, 2013; Ochmański, Modoni and Bzówka, 2015). The literature covered in this review consider construction, modelling and parameter selection of jet grouted material.

Pichler *et al.* (2004) attempted optimization of jet grout support in NATM tunnelling. The construction technique studied consisted of 37 horizontal jet grouted columns in an arch. A time dependent hydration process of the jet-grouting installation was modelled, and comparison of the support with and without jet grout support. The jet grout supported tunnel was modelled with full face excavation and simple sprayed concrete lining with staggered excavation. Results show that settlements of the jet grouting procedure were depended on the horizontal length of each jet grout screen. A reduction in the number of jet grout columns could result in larger settlements than with solely sprayed lining configuration. The study did not evaluate groundwater or thermal properties (Pichler *et al.*, 2004).

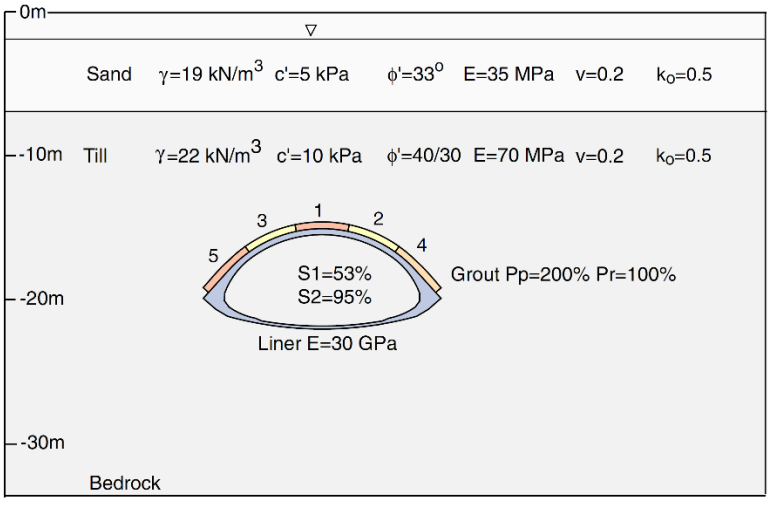

Figure 2.20: Finite element model used by Coulter and Martin (2006).

Coulter and Martin (2006) performed a FEM numerical back-calculation analysis, the modelling procedure shown in Figure 2.20, using FEM-program Phase2 with correspondence to the measured settlements. To account for 3D-effects a stiffness reduction method was applied. The stiffness reduction method consists of lowering the

elastic modulus of the soil prior to the approaching tunnel excavation. This enables cavity convergence in the two-dimensional model prior to excavation (Coulter and Martin, 2006).

Modelling of the jet grout was done using 5 sets with different installation times. The analysis suggested that the settlements occurred due to high jet-grouting pressure and the associated soil yielding with a strain-weakening model. The reason for this was that jet-grout pressure exceeded the overburden pressure and formed narrow shear bands allowing a soil block above the tunnel centreline to move down. Due to finite element mesh possibly producing some falsely produced shear bands, several meshes were investigated (Coulter and Martin, 2006).

Barla and Bzowka (2013) performed a comparison of different numerical alternatives to model jet grouting in tunnels. The paper used the Aeschertunnel as a well described model. The goal of this comparison was to compare different approaches to numerical analysis of jet grouting. All material models except tunnel lining were simulated according to the Mohr-Coulomb model. The tunnel lining was assumed under elastic behaviour. A stress release was assumed prior to excavation (Barla and Bzowka, 2013).

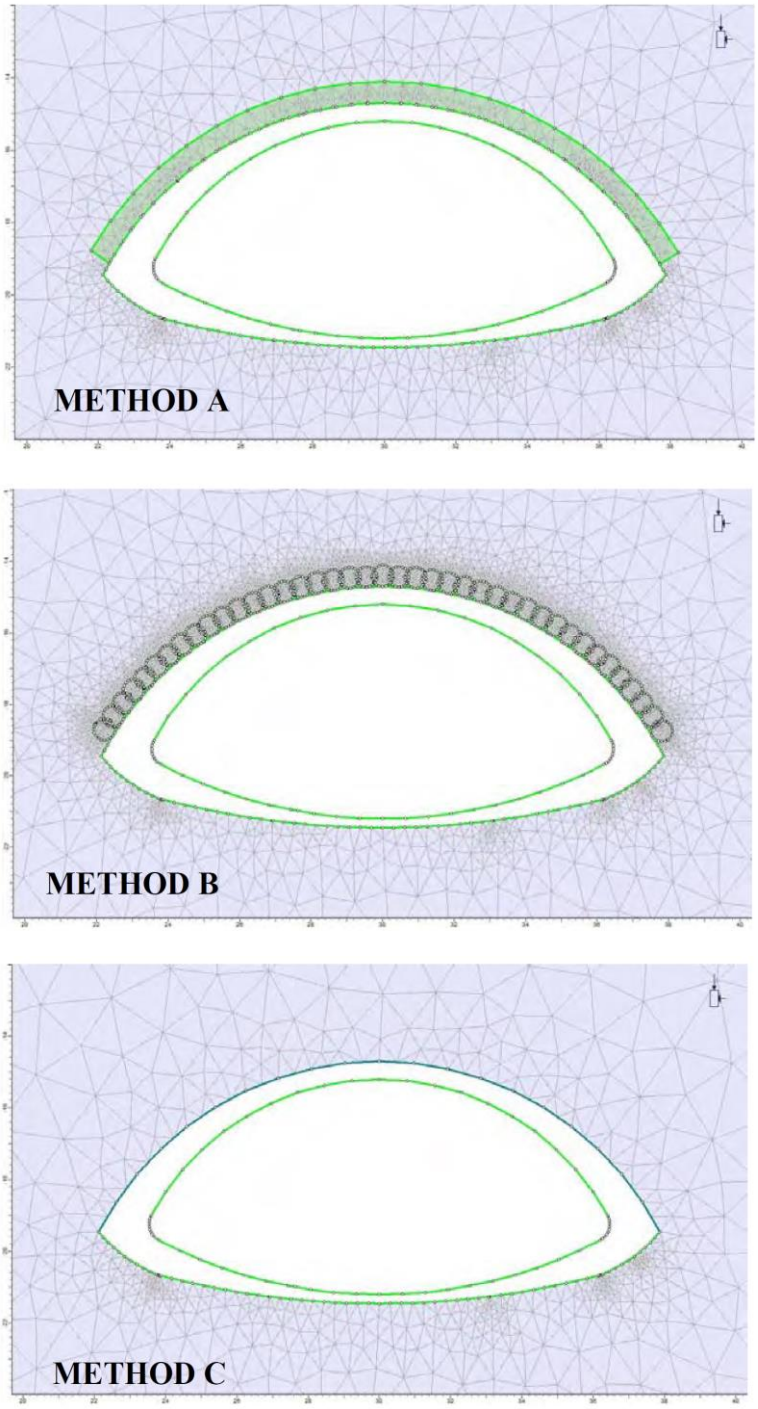

Figure 2.21: Numerical alternatives to model jet grouting from Barla and Bzowka (2013).

Three different methods of modelling the jet grout arch were assessed as shown in Figure 2.21. Method A consisted of a continuous soil arch, Method B of individual jet grout columns and Method C with a beam. In method A and B, a full bonding, implying no sliding and full stress transfer, between moraine and reinforced soil was assumed. Barla and Bzowka (2013) states that the difference in settlements between the methods are small. Therefore, the study recommends choosing the model based on computational time and easiness (Barla and Bzowka, 2013). A similar conclusion was reached by Ochmański, Modoni and Bzówka (2015), stating that the hardening of jet grout is relatively fast and that the jet grout canopy acted as a whole.

Numerical analysis performed by ILF on the Untersammelsdorf tunnel, previously mentioned, showed that almost the entire ground load could be taken by the jet-grout arch (Höser *et al.*, 2018). Ochmański, Modoni and Bzówka (2015) did an extensive study on numerical analysis of tunnelling with jet grouted canopy. Both 2D- and 3D calculations were performed with several different soil models. The analysis includes cement hydration of both jet grouting, sprayed concrete- and concrete lining. Results showed how 3D calculations and accurate soil non-linearity behaviour are less important for extracting internal forces (Ochmański, Modoni and Bzówka, 2015).

Displacements due to the jet grouting process is a realistic problem considering drilling and high grouting pressure, and particularly in clayey soils (Pinto *et al.*, 2013). Literature reviewed focuses mostly on lateral displacements. Wong and Poh (2000) stated that vertical displacements are often lower in comparison to lateral displacements with vertical jet grouting. Most relevant literature for jet grouting pressure modelling is based on the cavity expansion theory (Chadwick, 1959; Vesić, 1972). An analytical solution to this process in cohesive frictional soil was suggested by Carter, Booker and Yeung (1986). In terms of numerically simulating the ground displacement due to the jetting process, several engineers have implemented volumetric strain as a key modulator (Carter, Miura and Zhu, 2009; Pinto *et al.*, 2013; Wang, Bian and Wang, 2017).

A numerical approach to simulate ground displacements by jet grouting using finite element program Plaxis was performed by Wang, Bian and Wang (2017). It was based on horizontal jet grout columns. The approach features determining an influence radius of injection pressure, volumetric expansion strain of fluid injection and running a numerical simulation. Results indicate that Mohr Coulomb and a Hardening Soil model can provide a suitable ground response in horizontal jet grouting activity. The article concluded that proper spoil control can mitigate disturbances to the surroundings during jetting (Wang, Bian and Wang, 2017).

Modelling and verification of jet grouting as structural support

Realistic modelling of jet grout columns can be a problem. It is hard to predict exact shape and strength parameters of in-situ jet grouted columns. In the execution standard for jet grouting, two methods are proposed to find the material strength. For 4 to 9 test samples the characteristic unconfined cylindrical strength should be based on the minimum value. With more than 9 samples tested, a statistical approach to determine the material strength can be applied. Design values are derived through application of design factors such as from the concrete standards (CEN, 2019)

When using numerical analysis in design, it is important to understand if the structure is limited to provisional use or capable of permanent structural abilities. The design capabilities are often described in design criteria by the client. The common belief that jet grouting parameters cannot be correctly determined has led to a more empirical approach to find parameters. Croce, Flora and Modoni (2014) stated that use of jet grouting for support and waterproofing in tunnel design is commonly considered provisional. For applications such as foundations or retaining structures, a jet grout structure is commonly considered permanent. The authors also suggest that the limited confidence on the effectiveness of jet grouting could be the reason for provisional design (Croce, Flora and Modoni, 2014).

Discontinuities in jet grouting is a major concern in construction. 2D analyses of curved jet grouted structures have shown that discontinuities could lead to a local failure. According to Croce, Flora and Modoni (2014) the local failures observed are conservative since three-dimensional structures like jet grout canopies can carry loads even if they are non-continuous. A simplified three-dimensional analysis by Flora *et al.* (2012) showed that discontinuities don't necessarily cause structural failure. Exceptions to this is large discontinuities, up to 1 metre, and low strength values. It was concluded that two-dimensional analysis holds an extra safety factor in comparison to three-dimensional analysis (Flora *et al.*, 2012).

As previously mentioned, the structural integrity and homogeneity of jet grouting columns can be hard to verify. The construction quality and close monitoring is essential to achieve the required performance. Several methods exist to perform verifications on the structure. Instrumented drilling is a technique used to record rotation, advancement, thrust, torque and fluid pressure during perforation. This is applicable to most drilling processes to receive qualitative information. Dynamic tests represent another way to verify the structure. Wave propagation velocity measured by an oscilloscope can indicate the homogeneity through stiffness estimates, but special care is needed in saturated ground. Sonic logging measures the compressive wave velocity and give clear indications of heterogeneity of the ground. Creating a tomography of compression or shear wave velocity from cross-holes is regarded as the most effective and complete view of the jet grouting effects. However, this method can be time consuming and expensive. Standard tests exist for both downhole and crosshole seismic testing (Croce, Flora and Modoni, 2014).

Cordon (1962) established that soil-cement mixes are generally exposed in the same manner as concrete to sulphate attack. Shihata and Baghdadi (2001) investigated long-term strength and durability of soil-cement. This study showed when subjected to saline water, a peak strength occurs after 90 days and a residual strength after 270 days. The authors indicated that after reaching the residual strength, negligible impacts on durability is assumed. Hasan and Canakci (2022) studied durability of jet grouted columns in clayey soil with particular focus on degradation due to seawater and magnesium sulphate. It was concluded that the improved ground was most affected by magnesium sulphate attacks, which have an impact on mass change and strength properties. This study did not involve long-term deterioration of the material (Hasan and Canakci, 2022).

2.7.3 Summary on numerical analysis

Reviewed literature has shown that two-dimensional models can be used to simulate the three-dimensional behaviour of the driving face, although the procedure is difficult. It is important to consider the 3D effects in the model to avoid unrealistic internal forces. Literature states that the plane strain model without stress release simulates upper-limit stresses induced on the lining systems. This would be unrealistic due to the pre-convergence of the tunnel. In order to find the proper stress-release a simplified three-dimensional model can be studied, experience-based assumptions can be used, or the release is found by models from literature.

Literature with numerical modelling of jet grout canopies have proven that the assumption of a continuous volume element for the jet grout column scheme can give adequate results. In addition, discontinuities due to the installation process, does not necessarily lead to a local failure due to three-dimensional effects. Simulating displacements due to the jetting process have been attempted using volumetric strain as a key modulator. In design of tunnels, jet grout is commonly considered a temporary support. Reasons for this assumption are the difficulty of verifying strength parameters and concerns regarding the integrity of the structure in short- and long-term situations. Additional information on how the jet grout structure could contribute in long-term for a soil tunnel should be established, since technology for verification of structural capabilities are presents.

2.8 Review summary

Based on the recent urban development, more underground works are expected to be constructed in the future. To build safely and meet environmental sustainability goals, it is important to gain more experience in design and construction of soil tunnels. Choosing a feasible solution to different ground conditions is important for a successful process. Increased experience on construction of soil tunnels and design will be valuable for Norway in the years to come, especially since expertise is often hired from other European countries.

Common soil tunnel designs today consider both the primary sprayed lining and jet grouting supports as provisional. Literature states that sprayed concrete may be designed for a longer life span with application of newer technology such as fibre-reinforced shotcrete. Sprayed concrete with steel reinforcement such as lattice girders and wire mesh are prone to corrosion. To account for long-term degradation, techniques of modelling a degradation of sprayed concrete in numerical models provides an alternative design method.

In the future, design standards at European level could be established, and potentially contribute to further improvement of design. A standardization could improve the engineer's design confidence, and then possible lead to more environmentally friendly underground works. Improvements in technologies such as spray-on membranes, as opposed to frictionless membranes, can lead to new design practices for tunnel linings. Therefore, it is important to evaluate the current design practice and investigate future design possibilities.

There are several approaches to investigate and design soil tunnels, and the engineer is responsible for choosing a suitable method. Experience suggests that use of two- or three-dimensional numerical analysis should be decided based on the goal of the analysis. Plane strain models without stress release yields upper limit lining forces that is generally unrealistic due to relaxation of the driving face. To simulate three-dimensional effects in plane strain models, a stress release approach may be applied. Beam-spring models may provide efficient final lining design but could induce higher forces due to not sufficiently considering the beneficial arching effect. This arching effect can be automatically accounted for with a continuous finite element model.

Ground improvement with jet grouting, even though being a relatively new technology, have shown good capabilities in underground works. Appropriate modelling of both jet grout support and lining configurations is difficult and must be evaluated carefully. Literature proposes some degradation of soil-cement ground without reinforcement, but shows that a residual strength occurs relatively fast. In the future, new tunnelling materials, knowledge and construction improvements can lead to reduced environmental impact and contribute to more economical construction.

Modelling of jet grout degradation was not found in literature. It seems that structural uncertainties are the main factor for not including jet grouting in the long-term design of the structure. With growing experience, confidence and better monitoring techniques, more permanent considerations could be feasible. For this reason, it is relevant to investigate the internal forces in the secondary lining due to partial contribution from jet grout supports.

3 Theory

This theory chapter elaborates briefly on the theoretical methods or phenomena relevant for the analyses.

3.1 The Finite Element Method

The finite element method (FEM) is well-known method in numerical analysis. Complex interaction and behaviour can be simulated, which would otherwise be difficult to understand. Zienkiewicz, Taylor and Zhu (2005) explains this method in detail in their book. The finite element method consists of discretization a model into a finite number of elements. Continuous problems can be solved with the means of mathematical differential equations. The method is an approximation, that with enough iterations and elements hopefully converges on a true continuum solution (Zienkiewicz, Taylor and Zhu, 2005).

The elements that have been discretized can vary in shape and form. Generally, triangular or rectangular shaped elements built up by nodes with defined degrees of freedom are connected with nodes of neighbouring elements. Each node is generalized with forces and displacements that reacts with external loads. Forces and displacements are collected in matrices and material properties of the elements used are collected in material stiffness matrices. Equilibrium and compatibility requirements need to be fulfilled in order for a complete solution (Zienkiewicz, Taylor and Zhu, 2005).

3.2 Plaxis Geotechnical Software

Plaxis 2D and 3D are finite element programs for geotechnical engineering that can be used to perform deformation-, stability- and flow analysis. Plaxis 2D can model with plane strain or axisymmetric models. Depending on the purpose the uses can operate with either 6-noded triangle elements or 15-noded triangle soil elements shown in Figure 3.1. The 15-noded triangle elements are default and provide the most accurate stress result. Fourth order interpolation and twelve Gauss points provides compatibility and high quality. Today's computer capacity would normally not have problems running these 15-noded elements, but 6-noded triangle elements may be used to reduce computational effort. Use of 6-noded triangle elements would need to be justified in terms of correct results. In addition to finite elements, structural plate-, geogrid- and interface elements are used. Plates are modelled by the Mindlin beam theory, so that bending and shear deformation are accounted for (Bentley, 2021a).

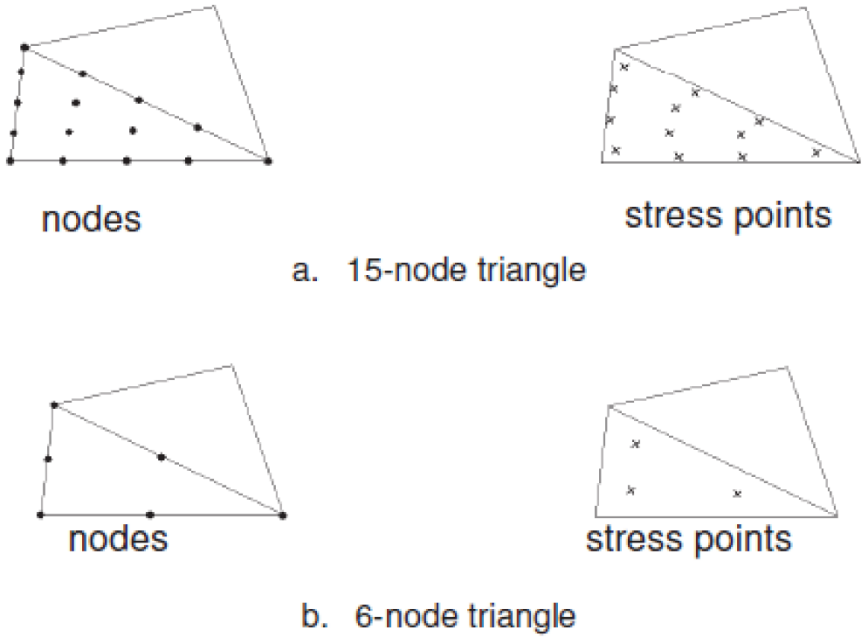

Figure 3.1: Finite elements in Plaxis 2D (Bentley, 2021c).

In Plaxis 3D the basic soil element is a 10-noded tetrahedral element. Beams are simulated with 3-node line elements, plates and geogrids by 6-noded elements and soil-structure interaction with 12-node interface elements. The interface elements in both 2- and 3D replace single nodes with a nodal pair, at exact same location (Bentley, 2021a).

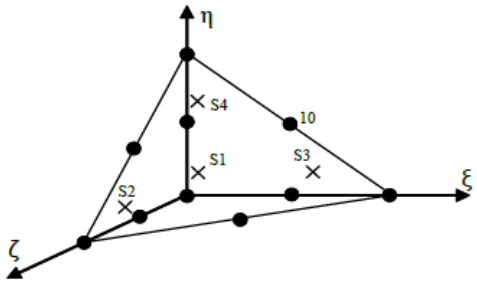

Figure 3.2: 10-noded tetrahedral element in Plaxis 3D (Bentley, 2021a).

3.3 Convergence-confinement method

The Convergence-confinement method (CCM) is an approach in tunnelling which enables plane strain simulations to account for three-dimensional effects and deformations due to an unsupported tunnel face (Bentley, 2021c). Convergence-confinement method, also named β-method or characteristic curve method, is based on analytical and empirical formulations to create relevant design approaches in plane strain conditions (Schikora and Fink, 1982; Panet *et al.*, 2001; Panet and Sulem, 2022). However, a preliminary three-dimensional analysis can be used to find the displacement prior to lining installation (Panet and Sulem, 2022).

Three different curves called the Longitudinal Displacement profile (LDP), the Ground Reaction Curve (GRC) and the Support Confinement Curve (SCC) are used to determine the deconfinement ratio. Panet *et al.* (2001) defined the reduction from a three-dimensional problem to a plane strain problem by equation 3. In the equation, λ is the coefficient for deconfinement ratio, varying from 0 to 1 depending on the face advance, σ is the radial stress on the tunnel wall and σ_0 is the natural stress in the ground (Panet *et al.*, 2001).

$$\sigma = (1 - \lambda)\sigma_0 \tag{3}$$

The coefficient is derived from the LDP curve, which is a function of radial displacement at the tunnel wall in relation to support distance from the excavation face. The GRC shows the ground reaction due to excavation without lining support action. The SCC characterizes the confinement due to installation of a support at a distance from the excavation face (Panet and Sulem, 2022).

3.4 Hypothetical Modulus of Elasticity

The theory of using a hypothetical modulus of elasticity (HME) to model sprayed concrete was first established by Pöttler (1985). Viewing the sprayed concrete as pseudo-elastic, he showed that using a gradient of the stress-strain curve could be regarded as a hypothetical modulus of elasticity. HME consists of reducing the modulus of elasticity to account for the hardening, time-dependent history, load and creep of sprayed concrete. Through parametric trials he showed that a short-term elastic modulus of 7 GPa induced the highest stresses in the lining. Pöttler (1990) also indicates that the HME can be used for long-term behaviour in a similar manner. Thomas (2008) explains that the choice of HME is empirical and can be combined with the relaxation of ground stresses. The method applied in numerical modelling will result in lower stresses acting in the lining, compared to using an immediate full stiffness (Thomas, 2008).

3.5 Composite behaviour

The principle of composite behaviour of linings is described by Bloodworth and Su (2018). Composite behaviour will occur when the surface between structural members has sufficient shear capacity and friction to take the transverse shear from bending or shearing. The theory is well established in terms of how laminated timber beams and steel/concrete composite beams work. The transverse shear occurring between the beams will either cause a slip/gap behaviour or induce a composite behaviour allowing the structural members to share the stresses as shown in Figure 3.3. With a shared stress situation, the beams act together.

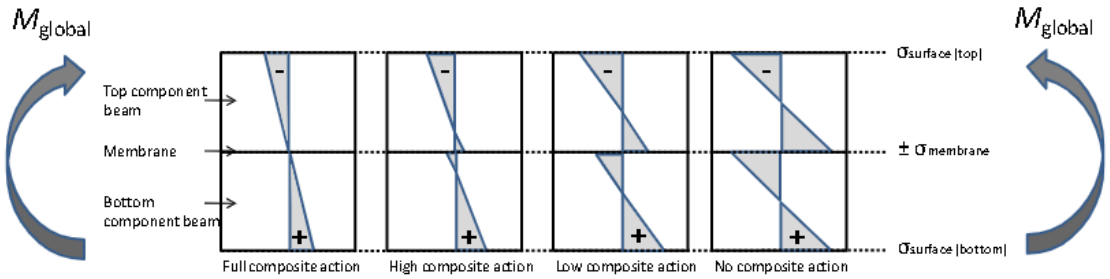

Figure 3.3: Illustration of composite behaviour by Bloodworth and Su (2018).

4 Case study - UDK02

This chapter will provide information about the case study, construction procedure, geotechnical investigations, constructional design, geotechnical - and constructional parameters involved in this case study.

4.1 Project information

Project *UDK02 Concrete tunnel and soil tunnel* is the second contract of the Drammen-Kobbervikdalen railway project in Drammen, Norway. Location of the project is shown in Figure 4.1. It is an EPC- (Engineering, procurement and construction) contract as a part of the Intercity railway-line and was awarded to Veidekke Entreprenør by Bane NOR. UDK02 consists of creating a 540m concrete tunnel and a 290m soil tunnel. The railway line is dimensioned for speeds reaching 200 km/h (Backer and Hæstad, 2020).

Figure 4.1: Location of UDK02 extracted from Kartverket (2022).

Figure 4.2: Project overview of soil tunnel extracted from BaneNOR (2022).

To identify the best solutions and provide the best service to Bane NOR, a competitive dialogue was used to find a suitable tender. This involves prequalifying tenders to a dialogue phase. Here the involved parties can discuss technical solutions, timelines, economy, and organization of work. Dialogue phase leads to a tender procedure that awards the contract based on a competitive basis. The chosen solution for the soil tunnel was to use jet grouting to keep the cavity free from water and stabilize the ground during excavation procedure (Backer and Hæstad, 2020).

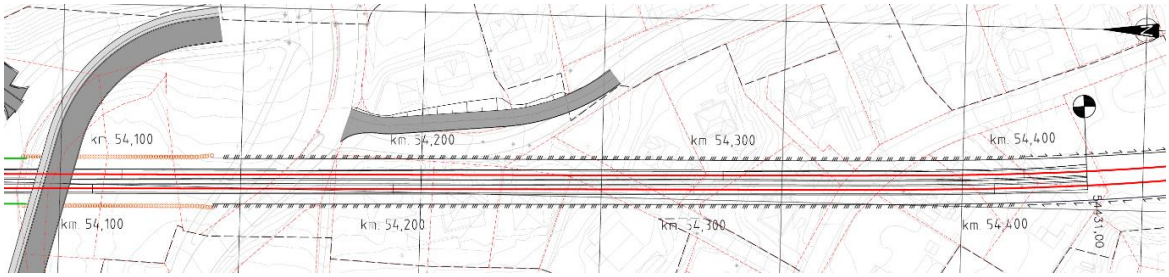

Figure 4.3: Plan overview for soil tunnel alignment from (NIRAS, 2020)

The soil tunnel stretches from profile km. 54,140-54,431 approx. as shown in Figure 4.3. Excavation of the soil tunnel is executed simultaneously with this study.

4.2 Geology

Geological soil conditions of the area consist of a deposition of glaciofluvial sediments. Experience suggest that these sediments consist of sand, gravel and some boulders with variable size. Along the tunnel alignment the surface increases by approx. 25 meters. The deposit generally thickens with increasing surface altitude. The sediment thickness above the rock tunnel interface is approximately 20-25 meters. The rock surface increases with the hillside, with some variations (NGI, 2020).

4.3 Technical design basis

The technical design basis states that the tunnel should be designed for a lifespan of 100 years and for speeds up to 250 km/h. Where higher costs are calculated, 200 km/h is the dimensioned speed. In addition, the permanent support is to be dimensioned to withstand all loads from earth- and water pressure, temperature and fire. Ground improvement and sprayed concrete lining is considered temporary in design. Potential use of spray-on watertight membranes must be designed to withstand freeze-thaw processes. According to agreement in dialogue phase the tunnel was to be excavated dry without influencing the ground water level for the area (Backer and Hæstad, 2020; BaneNOR, 2019).

4.4 Tunnelling method and design

ILF Consulting Engineers have designed the temporary - and permanent support for the soil tunnel (ILF, 2020a; 2020f). Designs are based on geological information by NGI (2020). The construction concept for the tunnel is to excavate using the sequential excavation method and support with a double-shell tube, or commonly known as double shell lining configuration. Due to restrictions in groundwater interference, a jet grout structure is established around the cavity from surface level, prior to excavation, to reduce inflow of groundwater and allow excavation in the cohesionless soil (ILF, 2020a; 2020f; 2020d).

The jet grout structure consists of either a full jet grout- block, ring or arch in the mixed face excavation with bedrock. Face stability is ensured by jet grout columns in the excavation and 50 mm sprayed concrete for face support. The jet grout rings consist of 12 compartments in longitudinal direction, separated by jet grout walls, which are to be drained by drilled wells prior to excavation. In addition to a compartment division, the

longitudinal profile is also divided into 25 different 12-meter blocks with pre-determined reinforcement properties for the sprayed lining as seen in Figure 4.7. After the temporary lining installation is completed and deformation is controlled, a sheet waterproofing membrane is applied. Finally, the secondary lining is installed as in-situ permanent concrete lining (ILF, 2020a; 2020f).

4.4.1 Excavation sequence

Temporary support schemes vary across the trajectory of the tunnel. Excavation sequence consist of excavating the top heading to the rock tunnel transition. After the full completion of the top heading, the bench will be driven with the invert either excavated 20 meters behind or linked with a deformation ratio. Depending on the support class of the section, the unsupported excavation lengths vary slightly. Generally, the unsupported lengths are short according to methodology of NATM (ILF, 2020c; 2020e).

4.4.2 Geometrical definition of tunnel section

The geometric tunnel profile is separated into three different sections. Geometric cross-section 1, hereby referred to as GCS1, is used generally in the soil tunnel. GCS3 is used in the transition from cut & cover to soil tunnel, which relates to the first 10 meters of the soil tunnel. GCS2 refers to the transition from soil tunnel to the rock tunnel. GCS1 is relevant for the case study and is shown in Figure 4.4.

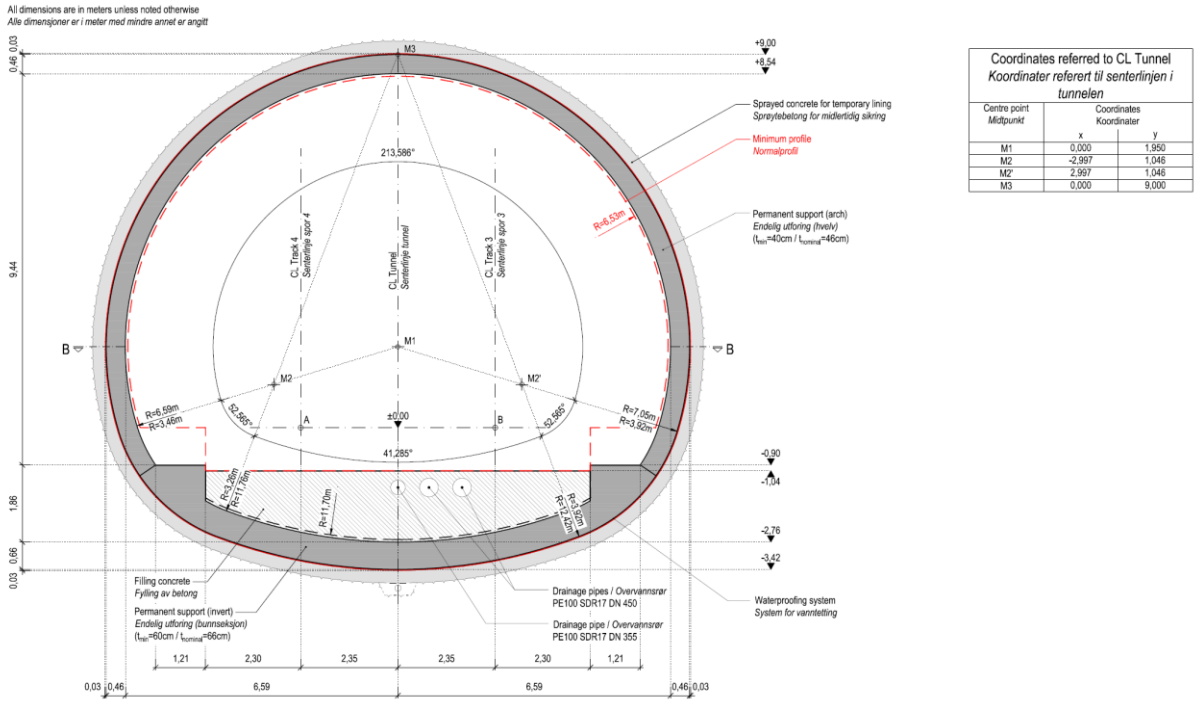

Figure 4.4: Geometrical definition of GCS1 from ILF (2021a).

4.4.3 Temporary support design

The temporary support consists of a jet grout block/ring/arch and a temporary sprayed concrete lining with reinforcement. Jet grouting thickness differs slightly from the initial starting block to the transition to rock tunnel. Generally, the jet grout ring has a thickness of 2.5 to 2 meters. From compartment 8 to the rock tunnel, the face excavation is a mix of rock and soil tunnelling as shown in Figure 4.5 (ILF, 2020a). The design procedure uses the method of a hypothetical modulus of elasticity and cavity relaxation of the elastic modulus to account for three-dimensional effects (ILF, 2020a; Kielbassa and Duddeck, 1991).

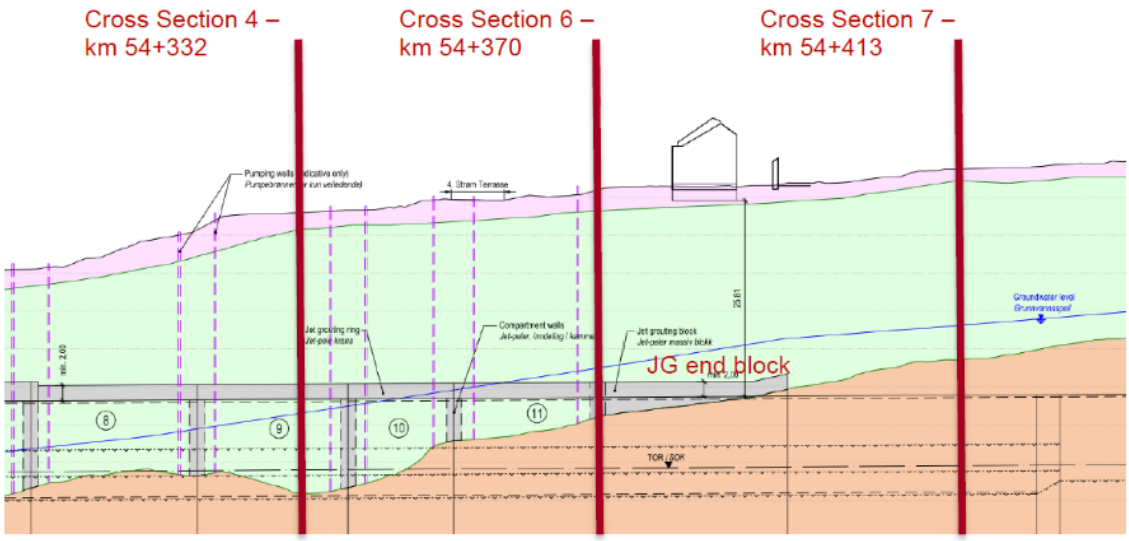

Figure 4.5: Longitudinal section of mixed face excavation from C8-12 from ILF (2020d)

The temporary supports are separated into two support classes. Support class SC1 refers to the support for the jet grout block in the transition between cut & cover-section and the soil tunnel. Support class SC2 is used for the cross section with a jet grout ring. The sprayed concrete thickness is set to minimum 30 cm for both classes and has a quality of C25/30. Supports besides sprayed concrete include lattice girders, mesh – and bar reinforcements. Reinforcement material type is B500C and B500NA for mesh. An elephant foot is used for primary lining in the top heading shown in Figure 4.6 (ILF, 2020a).

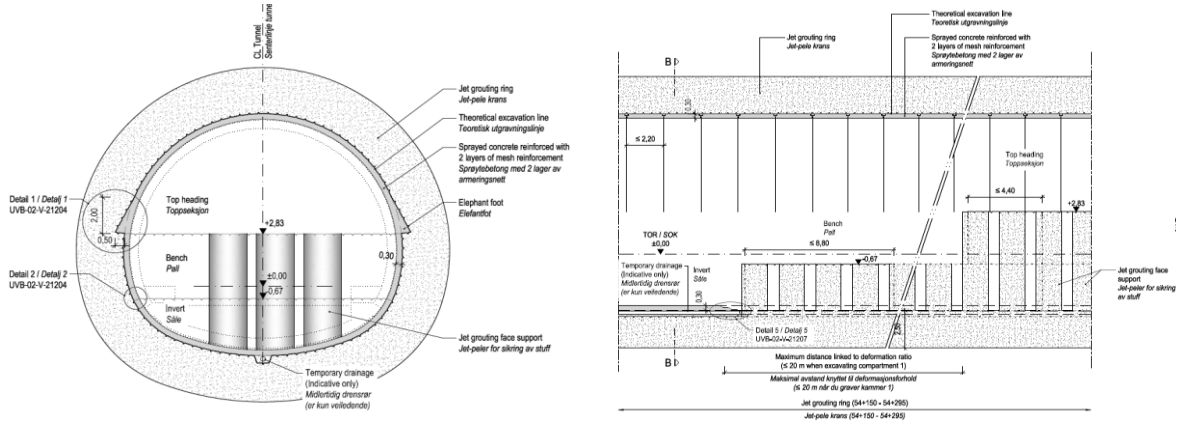

Figure 4.6: Support class 2 from (ILF, 2020b).

4.4.4 Permanent support design

The permanent support design varies from the different cross-section types. Geometric cross sections 1 and 3, requires a minimum 40 cm concrete thickness in the arch and a minimum 60 cm thickness in the invert. Nominal thickness is considered slightly higher with 46 and 66 cm. Demands for reinforced structural concrete B35 and a durability class MF45 is given. The reinforcement used is B500NC. This system is shown in Figure 4.4. The concrete fill above the invert is of concrete class C12/15 (ILF, 2021a). Cross section 2 is a mixed excavation cross-section and has no concrete invert. Therefore, CS2 features a secondary lining with solely a minimum 40 cm thickness in the arch (ILF, 2020f).

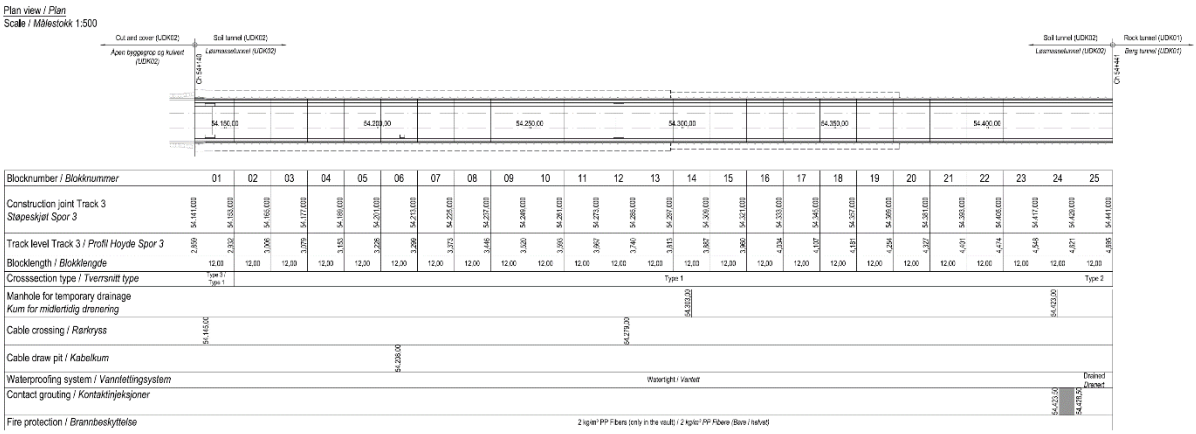

Figure 4.7: General overview of permanent support (ILF, 2021b).

After deformations are controlled for the temporary supports, a watertight membrane of PVC-P with minimum thickness of 3 mm and at least 900 g/m^2 of geotextile will be placed prior to the in-situ cast lining. From 0.5 meters above invert, reinforcement of at least 3 mm of PVC protection membrane is to be installed outside the watertight membrane. Design of the secondary lining was performed with a beam-spring model (ILF, 2020f).

4.5 Geotechnical parameters

Norwegian Geotechnical Institute (NGI) has performed several ground investigations and made a faction report over the soil conditions of the soil tunnel (NGI, 2020). The ground investigations, both field and laboratory, are reported by Norconsult AS in a geotechnical data report (Norconsult, 2019b). Total soundings in close vicinity of the soil tunnel are shown in the Figure 4.8.

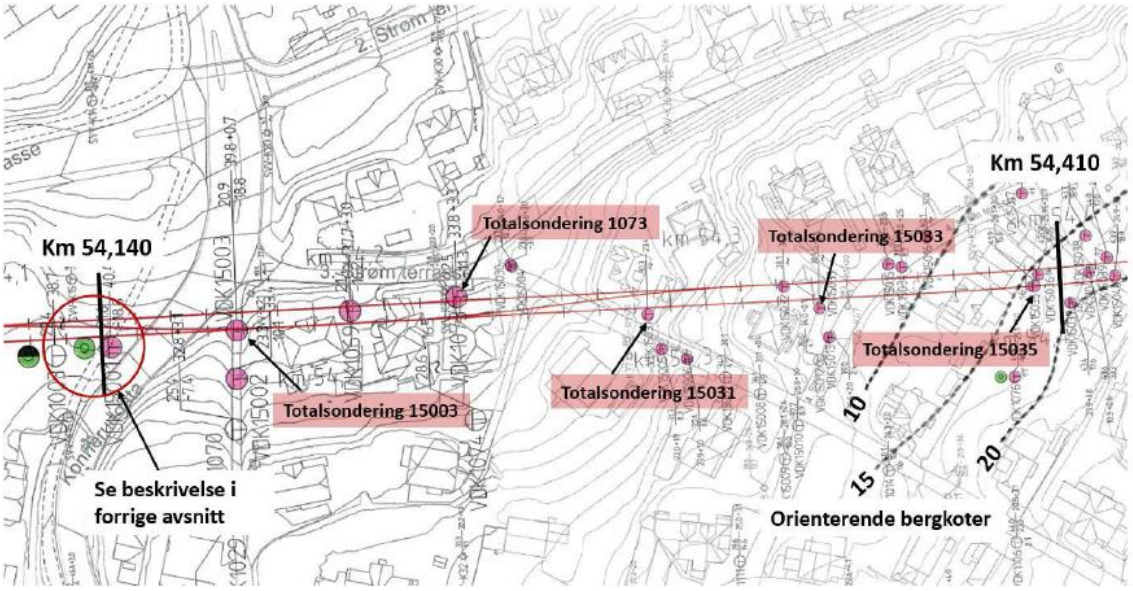

Figure 4.8: Site investigations between km 54,140 and 54,410 from NGI (2020).

The soundings 15003, 1073, 15031, 15033 and 15035 forms the basis of the layering profile for the centreline as shown in Figure 4.8.

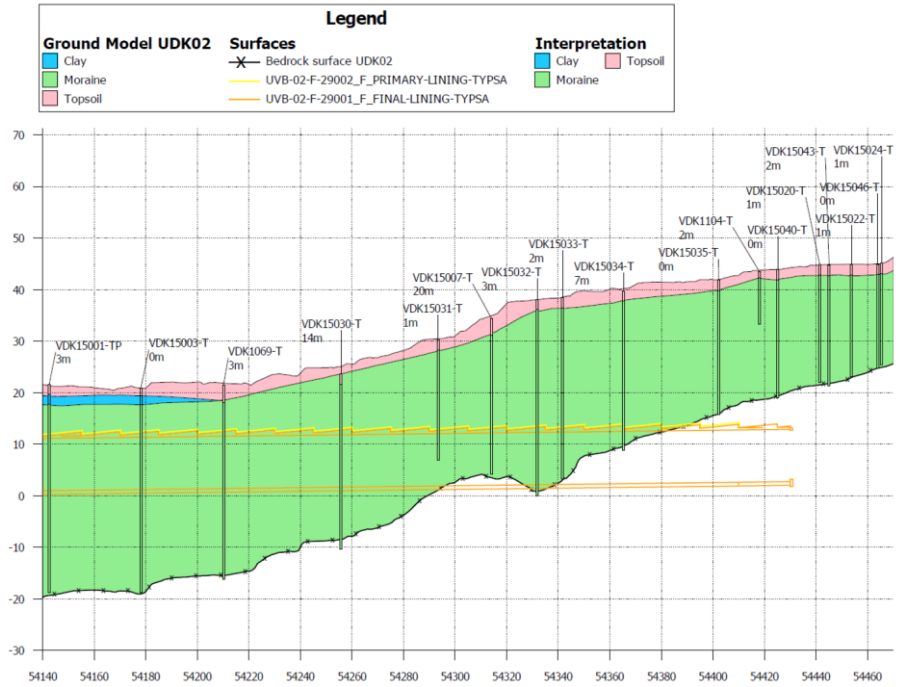

Figure 4.9: Longitudinal profile based on soil investigations extracted from NGI (2020).

Based on previous reports several interpreted geotechnical parameters have been collected. In 2017, Norconsult reported parameters for the soil tunnel part as shown in Figure 4.10.

Based on the geotechnical information provided by NORCONSULT, the following table summarizes the geotechnical parameters considered up to now.

Table 5. Geotechnical Characteristic Parameters

Lithology	g (kN/m³)	c' (kPa)	F' (º)	E (MPa) z(m)	n	K₀
Dense granular soil	21	5	40	75·(1+0.04·z)	0.3	0.357 (*)
Fractured rock	21	80	40	16 000	0.3	0.429 (**)
Rock (***)	27	1 000	60	22 000	0.18	0.5
Improved ground	23	100	40	800	0.25	-

(*) 1-sinF' (**) n/(1-n) (***) Rock parameters have been obtained from the intact parameters obtaining the rock mass parameter from an estimation of the GSI

The main conclusions in relation to the geotechnical conditions of the soils encountered in the tunnel area are:

- The **glaciofluvial sediments soil** seems to be mainly **granular materials** with an average **fine content lower than 10%**.
- The elasticity modulus of these materials seems to increase with depth and the average value could be close to 75 MPa, so they have a **dense to very dense compactness**.
- This geological unit typically could contain boulders of different size. But according to the information available up to now, their presence is not foreseen to be significant or important.
- The contact between the rock and the soil has been defined based on the geotechnical site investigations available up to now. More information could give a more accurate approximation to this contact.
- At this stage of the Project the GWL is going to be assumed at level +5 (max. expected value) at the beginning of the alignment, increasing along it and more or less parallel to the contact between soil and rock. As in the case of the rock contact, the more information is available the more accurate will be the interpretation of the GWL location.
- In relation with the permeability coefficient of the materials encountered in the tunnel area, based on the grain size distributions **the permeability of the materials is medium to high (10^{-4} to 10^{-5} m/s)**.

Figure 4.10: Soil tunnel parameters from Norconsult (2017).

Based on parameters from the soil tunnel report, further interpretation has been conducted to form Plaxis-parameters. Figure 4.11 displays parameters interpreted by Norconsult, which also accounts for calculations performed on the cut and cover tunnel excavation pit. *Dense granular soil* from Figure 4.10 correlates with *Glasifuviale masser* from Figure 4.11. ILF (2020a) used soil parameters according to Figure 4.10, but conservatively neglected the increase in elastic modulus by depth in the temporary design reports.

4.2.2 Inputparametere Plaxis – løsmasser

Tabell 2 Jordparametere Plaxis - friksjonsmasser

Identification		Tørrskorpe	Sand	Glasifluviale masser
Farge		Grønn	Blek gul/ rødbrun**	Mørk grå
Material model		Hardening soil	Hardening soil	Hardening soil
Drainage type		Drained	Drained	Drained
γ_{unsat}	kN/m³	19	17	19
γ_{sat}	kN/m³	19	17	19
E_{50}^{ref}	kN/m²	2,00E+04	3,00E+04	4,00E+04
E_{oed}^{ref}	kN/m²	2,00E+04	3,00E+04	4,00E+04
E_{ur}^{ref}	kN/m²	6,00E+04	9,00E+04	12,00E+04
$power\ (m)$		0,5	0,5	0,5
e_{init}		0,5	0,5	0,5
c_{ref}	kN/m²	0/3,12*	0/3,25**	0
$\varphi\ (phi)$	°	32	33	42
$\psi\ (psi)$	°	2	5	10
ν_{ur}		0,2	0,2	0,2
p_{ref}	kN/m²	100	100	100
K_0^{nc}		0,4701	0,4554	0,3309
R_f		0,9	0,9	0,9
ν_u		0,495	0,495	0,495
R_{inter}		0,6	0,7	0,7
δ_{inter}		0	0	0
$K_0, x\ =\ K_0, z$		Yes	Yes	Yes
K_0, x		0,4701	0,4554	0,3309

*For ett beregningssnitt er det lagt inn attraksjon på 5 kPa i tørrskorpen for å unngå lokale brudd helt i kant på utgraving som ikke er reelle

**For ett beregningssnitt er det lagt et lite element med sand med 5 kPa i attraksjon for å unngå lokale brudd under utgraving som ikke er reelle

Figure 4.11: Plaxis parameters for the cut and cover section by Norconsult (2019a).

4.6 Jet-grout parameters

Ground improvement specialist, *Trevi Spa,* stated conservative experience based characteristic parameters for jet grout columns as shown in Figure 4.12 (ILF, 2020a). Elastic modulus, Poisson's ratio and unit weight are extracted from Figure 4.10. The jet grouting method used is a double fluid method. These parameters are used in the temporary design report for the project. Friction angle are similar to that of the moraine (ILF, 2020a).

Table 2 – Characteristic jet grout parameters

		Improved Ground (Jet grout)
E	[MPa]	800 [1]
ν	[-]	0.25 [1]
γ	[kN/m³]	23 [1]
c'	[kN/m²]	466 (deducted from σ_{Gc} and φ')
φ'	[°]	40
σ_{Gc} (characteristic uniaxial compressive strength)	[MN/m²]	2.0 (Source: design meeting 19.03.2020 Soil Tunnel)
k_{st}		10^{-8} m/s (Source: TREVI, design meeting 13.02.2020)
Deducted from σ_{Gc} (see section 7.3.4) $\sigma_{Gc}=(2*c*\cos\varphi)/(1-\sin\varphi)$		

Figure 4.12: Characteristic jet grout parameters from ILF temporary design report (ILF, 2020a).

After completion of the jet grout columns, core samples in each compartment have been extracted (Trevi, 2021a; 2021b; 2021c; 2021d; 2021l; 2021k; 2021e; 2021f; 2021g; 2021h; 2021i; 2021j). The results and number of samples for each compartment are shown below. Lab tests, performed by SINTEF Community, are used to find specific weight, uniaxial compression strength and elastic modulus of the treated material. Standard unconfined compression tests were performed according to NS-EN 12716:2018 Annex. In addition, in situ permeability was measured with Lefranc tests by Trevi SPA. Results from these tests are shown in Table 4.1.

Table 4.1: Jet grout corings tested for the different compartments

Compartment	Samples	Average permeability [m/sec]	γ_{ave} [kg/m^3]	UCS [Mpa]			E_{ave} [Mpa]
				Max	Ave	Min	
1	8	3.9E-08	2297	15.25	9.51	5.43	1826
2	8	2.2E-08	2372	20.81	9.37	5.16	1523
3	16	7.8E-08	2295	21.01	11.8	5.98	1840
4*	12	7.2E-08	2233	28.66	11.6	3.76	1792
5	12	7.3E-08	2182	19.05	10.1	4.4	1896
6 *	8	3.3E-08	2254	12.71	6.66	4.36	874
6_{field}	8	3.3E-08	2153	24.85	12.8	1	2198
7*	12	2.3E-07	2203	24.97	10.38	3.03	1935
8***	12	1.8E-07	2190	17.72	10.24	2.98	1666
9***	12	1.7E-07	2215	61.14	17.55	4.13	1518
10***	10	2.0E-07	2052	18.92	8.45	1.25	2434
11***	8	3.4E-07	2397	8.18	2.26	1.12	496
12**	5	3.0E-07	2262	30.97	13.92	1.69	1458
Average	*131*	*1.36E-07*	*2239*	*23.40*	*10.36*	*3.41*	*1650*
*	Some samples contained larger stones (>4mm).						
**	Presence of boulders, usually confined by grout.						
***	Larger stones and presence of boulders.						

In compartment 8 a layer of silty/clayey silt was discovered in the bottom of the treatment with a variable thickness of up to 2 meters (Trevi, 2021f). The presence of boulders in some samples were reported, suggesting that this could cause a "shadow effect", where a boulder behind the nozzle could prevent a spread of fluid. This could lead to a smaller diameter column. However, as part of the global treatment system it would, according to Trevi, be confined by jet grout and not cause problems for the tunnel excavation (Trevi, 2021f).

4.7 Extended control

In accordance with Intercity Design Basis and Eurocode, an independent third-party control is required with reliability class 3 and execution control class 3 (UKK3) (CEN, 2016; BaneNOR, 2019). The control was performed by Norconsult on the permanent structure. Two sections were investigated, where a GCS1 at km. 54+332 resulted in the largest internal forces on the structure. The critical cross section, named CS3, has an estimated 25-meter overburden and the bedrock was conservatively assumed just below the lining. Calculations were performed for both high and low groundwater level in finite element. The calculations regarding long-term actions for the inner lining, did not introduce relaxation or three-dimensional effects due to jet grouting, excavation and primary lining. Bedding reaction between moraine and concrete was simulated with moraine interface properties as shown in Figure 4.11.

4.8 Project experience

Current experiences from the project suggest that the jet grout ring is sufficiently watertight. During top heading excavation no water ingress was observed. In addition, the excavation progress was faster than planned (Mork, 2022). Current settlement and displacement monitoring has shown surface settlements and tunnel extrados displacements mostly below 10 mm. Measurements performed at km. 53+335 is shown in Figure 4.13. At this point the bench is excavated to km. 53+365. The tunnel displacements occurring ahead of the excavation face are not considered (Veidekke, 2022). At km. 51+360 the surface settlements are measured to approx. 17 cm.

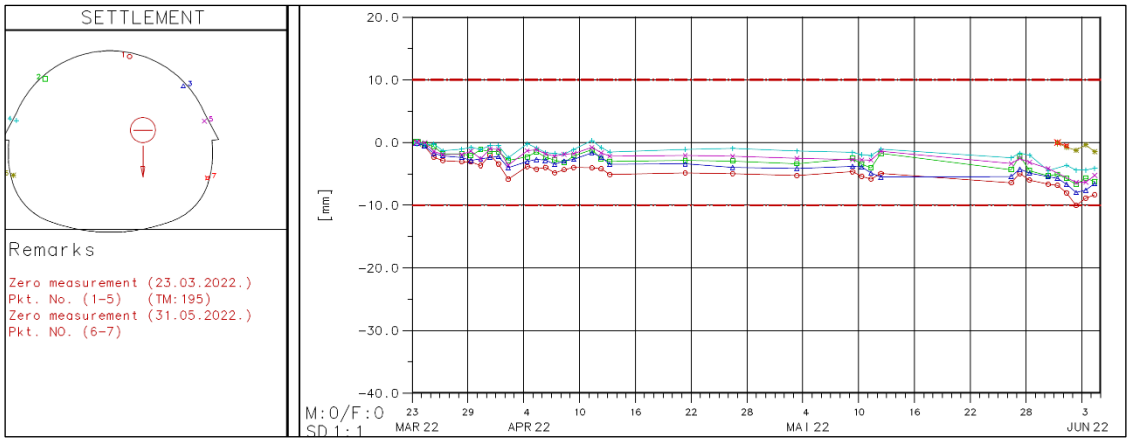

Figure 4.13: Monitored vertical displacement as om 06.06.22 from Veidekke (2022).

5 Modelling

The method for this thesis is to use gathered material parameters and establish numerical models using finite element program Plaxis 2D and 3D. Plaxis can model soil-structure interaction, making it possible to investigate the effect of the temporary supports, and compare structural forces and interaction behaviour for the lining configurations. Approaches and methods found in literature will be applied according to suitability. As a basic rule, a finite element analysis should be controlled using basic established theories. However, due to the complexity of the case study and that design is not within scope of the study, basic theories are not used. Calculation results will be roughly compared with the unpublished design reports, mainly to evaluate the force distributions. Since the design reports for the project are based on different assumptions and methods than what is used in this study, a full comparison is not considered relevant.

5.1 Numerical modelling

Numerical analysis of this problem includes several simplifications to provide sufficiently comparable results. The investigations are not performed to design or alter the current design of the case study. Because the case study is not fully excavated, and monitoring not completed, a back-calculation is not performed.

5.1.1 Model geometry

In accordance with the extended control and the permanent design report, cross section 3 forms at km. 53+332 the basis for the model geometry. The equivalent cross section is named cross section 4 in the temporary design report shown in Figure 4.5 (ILF, 2020f). Based on ground investigations an approx. 2-meter-thick layer of topsoil is followed by a layer of dense granular soil stretching to bedrock. Potential clay deposits found during jet grout testing is neglected. At this section the overburden is set to 25 m and the jet grout ring has a thickness of 2 meters. The longitudinal profile suggest that rock surface is 1 meter above the invert (NGI, 2020). As a conservative approach and to simplify the model, bedrock is assumed 1 meter below the invert. The transition to bedrock is modelled with a rigid boundary, as the stiffness is considered significantly higher than the moraine. A sensitivity analysis has been performed which confirmed the consideration. The sensitivity analysis is not shown in the thesis. The cross section is divided into a top heading, bench and invert. The modelled geometry of the tunnel profile and structural elements are shown in Figure 5.1.

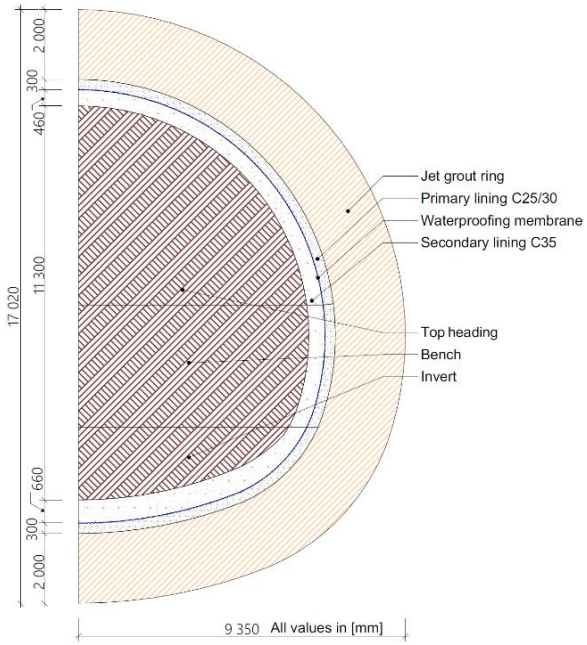

Figure 5.1: Modelled geometry according to support class 2. Drawing produced in AutoCAD 2022 and ArchiCAD 25.

The vertical boundary of the model is for both 2D and 3D analysis modelled 60 meters from the centreline, more than 4 times the tunnel diameter. Equivalent boundary conditions apply to both models as shown in Figure 5.2. All vertical boundaries in the models are set to normally fixed, allowing vertical displacements. The lowest horizontal boundary is modelled as fully fixed, preventing any displacement due to assumed stiffness ratio of bedrock and moraine. The surface boundary is modelled as free. The total height of the models are 41 meters. In the 3D model, the model length perpendicular to the plane model will be 44 meters initially, and 88 meters for an enlarged model. Due to computational power available, this is not further increased.

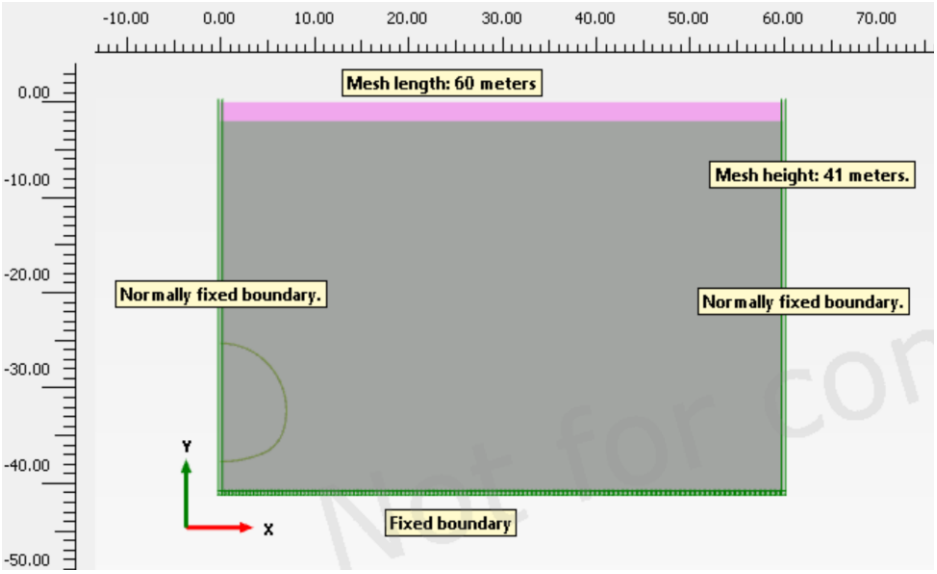

Figure 5.2: Two-dimensional model geometry from Plaxis 2D.

5.1.2 Modelling evaluations

To enable use of half-symmetry modelling, the surface is considered flat. The elephant foot for the sprayed lining is neglected due to potential meshing difficulties, which will affect the bearing and stress distribution. Surface- and traffic loads are disregarded to simplify evaluation of internal forces. To avoid increased computational costs and potential numerical problems, the concrete and gravel fill above the invert, which are used to create a traffic platform, are neglected. This includes the notches seen from Figure 4.4, which are part of the permanent invert design. These notches are neglected due to possible implications they might give in the finite element model, especially in terms of obtaining forces. As a result, the nominal thickness of the secondary lining, 660 mm, is used in the models (ILF, 2020f).

Full bonding between jet grout ring, moraine and sprayed concrete is assumed. Due to adhesive behaviour of sprayed concrete and the jet grout mixture with high pressures, this is considered realistic. With this assumption, no interface is deemed necessary to simulate any reduced strength behaviour between the mentioned materials. Full bonding is also assumed between the sprayed concrete lining and jet grout ring. Each concrete lining is assumed with no jointed behaviour, which leads to a full moment transfer in the entire lining. This assumption would in a design situation have to be justified, especially for the connection with reinforcement between bench and invert in the secondary lining.

5.1.3 Groundwater modelling

The groundwater (GW) is modelled at a depth of 25 meters, at the top of the primary lining. To model the groundwater pressure on the secondary lining, both primary lining and jet grout ring must be modelled as drained materials to allow groundwater pressure. The secondary lining, which is considered dry in all phases, can be modelled as non-porous. Prior to secondary lining activation, the primary lining and jet grout ring can be set to dry manually, which causes the groundwater pressure to act on the extrados of the jet grout ring. For a shared groundwater load between the primary and secondary lining, the jet grout ring is modelled with global water level. With the groundwater pressure acting only to the secondary lining, both primary lining- and jet grout volumes are manually set to global water level. This procedure is shown in Figure 5.3 where grey volumes are manually modelled with dry water conditions.

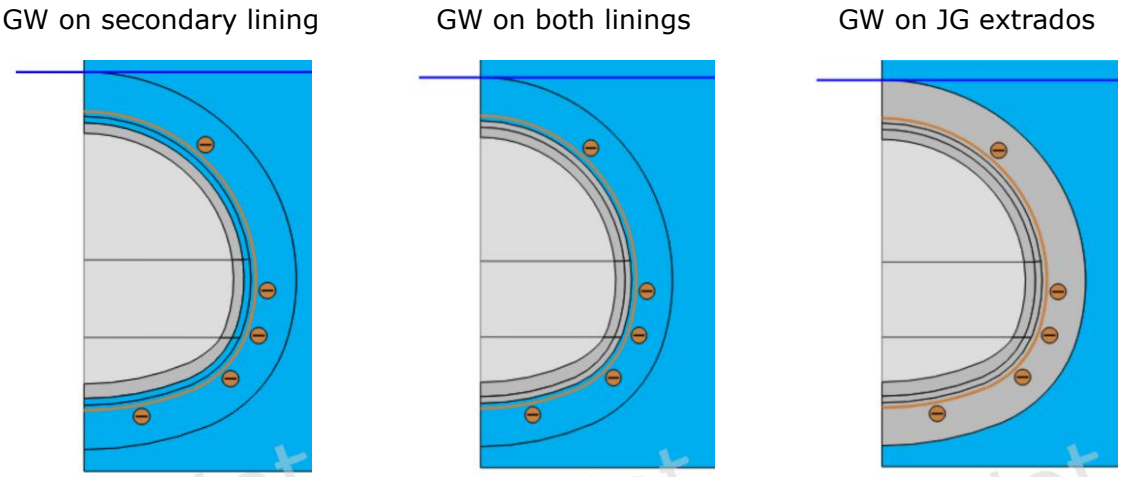

Figure 5.3: Modelling of groundwater pressure.

5.1.4 2D-modelling

2D analysis will be performed using Plaxis 2D v22. The layering and geometrical model is as previously discussed extracted from the permanent design report for the project. The geometric cross section consists of three arches as shown in Figure 4.4. Therefore, AutoCAD 2022 by Autodesk was used to draw tunnel geometry and then profile contours were created with an offset. In an attempt to model the tunnel accurately, volume elements were chosen for evaluating internal forces in the 2D model. Special attention to the transitions between heading, bench and invert is needed due to the sudden change in radius between the curves used to form the geometry, which may cause some numerical issues from the mesh. The change in radius could potentially be solved by using a clothoid (Euler spiral) or a continuous spline, but this is not featured in this study.

The method chosen to evaluate the internal forces of the structural volume elements is the tool *Structural forces in volume plates*. This tool integrates the perpendicular stress points along a cross-section centreline. Application of this tool requires that an adequate amount of stress points exists to be integrated in the volume element (Bentley, 2021c). As an alternative to this tool a "dummy plate" with no structural contribution could have been used to extract forces. However, this process would be complicated to implement for both jet grout, primary and secondary lining volumes with a staggered modelling. It is considered that, with a locally refined mesh, the integrations of stress points tool will be accurate.

Quality verification of the mesh will be performed with the tools *Quality/ Quality Spheres*. The Quality tool defines the quality of each finite element based on dividing the inner circle of the tetrahedralis elements by the outer circle. A equilateral triangle will be normalised at 1, given as the best quality element. Non-equilateral element is assumed to provide increasingly worse element quality, and could affect the mesh quality (Bentley, 2021b).

Including time-dependency and 3D-effects of sprayed concrete in a plane strain model is a difficult and often unprecise task. Therefore, a simplification has been made. Factors such as humidity-, creep- and shrinkage of shotcrete are considered with the Hypothetical Modulus of Elasticity method. Simulating time-dependent behaviour is performed by using two separate material models for sprayed concrete with different strength and stiffness parameters. After excavation the lining is wished-in-place with early-age strength. When the next staggered excavation is performed, the primary lining will be replaced with a constitutive model representing a hardened sprayed concrete. The jet grouted columns for face support will be modelled with a homogenized improved ground.

Pre-release of stress will be used to simulate deformations due to cavity pre-convergence and unsupported excavation length. The deconfinement method for use in Plaxis is based on the convergence-confinement method and a calculation method by Schikora and Fink (1982) (Bentley, 2021c). Few models found in literature account for support provided by the pre-existence of a jet grout ring. Because of this, the deconfinement ratio will be found using a preliminary three-dimensional analysis with improved ground in the advancing core.

Workflow in 2D:

1. Establish materials, geometry and layering model in Plaxis 2D.
2. Import a geometric cross section from a suitable format to the tunnel designer. The lining interface are established within the tunnel designer.
3. Meshing of the model. Special attention is needed to create a suitable mesh. Small and slender structures should be locally refined and quality checked.
4. Define construction stages in staged construction. Initial stage is set to K_0-procedure for horizontal layering models.
5. Next phase activates the wished-in-place jet grout ring and drains the cavity.
6. The following phases defines the tunnel excavation process of the soil tunnel as shown in Figure 5.4. For the first tunnel excavation step the previous displacements should be reset, otherwise this needs to be considered during post-processing. The steps considers relaxation, deactivation of elements and wished-in-place installation of linings.
7. The following phases after the secondary lining installation will feature the degradation of temporary supports. The displacements occuring in the analysis from degradation will not be accounted for, since they are considered unrealistic.

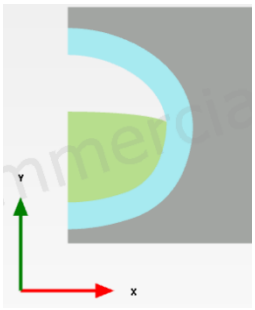

Relaxation top heading

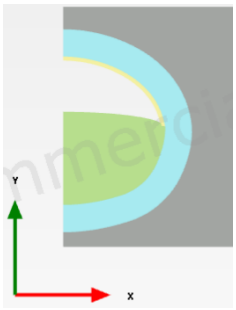

Top lining

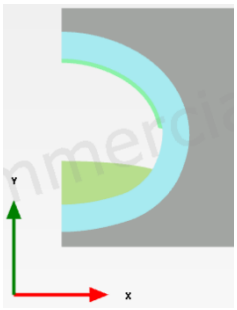

Relaxation bench

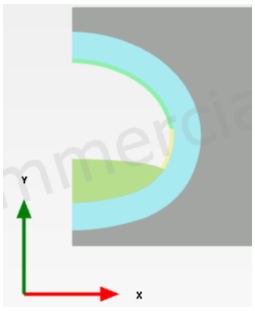

Bench lining

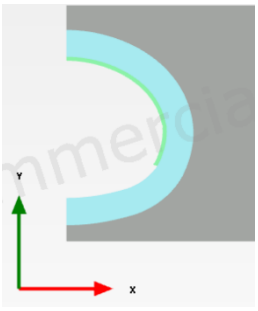

Relaxation invert

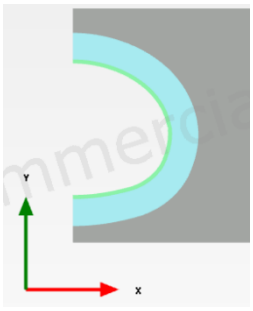

Invert lining

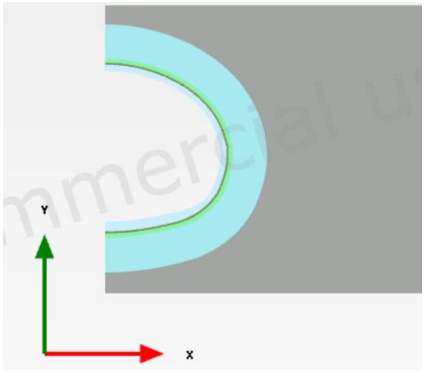

Installation of secondary lining and activation of interface

Figure 5.4: Staged excavation performed in Plaxis 2D with a stepwise process.

5.1.5 3D-modelling

The three-dimensional analysis is performed using Plaxis 3D v21. Three-dimensional analysis is used to examine the effects of sequential excavation and unsupported length. The preliminary results will be utilized to select a deconfinement parameter suitable for describing displacement and stress-release prior to lining installation in the following two-dimensional analysis. Therefore, modelling of the secondary lining is neglected for the three-dimensional model.

The geometry is modelled according to previous discussion with two different model sizes and a half-symmetrical approach. This choice was due to computational savings, which is useful for three-dimensional models. It is assumed that 44 meters of tunnel length is sufficient to extract primary deformations, but it can be argued that a larger longitudinal length should be used for a fully developed deformation. This will be performed by increasing the longitudinal length to 88 meters in the final preliminary analysis used to calibrate the stress-release in 2D.

Due to difficulties with meshing the primary lining as a volume element, two different configurations are performed for verification. The first analysis models the primary lining as a volume element and the other analyses will model the primary lining as a plate. If verified, the plate lining configuration will be used for investigating the enlarged mesh model, since it requires more computational power. The groundwater table is modelled hydrostatic, with a dry behaviour of the jet grout ring and the tunnel cavity for both configurations. Thus, the hydrostatic loads are acting on the extrados of the jet grout ring which can be argued as unrealistic. This assumption was equally applied to 2D calculations prior to secondary lining installation.

All variations in bedrock and surface are disregarded. Thus, the model is only considered useful for the chosen cross-section in the two-dimensional model. It is expected that in the real situation the relatively higher level of bedrock will reduce the displacements. To reduce computational costs and avoid potential meshing difficulties, the jet grouted columns within the cavity will be modelled with a homogenized improved ground. This is performed to uncover a potential effect of an improved advancing core on pre-convergence.

For three-dimensional analysis an unsupported length of 2.2 meters for top heading, 4.4 for bench and 8.8 for invert is considered. Each step for three-dimensional analysis is performed with 2.2-meter steps. The full length of top heading is excavated prior to bench excavation. In the project description, the invert is excavated no further than 20 meters behind the bench or controlled by a deformation ratio. In the analysis a full excavation of bench prior to invert is assumed. Information from the project shows that a large length of the bench was excavated prior to invert excavation (Mork, 2022). To prevent numerical failure as a result of a collapse in the excavation face, a fixed displacement in the longitudinal direction is applied to the free faces during excavation as can be seen in Figure 5.5. This assumption may yield some differences compared to a realistic situation but is applied to find reasonable results.

Workflow in 3D:

1. Establish materials, geometry and layering model in Plaxis 3D.
2. Import the geometric cross section to the tunnel designer from suitable format. Jet grout geometry is later extracted and modelled as a surface independent of the tunnel designer. This ensures that no numerical issues are caused between jet grout and the tunnel designer when meshed. With JG modelled as an independent surface, the ring can be activated prior to excavation. Special care is taken that both tunnel and jet grout ring have same base coordinates. Interfaces and plates, if any, are established within the tunnel designer.
3. Decide tunnel length, trajectory, segment length, segment number and excavation sequence. The sequence is defined with steps, so that the first step is equivalent to the face of the excavation. Steps following the first step decides the supports and when the next staggered excavation starts. Supports feature a early-age strength sprayed concrete until next staggered excavation with the HME method. When the next staggered excavation is started, a full strength is given which is considered equivalent to the 2D procedure. The invert sprayed concrete is given full strength immediately, since it is assumed to produce little difference for the results. Excavation sequence is shown in Figure 5.5 for the modell with a longitudinal length of 44m. Same procedure applies to the enlarged mesh.
4. Meshing of the model. Special attention is needed to create a suitable mesh. Quality spheres tool will be used to verify the mesh. Small and slender structures should be locally refined.
5. Define construction stages in staged construction. Initial stage is set to K_0-procedure for horizontal layering models.
6. Next phase activates the wished-in-place jet grout ring and drains the cavity.
7. The following phases defines the tunnel excavation process of the soil tunnel as shown in Figure 5.5. For the first tunnel excavation step the previous displacements should be reset, otherwise this needs to be considered during post-processing. Each new phase advances the tunnel one step, and deactivates the soil volume. Due to large quantity of steps, it is considered considerably more efficient to use a script to simulate this. Bentley have created a Python script, called *tunnel_advancement_tool,* which can be downloaded from their Bentley's website (Sloot, 2019).

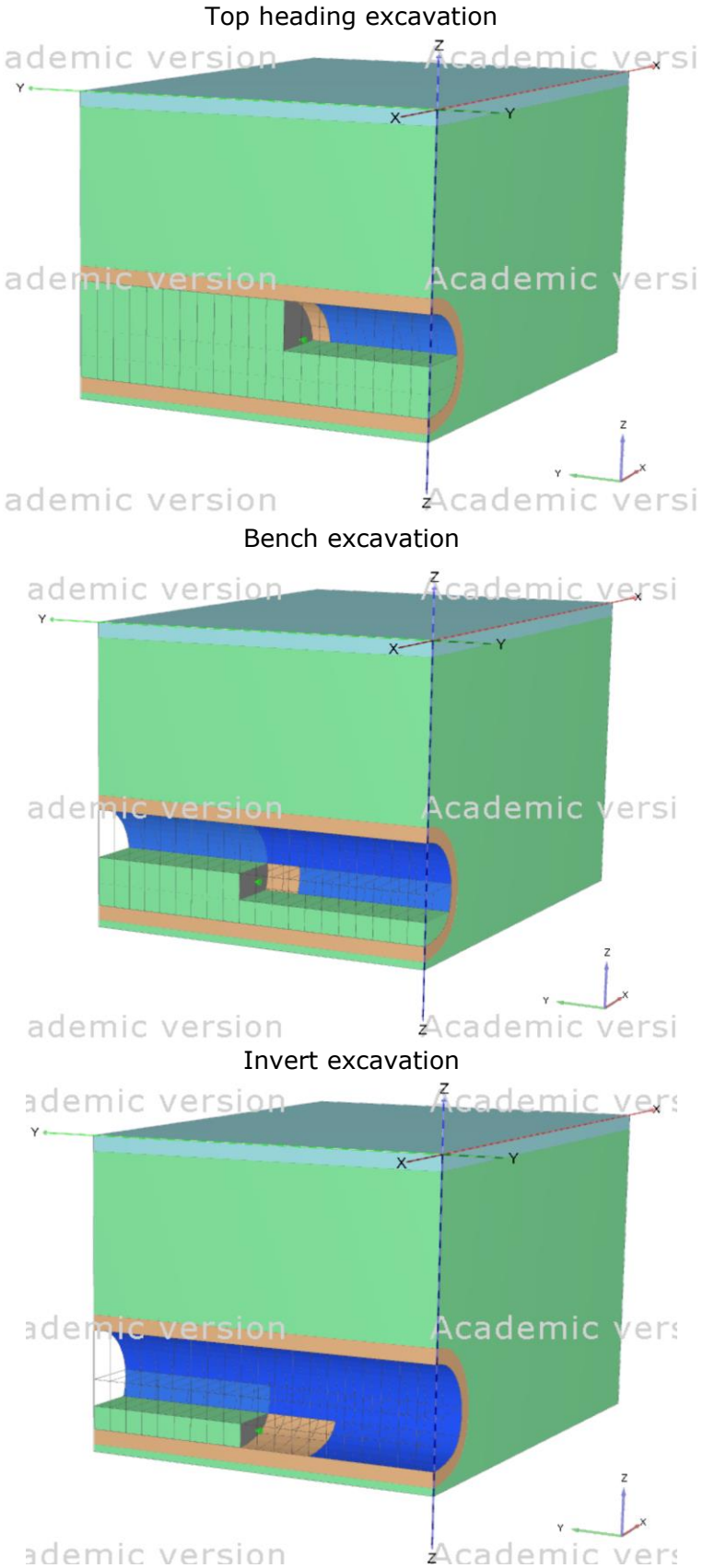

Figure 5.5: Staged excavation performed in Plaxis 3D with a stepwise process.

5.2 Material models

5.2.1 Geotechnical parameters

Geotechnical parameters are extracted from previously named reports and used to form constitutive Plaxis material models. All parameters not covered are set to default value. The soil parameters used for top soil and moraine in Plaxis are extracted from NGI (2020).

Identification		Top Soil	Moraine
Material model		Hardening soil	Hardening soil
Drainage type		Drained	Drained
$\gamma_{unsat} = \gamma_{sat}$	kN/m³	19	19
E_{50}^{ref}	kN/m²	2.00E+04	4.00E+04
E_{oed}^{ref}	kN/m²	2.00E+04	4.00E+04
E_{ur}^{ref}	kN/m²	6.00E+04	1.20E+05
power (m)		0.5	0.5
e_{init}		0.5	0.5
c_{ref}	kN/m²	0	0
$\varphi\ (phi)$	°	33	42
$\psi\ (psi)$	°	3	10
ν_{ur}		0.2	0.2
p_{ref}	kN/m²	100	100
Tension cut-off		Yes	Yes
Tensile strength	kN/m²	0	0
R_{inter}		0.6	0.7
$K_{0,x} = K_{0,z}$		Yes	Yes
$K_{0,x}$		0.4554	0.3309

Parameters for jet grout

Eurocode for execution of special geotechnical work, EN 12716, regarding jet grouting works has established a method to determine the material strength parameters (CEN, 2019). Annex A describes that with a minimum of 10 samples, the unconfined cylindrical compressive strength can be calculated using a statistical approach. The characteristic unconfined cylindrical compressive strength can be found using equation 4.

$$f_{m,k} \leq \eta_d \exp(m_y - k_n s_y) \quad (4)$$

In this formula η_d is a conversion factor, typically set to 1, to consider uncertainties not covered by other safety factor. Variable m_y is the mean value and s_y is the standard deviation of the natural logarithm of the strength for the individual samples. Variable k_n is the acceptance factor for jet grouting material and is typically 1,28 as a 10-% fractile. Based on the characteristic strength a design value can be depicted using typical values from EN 1992-1-1 as seen in equation 5.

$$f_{m,d} = \alpha * \frac{f_{m,k}}{\gamma_m} \quad (5)$$

In this equation α is the factor for long term effects of the strength and γ_m is the partial factor for the jet grouted element. As explained by Croce, Flora and Modoni a Mohr-Coulomb failure criterion is often adopted for grouted material in massive treatments (Croce, Flora and Modoni, 2014).

Table 5.1: Statistically determined jet grout parameters based on EN 12716.

Identification	Value	Unit
Number of samples	131	-
Average unconfined compressive strength, UCS	10.36	MPa
Average elastic modulus by SINTEF, E	1650.46	MPa
Conversion factor, η_d	1	-
Acceptance factor, k_n	1.28	-
Mean deviation natural logarithmic , m_y	2.102	
Standard deviation $\log_e$ C1-12, s_y	0.756	
Characteristic strength C1-12, $f_{m,k}$	3.111	MPa
Design strength C1-12, $f_{m,d}$	1.76	MPa
Mean deviation natural logarithmic C1-10, m_y	2.204	
Standard deviation $\log_e$ C1-10, s_y	0.622	
Characteristic strength C1-10, $f_{m,k}$	4.085	MPa
Design strength C1-10, $f_{m,d}$	2.31	MPa

The average characteristic strength of the jet grout, using a statistical approach accounting for all compartments, yields a higher characteristic strength than that of the

project criterium. In addition, the hardening process of the jet grout is considered sufficient to be excluded from analysis. This is reasonable considering the installation of columns is performed in a sufficient period of time prior to excavation.

The material models used for numerical analysis are shown in Table 5.2. Friction angle of jet grouted material is similar to that of the moraine, as found by Balmer (1958) during soil-cement testing. To be conservative, the friction angle is set equal to that of the temporary design report (ILF, 2020a). Jet grout strength parameters are deducted from the uniaxial compression strength. Young's modulus and cohesion are varied to study the effect of upper and lower bound solutions. Design value (DV), characteristic value (CV) and average value (AV) are abbreviations used to show variation in stiffness and strength parameters. The design value of unconfined compressive strength is set to 2 MPa, slightly higher than 1.76 MPa from Table 5.1, as compartments 8-12 showed large deviations in results. These compartments are realistically in a mixed face excavation and the model geometry is already set conservatively. Tensile strength, f_{jg}, is estimated from equation 6 based on jet grouting in sand (Croce, Flora and Modoni, 2014).

$$f_{jg} = 0.3 q_u^{0.8} \tag{6}$$

A realistic value of tensile strength could be achieved with an indirect tensile test, which is not covered by scope of the thesis. Initial thoughts are that a tensile strength is not critical for the analysis since the jet grout arch under loading is assumed to be a compressive arch. Cohesion is calculated using uniaxial compressive strength inserted into equation 7 proposed by Mitchell (1976).

$$c\ [kPa] = 48.265 + 0.225 q_u \tag{7}$$

The geotechnical parameters utilized for the jet grout ring is shown in Table 5.2. A system with separate names for different strengths and stiffnesses according to abbreviations are given in the heading row.

Table 5.2: Geotechnical parameters of jet grouted material for Plaxis.

Identification	Unit	JGLE	JG1, JG2, JG3 (DV, CV, AV)
Material model		Linear-Elastic	Mohr-Coulomb
Drainage type		Drained	Drained
$\gamma_{unsat} = \gamma_{sat}$	kN/m³	23	23
E	kN/m²	800E3	500E3, 800E3, 1600E3
$\nu\ (nu)$		0.25	0.25
UCS (q_u)	MPa	4	2, 4, 10
c_{ref}	kN/m²	950	500, 950, 2300
φ	°	40	40
Tensile strength	kN/m²	-	522, 909, 1893
k_x	m/day	1E-7	1E-7
k_y	m/day	1E-7	1E-7
R_{inter}		1	1
$K_{0,x} = K_{0,z}$		Yes	Yes
$K_{0,x}$		1	1

Improved advancing core

The cavity within the jet grout ring is improved using three jet grouted columns per excavation length with a 2-meter diameter with centre distance of 2.2 meters in longitudinal direction. This will contribute to a strengthening of the soil inside the cavity. To simulate this numerically in the models, improved behaviour by a homogenization of the volume elements inside the cross section is used. Stiffness of moraine according to the Hardening Soil Model is considered at 21 meters, and thus is considered a conservative approach.

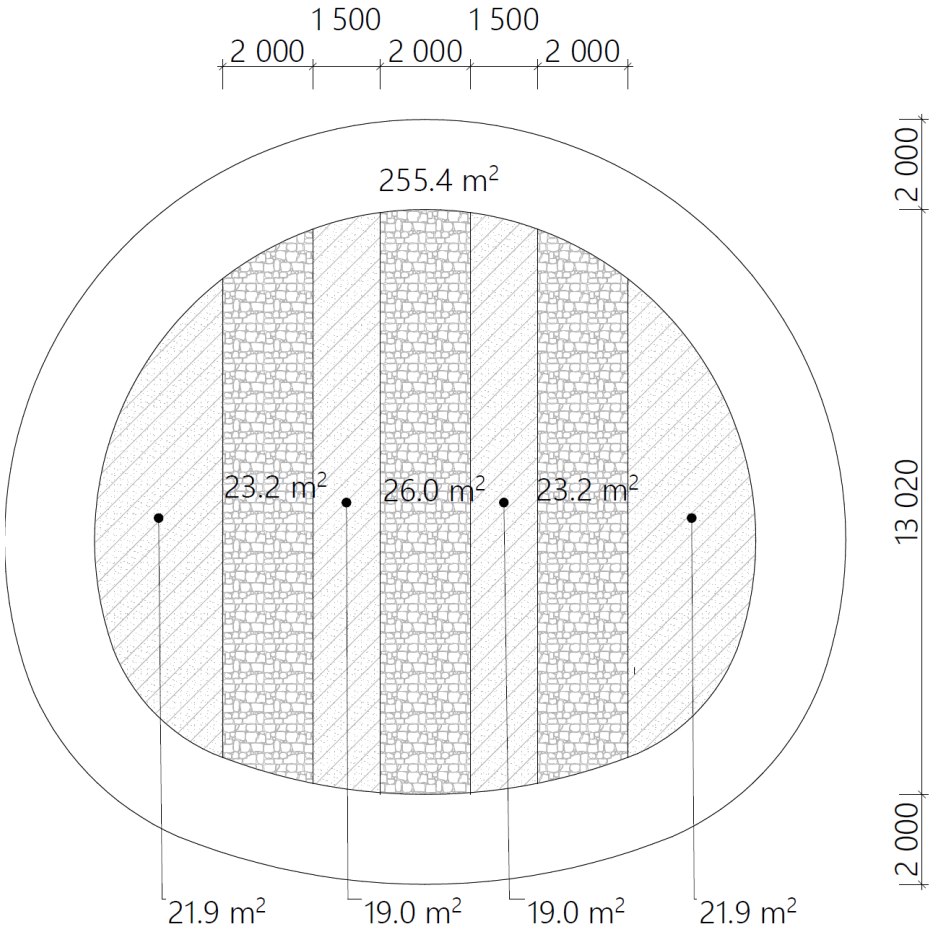

Figure 5.6: Drawing of 2D-areas in the cross section with ArchiCAD program.

The untreated part due to circular columns in longitudinal direction need to be considered. To account for the reduced volume for an excavated length of 2.2 meter, due to the circular shape and 2-meter diameter the jet grout columns cover approximately 33% of the volume. The strength and stiffness are evaluated by an average value of the parameters compared to their relative volume. The weight of the material is set to be equal to the moraine, and therefore the effects of the potential unit weight increase is neglected for this thesis.

Table 5.3: Homogenization of improved advancing core.

Identification	Volume [m^3]	E-modulus [kPa]	Cohesion [kPa]	Weight [kN/m^3]
Jet grouted columns	113.7 m^3	800E3	950	23
Moraine	225.5 m^3	80E3	0	19
Total volume	339.2 m^3			
Homogenized		321E3	318	19

Using the homogenization showed in Table 5.3, the selected constitutive model for the advance core is given Table 5.4.

Table 5.4: Improved advancing core constitutive model

Identification	Unit	Improved advance core
Material model		Mohr-Coulomb
Drainage type		Drained
$\gamma_{unsat} = \gamma_{sat}$	kN/m³	19
E	kN/m²	321E3
$\nu\ (nu)$		0.25
c_{ref}	kN/m²	318
φ	°	40
R_{inter}		1
$K_{0,x} = K_{0,z}$		Yes
$K_{0,x}$		1

5.2.2 Structural parameters

Sprayed concrete

The sprayed concrete used is concrete class C25/C30. The unit weight is estimated slightly higher than similar studies, due to weight contribution of lattice girders and wire mesh in the lining. The Hypothetical Modulus of Elasticity method by Pöttler (1990) is used to simulate the sprayed concrete behaviour. In combination with the convergence-confinement method, Panet and Sulem (2022) suggests using an average stiffness of sprayed concrete at early-age, around 8 GPa, and long-term characteristics for the final support state. John and Mattle (2003) proposed values of early-age shotcrete between 1 and 7 GPa, where higher early-age stiffness should be chosen for sprayed linings with heavier reinforcement. For hardened sprayed concrete the authors proposed 15 GPa. These values were based on tunnels with low overburden and found through numerical analysis. Based on literature suggestions, the constitutive parameters are chosen. This assumption is similar to those applied in the temporary design report (ILF, 2020a; 2020d).

The strength of the lattice girders and mesh reinforcement are not accounted for in this study, but the early-age stiffness will be derived slightly higher as suggested by literature. The effect of higher early-age stiffness will assumingly increase the stresses in the primary lining. It is assumed that the tensile capacity is sufficiently covered in the primary lining and is not covered in this case study. Based on this assumption, a linear-elastic model has been assumed for the volume and plate lining properties. To simulate the degradation process, a user-defined soil model described in chapter 5.2.4 and the appendix will be attempted. Characteristic, design and mean value shown in Table 5.5 for C25/30 are extracted from Eurocode 2 (CEN, 2021).

Table 5.5: Sprayed concrete parameters

Identification	Value	Unit
Unit weight, $\gamma_{unsat} = \gamma_{sat}$	25	kN/m³
Characteristic compressive strength, f_{ck}	25	MN/m^2
Design compressive strength, f_{cd}	14.1	MN/m^2
Mean value of Young's modulus, E_{cm}	31	GPa
Long term value HME, E_h	15	GPa
Early-age HME, $E_{e\text{-}a}$	5	GPa
Poisson's ratio, v	0.2	-

Based on these parameters and information found in literature, consitutive models are used to simulate the sprayed concrete behaviour. The constitutive model for the volume lining is shown in Table 5.6.

Table 5.6: Linear-Elastic primary lining for volume modelling in Plaxis 2D and 3D.

Identification	Unit	C25 Early-Age	C25 Hardened
Material model		Linear elastic	Linear elastic
Drainage type		Drained	Drained
Unit weight, $\gamma_{unsat} = \gamma_{sat}$	kN/m³	25	25
E', elastic modulus	kN/m²	5E6	15E6
v'		0.2	0.2
G	kN/m²	2.083E6	6.25E6
$k_x = k_y = k_z$	m/day	0.1E-9	0.1E-9
R_{inter}		1	1
$K_{0,x} = K_{0,y}$		1	1

Table 5.7 displays the consitutive primary plate properties for Plaxis 3D. Verification of the plate lining simulation with a volume lining should be performed. This is needed because the primary lining modelled as a plate will not be at the geometrical equivalent position as the model with a volume lining.

Table 5.7: Primary lining plate properties in Plaxis 3D.

Identification	Unit	C25 Early-Age	C25 Hardened
Material model		Elastic	Elastic
Thickness, d	m	0.3	0.3
Unit weight, γ	kN/m³	25	25
Isotropic		Yes	Yes
E_1	kN/m²	5E6	15E6
v_{12}		0.2	0.2
G_{12}	kN/m²	2.083E6	6.25E6
Prevent punching		No	No

Secondary lining

The secondary lining used in the project is of concrete class C35 and parameters are chosen according to an uncracked concrete state. In a realistic design situation, cracking of the secondary lining would need to be accounted for. A simplification is made, by not including any reinforcement in the numerical analysis and using a linear elastic material. The purpose of this study is limited to regard development of internal forces and relaxation due to temporary supports, not the actual design of a secondary lining. The parameters used are according to NS-EN 1992-1-1 and in accordance with the extended control of the project (CEN, 2021). Safety factors have not been applied since no design is performed, and higher stiffness is considered to yield the largest stresses.

Table 5.8: Material parameters for secondary lining.

Identification	Unit	C35 - uncracked
Material model		Linear elastic
Drainage type		Non-porous
γ_{unsat}	kN/m³	25
γ_{sat}	kN/m³	25
E	kN/m²	3.40E+07
$\nu\ (nu)$		0.2
G	kN/m²	1.42E+07
E_{oed}	kN/m²	3.78E+07
V_s	m/s	2358
V_p	m/s	3850
R_{inter}		1
$K_{0,x} = K_{0,z}$		Yes
$K_{0,x}$		1

5.2.3 Membrane interface parameters

The membrane interface parameters vary based on which waterproofing mechanism is assumed in the design. The case project uses a sheet membrane, which in design adopts a slip surface with low shear stiffness in numerical analysis. Friction angle and cohesion is chosen as low values to not withstand shear and avoid numerical problems. The sprayed waterproofing interface parameters need to be estimated, due to lack of relevant data. In a realistic design situation, tests need to be conducted to verify the material model. Looking at the potential effects due to the bond the material produces is considered more relevant than simulating realistic material tests. Stiffness parameters for slip and bonded interface are modelled directly, which disables any interface reduction factor to the stiffness parameters. This will reduce the risk of numerical issues.

Mohr-Coulomb parameters are selected to form a constitutive model for unbonded and bonded interface. Studies have shown a significant effect from humidity on the sprayed water membrane (Holter, 2016; Su and Bloodworth, 2016; 2019). According to suggestions by Su and Bloodworth (2016), the long-term relaxation ratio of a sprayed membrane is set to 50% for all stiffness values. To account for this the shear stiffness is reduced according to suggestions in their study. Based on suggestions by Su and Bloodworth (2016) found in Figure 2.11, the interface properties are shown in Table 5.9.

Table 5.9: Interface properties between secondary and primary lining.

Parameter	Unbonded	Bonded	Unit
Material model	Mohr-Coulomb	Mohr-Coulomb	
Drainage type	Non-porous	Non-porous	
K_n, Tensile stiffness	4E6	4E6	kN/m^3
K_s, Shear stiffness	100	5E5	kN/m^3
c_{ref}, cohesion	2	1000	kN/m^3
Φ, friction angle	1	48	°
Tensile strength	0	500	kN/m^2
Consider gap closure	Yes	Yes	

5.2.4 Degradation of temporary supports

Modelling of degradation of the jet grout and primary lining will be performed with stepwise material reduction, or direct complete degradation. From the literature review, tests on soil-cement mixes showed that when residual values are achieved, the subsequent degradation process is negligeable. No approaches in literature have been found that consider the degradation of jet grouting. In this case study the goal of this degradation modelling is to look at the transfer of forces to inner structures and investigate the possibility of considering temporary supports with a certain structural contribution. Three different numerical degradation approaches are used in this study:

- Simulate a stepwise degradation of jet grout with Mohr-Coulomb model.
- Simulate a stepwise degradation of jet grout and sprayed concrete with a user-defined soil model with a Mohr-Coulomb failure criteria.
- Switch the jet grout material or sprayed concrete material back to moraine properties with the Hardening Soil model and keeping the unit weight of the concrete material.

Considering that design criterions of projects normally state the allowed long-term contribution of temporary supports, an appropriate way to find internal forces would be by a degradation process to redistribute stresses. For stress transfer the friction angle could be reduced, but this is neglected in this analysis since the friction angle is being approximately derived from moraine properties. The degradation process of the jet grout applied in this study can be seen in the Table 5.10.

Table 5.10: JG2 stepwise degradation.

Degradation factor JG2	E	G	v	c’	Friction angle
1	800E3	320E3	0.25	950	40
0.5	400E3	160E3	0.25	475	40
0.2	160E3	64E3	0.25	180	40
0.1	80E3	32E3	0.25	90	40
0.01	80E3	32E3	0.25	10	40

Degradation with the Mohr-Coulomb model will consider a reduction of Young’s modulus and cohesion. The second approach will adapt a user-defined soil model based on a Mohr-Coulomb model. The UDSM can disrupt equilibrium and induce a redistribution of stresses based on the new elastic stiffness. The model is created by the thesis supervisor Gustav Grimstad. Using Mohr-Coulomb model embedded in Plaxis, the strength capacity should be surpassed for stress distribution to occur. As a result, only plastic behaviour controls the stress transfer. The user-defined model will be able to re-distribute the stresses in terms of total elastic stiffness (elasticity using total strains rather than incremental strains) and a plastic behaviour. The final approach of degradation is to

consider the temporary supports completely degraded to the initial Hardening Soil model used for the moraine, but with increased unit weight.

It will be attempted to evaluate the degradation of primary lining using a similar approach as with the jet grout ring. However, since Plaxis use incremental steps, the change of a linear-elastic material will not alter the stress situation in the analysis. Only degradation through the user-defined model and full degradation to the Hardening Soil model will be used for the primary lining.

Table 5.11: Primary lining degradation.

Degradation factor Primary Lining	Elastic modulus, E_{new}	Shear modulus, G_{new}	Shear modulus, G_{old}
1	15E6	6.25E6	6.25E6
0.5	7.5E6	3.125E6	6.25E6
0.2	3E6	1.25E6	3.125E6
0.1	1.5E6	6.25E5	1.25E6
0.01	80E3	33E3	6.25E5

Since the primary lining is modelled as a Linear-Elastic material, a degradation of the material will be performed using the previously mentioned user-defined model. The cohesion is selected high to not consider any plastic behaviour. As a result, only stress transfer due to elastic stiffness reduction will be occur. The shear modulus is featured both with an updated and the previous shear modulus. In this way, Plaxis can re-calculate the stresses based on the updated stiffness.

Important considerations when applying the user-defined model is that it doesn't have knowledge about the initial stresses from initial state. At complete modelled degradation it is likely that the stresses in the volumes are lower than observed in the initial state of Plaxis, which is a source of error. Plaxis models are based on incremental elastic stiffness with incremental strain- and stress. The user-defined soil models, however, calculates the total elastic stiffness related with "total" strain and stress. This is important to consider when evaluating the results, and the methods should be compared.

Analysis of degradation of the sprayed concrete will be performed either with a fully degraded- or with a partly degraded jet grout ring. The purpose of these analyses is to investigate the extent of relaxation provided on the secondary lining if considering a partial structural contribution from the jet grout ring. With the partial degraded jet grout ring the sprayed concrete will be degraded to moraine properties directly.

6 Preliminary 3D analysis

The preliminary three-dimensional analysis will be performed according to specifications in chapter 5.1.5. Simulation of the primary lining is modelled both as a volume element and plate. Results from the analyses will be presented here, to calibrate the convergence-confinement method. Key differences of the four analyses are summarized in the Table 6.1.

Table 6.1: Key elements of the preliminary 3D analysis.

3D Analysis	Primary lining	Modelled tunnel length	Improved advancing core	Excavation phases
Volume lining	Volume	44 m	No	70
Plate lining 1	Plate	44 m	No	70
Plate lining 2	Plate	44 m	Yes	70
Plate lining 3	Plate	88 m	Yes	128

Method used for finding the displacements is to disregard all displacements happening in the process of draining and installing the jet grout ring. This will need to be subtracted from the other displacements. The crown displacements at the advancing excavation face and point of lining installation, are taken from the midpoint of the modelled trajectory from corresponding calculation steps. In addition, crown displacements are extracted from a point close to the start of the modelled excavation for comparison. The location of extraction of displacements are visualized on Figure 6.1. Section A-A from Figure 6.1 is equivalent to modelled midpoint and section B-B is equivalent to length 0.1m at the start of the excavation.

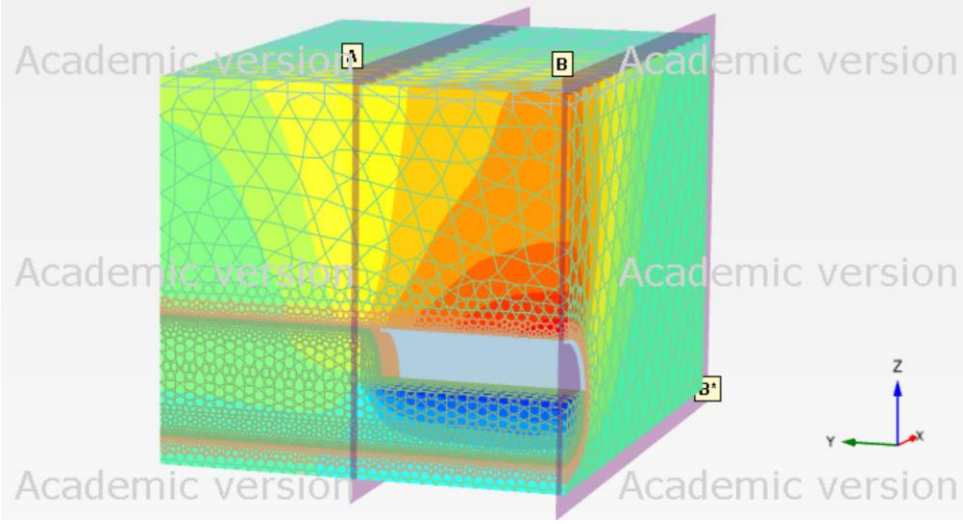

Figure 6.1: Vertical deformations in colouring plot with cross-section visualization.

The different meshes generated in the preliminary 3D-analyses are shown in Table 6.2. Mesh quality is considered sufficient for values of approximately 0.2 for quality spheres tool.

Table 6.2: Preliminary 3D analysis mesh specifications.

Identification	Volume lining	Plate lining 1	Plate lining 2	Plate lining 3
Element distribution	Medium	Medium	Medium	Medium
Coarseness	0.05	0.05	0.05	0.05
Relative element size	1	1	1	1
Element dimension	4.25	4.25	4.25	4.25
Enhanced mesh refinements	Activated	Activated	Activated	Activated
Global scale factor	1.2	1.2	1.2	1.2
Minimum element size factor	5E-3	5E-3	5E-3	5E-3
Elements	539191	39884	39884	63824
Nodes	736579	58904	58904	93465
Jet grout volume refined coarseness	0.3	0.3	0.3	0.25
Internal volume refined coarseness	0.5	0.5	0.5	0.5
Quality spheres min value	0.2	0.244	0.244	0.1839*
Calculation time staged construction	10 hours	1 hour	1 hour	2 hours
Primary lining volume refined coarseness	0.05	NA	NA	NA

* Quality spheres is smaller than 0.2 for only three elements. This is considered to have negligible effect on results.

6.1 Volume lining

Table 6.2 show the specifications of the mesh using volume element as primary lining. The mesh density necessary for a sufficient performance caused the project file to be larger than 30 GB. For this reason, extraction of curves and data from selected points are not feasible with the available computer capacity. Focus will be to compare crown displacements at selected sections with the plate lining configuration. The crown displacement for the volume lining configuration is shown in Table 6.3.

Table 6.3: Crown displacement from 3D simulation with volume primary lining.

Identity	Crown displacement, u_z [mm]
Draining and jet grout* (22 m)	4.25
Advancing face (22 m)	18.11
Lining installation (22 m)	23.79
Total crown displacement (22 m)	39.21
Total crown displacement (0.1 m)	43.02
*	In this table the draining and jet grout phase in not yet subtracted from other displacements.

To avoid issues due to the heavy project file, deformation at face of excavation and at lining installation is extracted from the neighbouring element of the primary lining crown. This is performed with the hint box tool, where information about any points can be acquired manually. A visualization of deformed mesh of the top heading excavation process is shown in Figure 6.2 with a scale of 1:25.

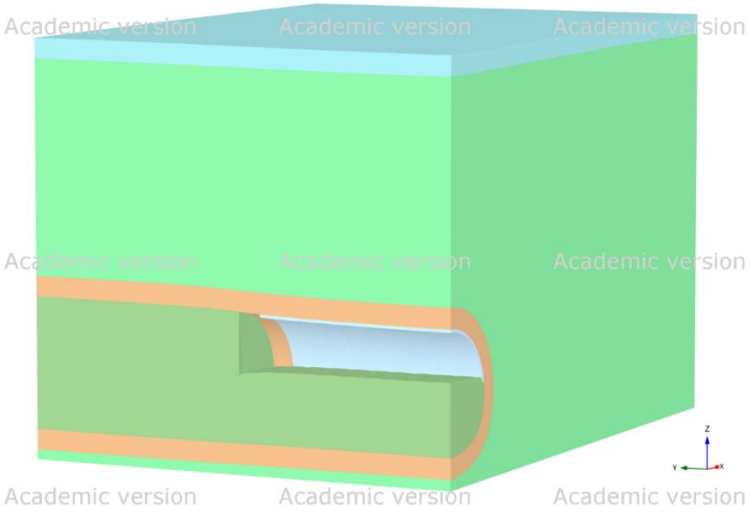

Figure 6.2: Deformed mesh during top heading excavation with volume primary lining.

6.2 Plate lining 1

In this chapter, the 3D analysis is performed with a plate lining without including the improved advancing core. Proper mesh generation is attempted through iteration of different mesh coarseness. The crown displacement for the plate lining 1 configuration is shown in Table 6.4.

Table 6.4: Crown displacement from 3D simulation with plate primary lining.

Identity	Crown displacement, u_z [mm]
Draining and jet grout* (22m)	4.25
Advancing face (22m)	18.57
Lining installation (22m)	23.72
Total crown displacement (22m)	39.88
Total crown displacement (0.1m)	42.85
*	In this table the draining and jet grout phase in not yet subtracted from other displacements.

With a plate lining it is possible to extract curves of the crown displacement to plot a longitudinal deformation profile, since the file is significantly smaller. Figure 6.3 shows a colouring plot of the vertical displacements with top heading excavation at modelled midpoint of the trajectory.

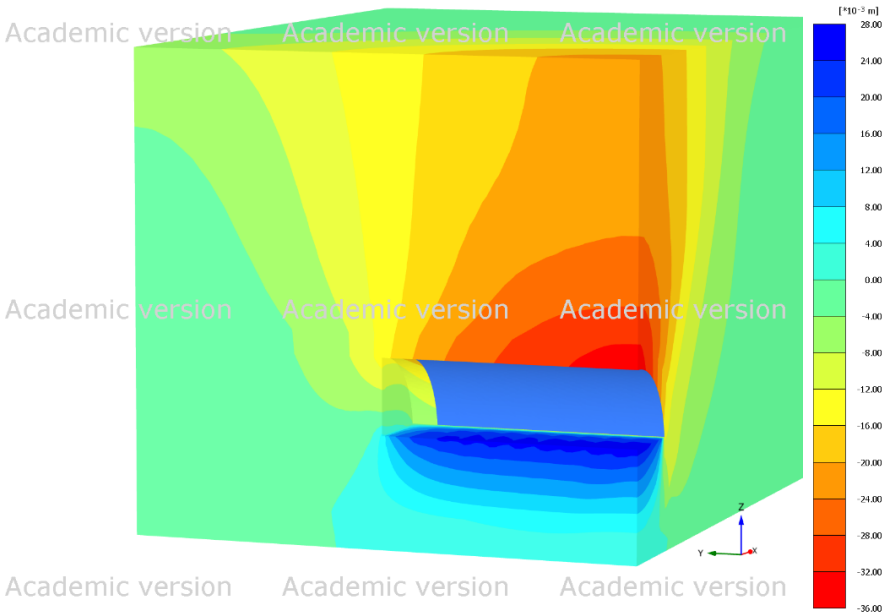

Figure 6.3: Vertical displacement from top heading excavation at 22 m without improved advancing core.

6.3 Plate lining 2

Table 6.2 shows the specifications and generation of mesh using plate as primary lining and accounting for the improved advancing core prior to excavation. Proper mesh generation is attempted through iteration of different mesh coarseness. The crown displacement for the plate lining 2 configuration is shown in Table 6.5.

Table 6.5: Crown displacement from 3D simulation with improved advancing core.

Identity	Crown displacement, u_z [mm]
Excavation face (at 22m)	9.17
Lining installation (at 22m)	15.40
Total crown displacement (at 22m)	35.93
Total crown displacement (at 0.1m)	38.74
*	In this model displacements due to draining and jet grout installation is subtracted from the other displacements.

Figure 6.4 shows coloured plot with the vertical deformation during top heading excavation.

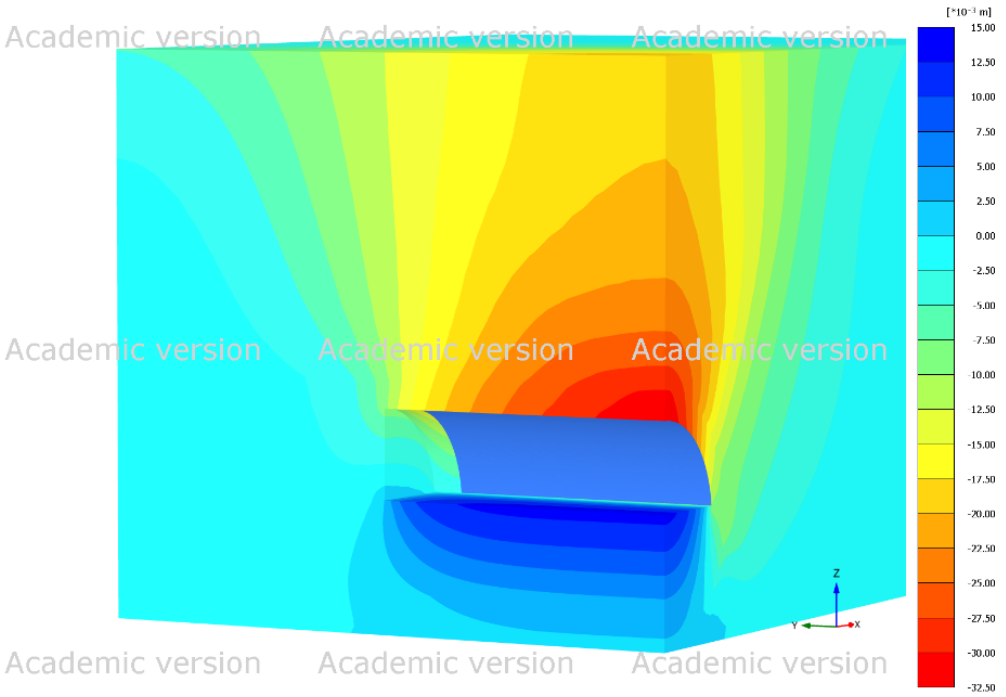

Figure 6.4: Vertical displacements with top heading at 22 m for an improved advance core.

6.4 Plate lining 3

Table 6.2 shows the specifications and generation of mesh using plate as primary lining with improved advancing core. In this analysis, longitudinal length of the tunnel is increased to evaluate a fully developed displacement and gain better understanding the displacements of the modelled start of excavation. This model is increased to perpendicular to the plane model for 88 meters, which increases the computational costs. The crown displacements results are shown in Table 6.6.

Table 6.6: Crown displacement from 3D simulation with improved advancing core.

Identity	Crown displacement, u_z [mm]
Advancing face (at 44m)	9.33
Lining installation (at 44m)	15.45
Total crown displacement (at 44m)	36.21
Total crown displacement (at 0.1m)	41.05
*	In this model displacements due to draining and jet grout installation is subtracted from the other displacements.

The vertical displacements are shown by the colouring plot in Figure 6.5 after complete excavation. The first meters of excavation show a larger variation than what can be seen from the middle section.

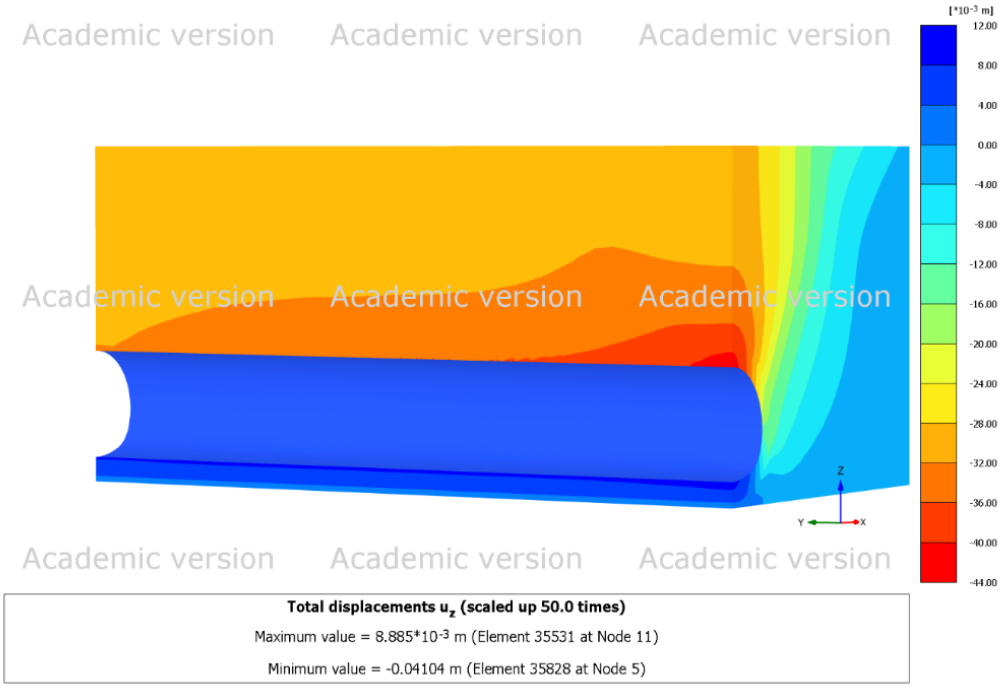

Figure 6.5: Vertical displacements from 3D analysis with enlarged mesh.

The displacements at the midpoint of the tunnel length, at longitudinal length of 44 meters, are presented graphically in Figure 6.6. The corresponding steps referring to the point where the excavation face and lining installation is at the given point is shown in the legend. At final displacements the entire excavation and primary lining installation is completed.

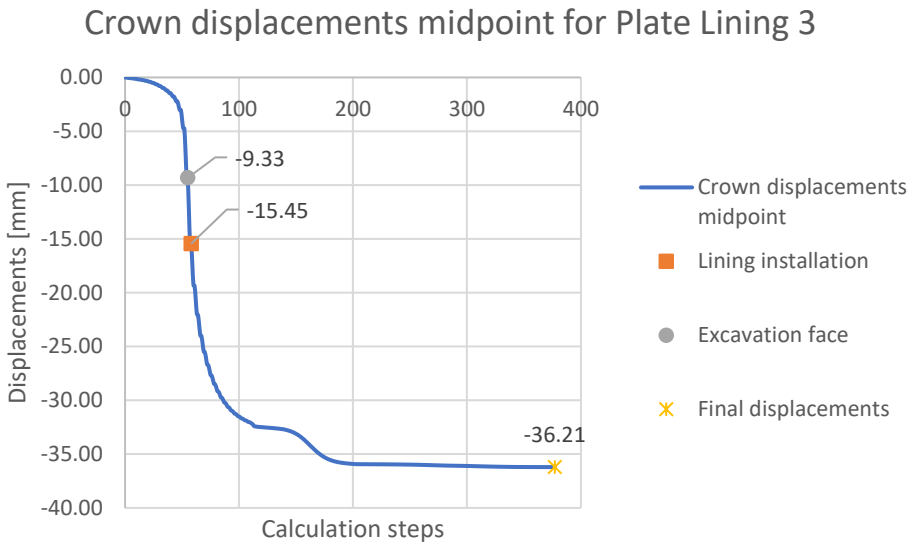

Figure 6.6: Crown displacements from midpoint of 3D-model with enlarged mesh.

6.5 Displacements from preliminary 3D analysis

Modelling the primary lining as volume element and plate gives approximately the same displacements prior to excavation face, displacements during unsupported length and total displacements. The difference can be seen in the Table 6.7 and is negligible for the unsupported length. Crown displacements are also relatively similar.

Table 6.7: Crown displacements for 3D analysis without improved advancing core.

Position	Plate lining 1	Volume lining	Difference
Excavation face	14.32	13.86	-3 %
Unsupported length	19.47	19.54	0 %
Crown [at the middle]	35.63	34.96	-2%
Crown [at the modelled start]	38.60	38.77	-0.44 %

For the subsequent analysis with improved advancing core the crown displacements are shown in Table 6.8. Displacements in the excavation face, the unsupported length and at the middle of the tunnel length is similar. Deviations are largest for the crown displacements at the start of the modelled excavation. Results from the preliminary results will be discussed further in chapter 8.1. Displacements from plate lining 3 configuration will be used to calibrate the 2D analysis.

Table 6.8: Crown displacements for 3D analysis with improved advancing core.

Position	Plate lining 2	Plate lining 3	Difference
Excavation face	9.17	9.33	2 %
Unsupported length	15.4	15.45	0 %
Crown [at the middle]	35.93	36.21	1 %
Crown [at the modelled start]	38.74	41.05	6 %

7 2D analysis

The 2D analysis will investigate the effect of the temporary supports in short- and long term on the secondary lining. The first chapter will investigate the jet grout ring capacity and how the stress distributes for varying jet grout material models. The second chapter consist of a 2D analysis without stress-release to enable comparison of internal forces and stresses with the converge-confinement method. The third chapter involves using the preliminary 3D analysis to calibrate the convergence-confinement method in 2D and consider both sequential excavation and arching effect.

7.1 Jet grout ring capacity

The jet grout ring capacity will be evaluated with a straight excavation method, without accounting for stress release due to excavation process and lining installation. It is assumed that all excavation is performed in a one-step manner since the primary lining is not included. The mesh is produced with very fine settings, in addition to using locally refined coarseness of the jet grout ring of 0.1. Internal soil elements are locally refined to 0.5 coarseness. Mesh consists of 5417 elements and 43623 nodes. No homogenized improved ground in the tunnel cavity is considered since it will be fully deactivated in one step.

Table 7.1: Methodology of 2D analysis on the jet grout ring.

Model	Support	Purpose and measuring.
JGLE	Jet grout ring with a Linear-Elastic model with characteristic parameters.	Extract crown displacement and forces in jet grout ring. A check of the structural integrity.
JG1	Jet grout ring with Mohr-Coulomb design model.	Extract crown displacement and forces in jet grout ring. A check of the structural integrity.
JG2	Jet grout ring with Mohr-Coulomb characteristic model.	Extract crown displacement and forces in jet grout ring. A check of the structural integrity.
JG3	Jet grout ring with Mohr-Coulomb average model.	Extract crown displacement and forces in jet grout ring. A check of the structural integrity.
JG1_R	Jet grout ring with a reduced Mohr-Coulomb design model.	Reducing cohesion by a factor of 0.4 and 0.6.

Figure 7.1 show the mesh generated for the analysis. The density of the stress points generated in the volume are shown and is regarded as suitable for an integration tool to calculate the internal forces. *Structural forces in volume plates* will create a centreline along middle of the jet grout and integrate the stress points perpendicular to the line.

Model mesh for jet grout ring capacity analysis

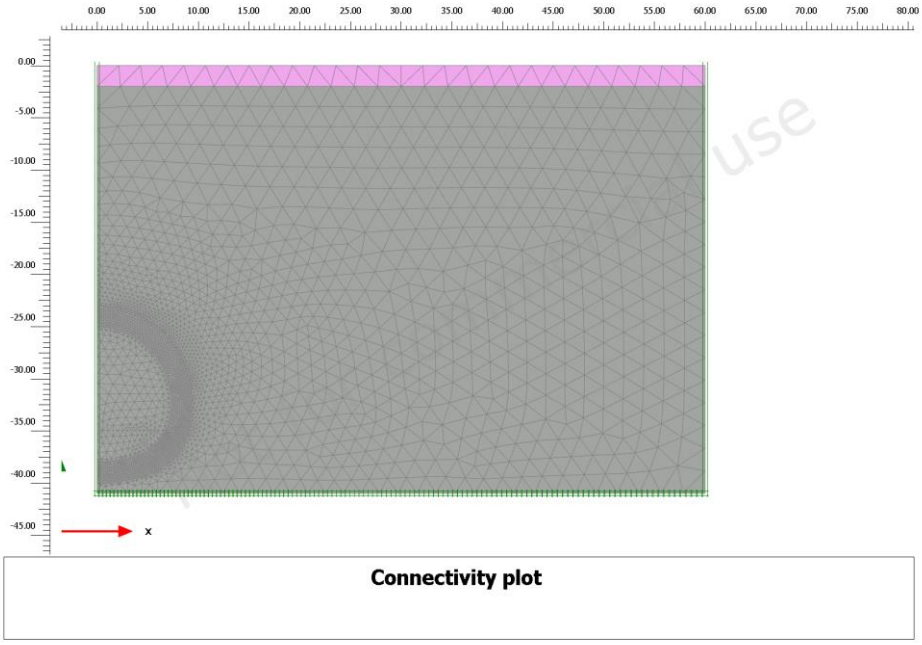

Stress points in the jet grout volume

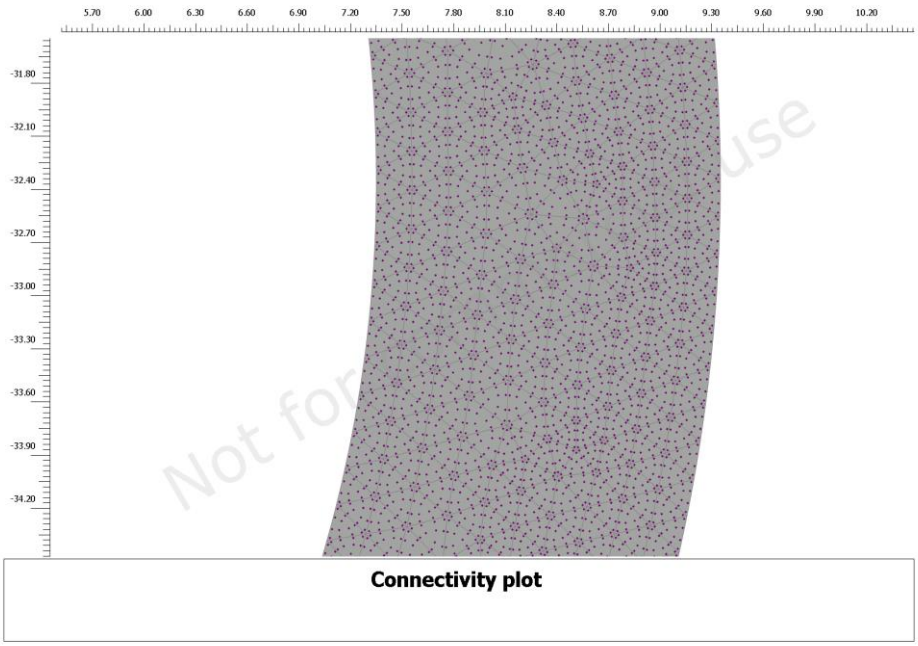

Figure 7.1: Mesh and stress points for the jet grout ring.

Figure 7.2 show calculation phase 2 and 3 for the JG1 configuration. The calculation phases used for the investigations is as follows:

1. Initial phase with a K0-procedure to establish initial stress situation.
2. Installation of the jet grout ring and draining of the cavity. The drained cavity extends to the extrados of the jet grout ring. Different calculation phases for varying jet grout parameters are used.
3. Full excavation of the cavity starting from the different jet grout phases. Displacement and internal forces are extracted. Since there are four different jet grout materials, four different excavation phases are used.
4. Calculation phase 4 is only applied for the reduced JG1 parameters. This phase is subsequent to calculation 3 with JG1. Here the JG1 cohesion is reduced by 40- and 60% to investigate if convergence is reached.

Phase prior to excavation

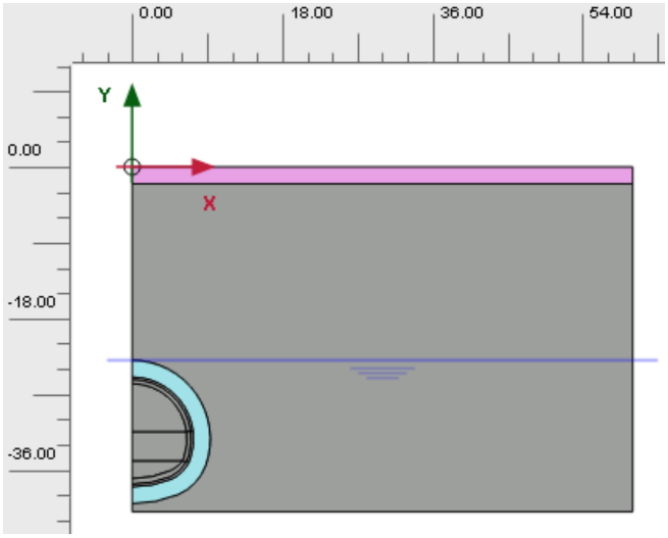

Complete one-step excavation

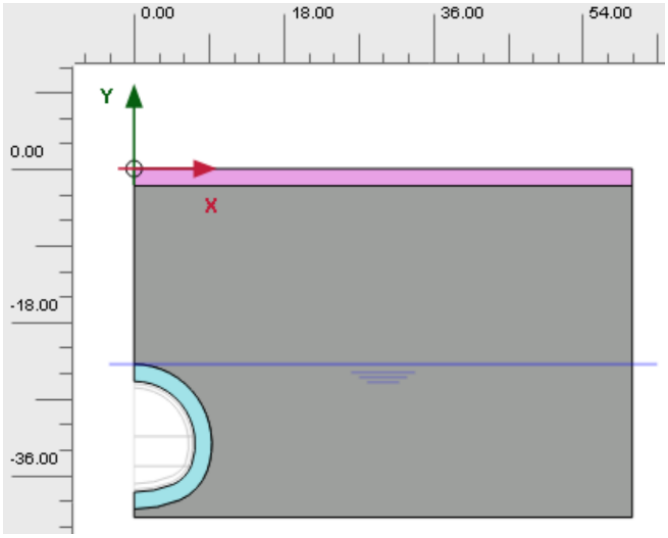

Figure 7.2: Modelling procedure for jet grout ring capacity.

7.2 Straight excavation method

To evaluate upper limit structural forces a straight excavation method is used. As found in literature this method does not consider any stress release or early-age strength of concrete prior to excavation. In practice this approach neglects all deformations happening prior to lining installation, unsupported length and creep deformations. According to literature this method should yield high stresses on the structural elements and yield unrealistic internal forces in the structure. Material model used for jet grout ring is JG2 with characteristic values. The homogenized improved ground is modelled in the tunnel cavity.

Table 7.2: Staged construction procedure with SE in Plaxis 2D.

Scenario	Support	Purpose and measuring.
SE1	Secondary lining wished-in-place with draining. Slip surface between lining and moraine to simulate sheet membrane.	Extract internal forces and compare with the converge-confinement method.
SE2	DSL. Secondary lining and primary lining directly with draining. Slip surface between linings.	Extract internal forces and compare with SE3.
SE3	CSL. Secondary lining and primary lining directly with draining. A bonded surface between linings.	Extract internal forces and compare with SE2.

The calculation phases used are as follows:

1. Initial phase with a K0-procedure to establish initial stress situation.
2. Full excavation of the tunnel with wished-in-place activation of the lining(s). Interfaces are activated with lining(s).

The purpose of these simulations is to show the internal forces in the structure without accounting for stress-release or temporary supports. SE1 will be used to evaluate the final forces acting on the secondary lining compared to the convergence-confinement method. SE2 and SE3 are performed to evaluate the difference in internal forces between a slip surface and a bonded membrane. The mesh established in the straight excavation method is equivalent of that used in chapter 7.3 shown in Figure 7.4.

7.3 Convergence-confinement method

To get realistic deformations, a stress-release to account for pre-convergence and unsupported length is attempted. This procedure is simplified by solely calibrating the crown displacement prior to lining installation. Deformations from preliminary 3D analysis will be compared to this approach. Calibration of the deconfinement parameter is performed with the following results from chapter 6.5 with an improved advancing core and enlarged mesh:

- Crown displacements at excavation face: approx. 9 mm.
- Crown displacements at lining installation: 15.4 mm.
- Crown displacements at complete analysis: 36 mm.

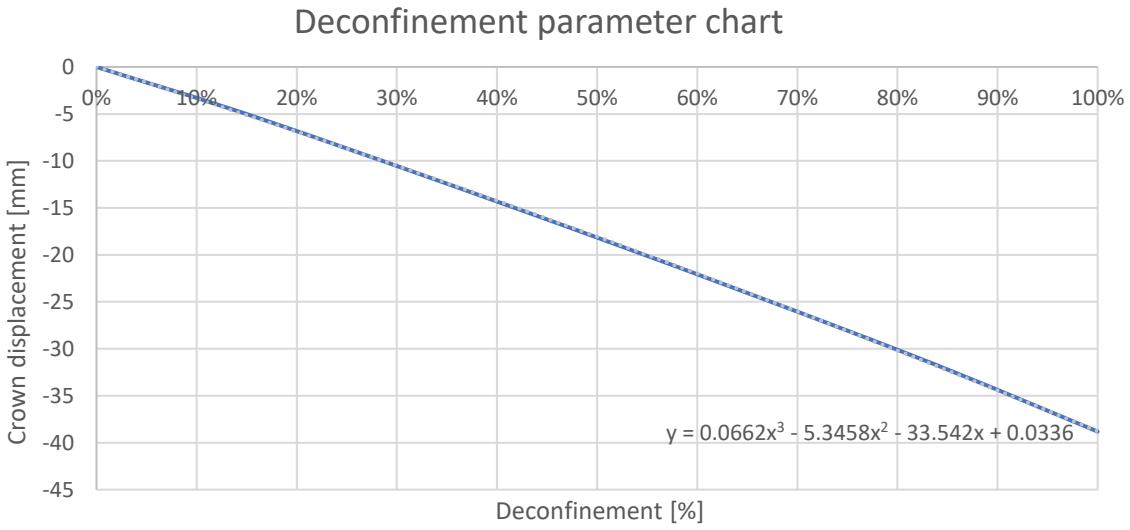

Figure 7.3: Calibration of deconfinement parameter.

Figure 7.3 shows a graph of deformation of the top heading for a complete unsupported excavation stage in Plaxis 2D with JG2 activated. The percentage is ∑Mstage, which is equivalent to the deconfinement parameter. Solving the equation in the chart for 15.4 mm pre-convergence results in a 42.87% deconfinement parameter. This parameter will be used to perform the two-dimensional analysis with the convergence-confinement method. As a simplification the same deconfinement parameter will be applied to the bench and invert.

The mesh elected for the 2D model is set to very fine with 0.03 global element coarseness. The primary lining volume, secondary lining volume and jet grout volume are all locally refined to 0.1 coarseness. The tunnel cavity is locally refined with 0.5 coarseness. The mesh generated consists of 8071 elements and 65420 nodes. The amount of stress points in the volume elements are considered sufficient to use an integration of stress points to generate internal forces. Lowest quality of the mesh in the tunnel designer volume is 0.5173, which is considered sufficient. The generated mesh and quality can be seen in Figure 7.4 and Figure 7.5.

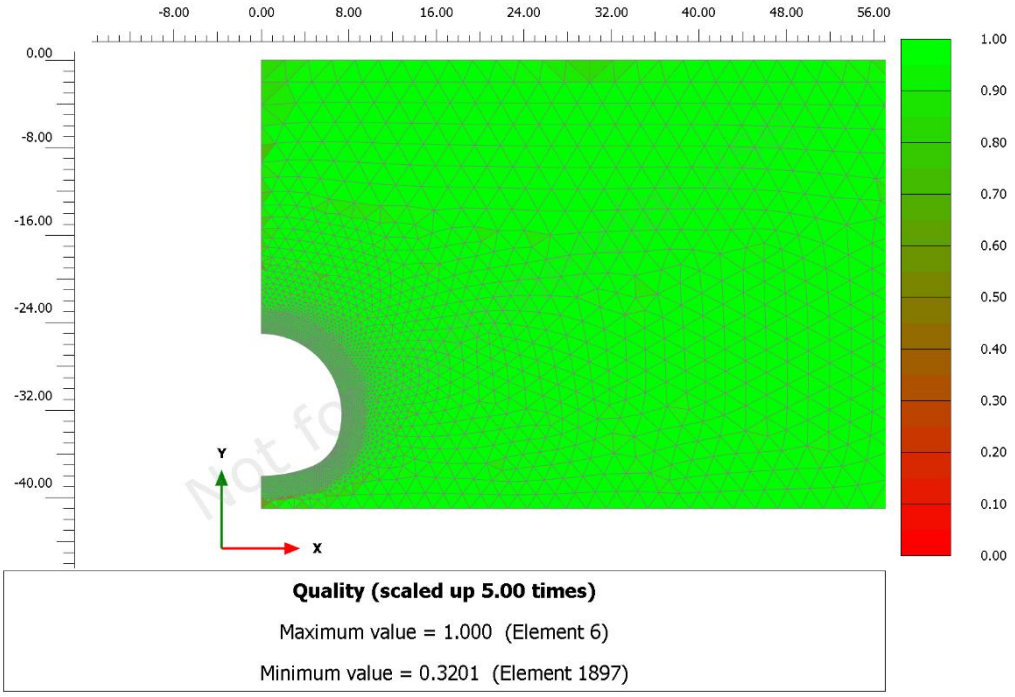

Figure 7.4: Model geometry and quality of mesh for 2D analysis.

The meshed volumes that will simulate the tunnel cavity, jet grout ring, primary and secondary lining are shown in Figure 7.5. The plot is normalised from 0.5173 to 1, so the red elements shown in the figure are not necessarily of poor quality.

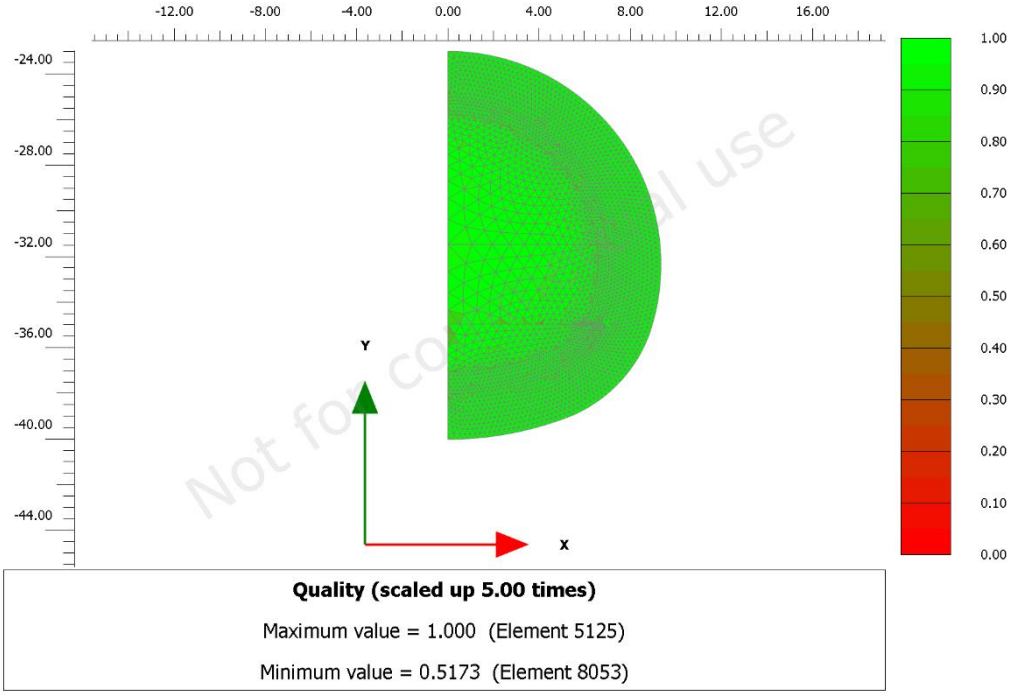

Figure 7.5: Mesh quality of the tunnel designer volumes.

The modelled excavation stages are shown in Table 7.3. The scenarios are explained to provide information of the procedure and the purpose of the stages.

Table 7.3: Staged construction procedure with CCM in Plaxis 2D.

Phase stage	Support	Purpose and measuring.
Top heading	Relaxation of top heading	Extract internal forces and displacements.
Top lining	Early-age top heading primary lining activated.	Extract internal forces and displacements.
Bench	Relaxation of bench. Top heading primary lining hardened.	Extract internal forces and displacements.
Bench lining	Early-age bench primary lining activated.	Extract internal forces and displacements.
Invert	Relaxation of invert. Bench primary lining hardened.	Extract internal forces and displacements.
Invert lining	Hardened invert primary lining activated. Full primary lining installed.	Extract internal forces and displacements.
DSL	Activation of secondary lining and lining interface with slip surface properties.	Extract internal forces and interface stresses.
DSL_JG	Stepwise or full degradation of jet grout ring with MC-, UDSM- or HS-models.	Extract internal forces.
DSL_JG_SC	Stepwise or full degradation of sprayed concrete with UDSM or HS-model, starting from a fully or partially MC degraded jet grout ring.	Extract internal forces.
CSL	Activation of secondary lining and lining interface with bonded properties.	Extract internal forces and interface stresses.
CSL_JG	Stepwise or full degradation of jet grout ring with MC-, UDSM- or HS-model.	Extract internal forces.

8 Main results and discussion

This chapter covers the main results from the analysis and discussion of the results. It is presented as main results since results from the preliminary 3D analysis already have been presented in chapter 6, for calibration of the convergence-confinement method. The displacements from the preliminary 3D- and calibrated 2D analysis will be displayed and compared. It is common to perform tunnel lining design with moment and thrust interaction diagrams. For this reason, most of the resulting internal forces are displayed with moment and thrust distributions that have been integrated from stress points for a given calculation phase. The terms thrust and axial force is equivalent.

8.1 Preliminary 3D analysis

8.1.1 Results

The results from the preliminary 3D analyses show final vertical crown displacement at the middle of the modelled trajectory of approximately 36 mm. The model with an enlarged mesh show that the final crown displacements at the middle of the trajectory does not increase significantly by the enlarged mesh.

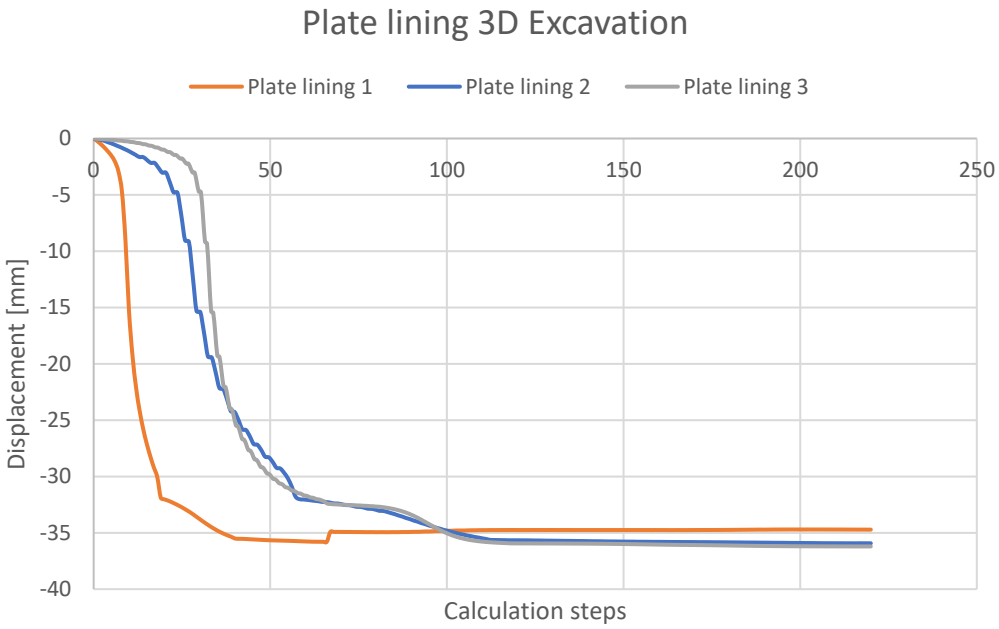

Figure 8.1: Crown displacements at midpoint of the tunnel length.

According to the four different 3D analyses from Table 6.1, the blue and grey lines from Figure 8.1 represent the models with a homogenized improved advancing core. The graph shows significantly less pre-convergence for this model, than the model without accounting for the improved advancing core. The graphs have different calculation steps, which does not leave a fully accurate representation. This fault can be seen from lacking overlapping of the blue and grey lines. The representation is however, considered good

enough to show the difference in cavity convergence rate. After full excavation it can be shown that both models seem to converge on a relatively similar total displacement.

Figure 8.2 show vertical displacement extracted from midpoint of the modelled mesh for Plate lining 3. The displacements from the surface are from a point directly above the tunnel centreline, while the boundary displacements are taken from surface level at the vertical boundary of the modelled midpoint of tunnel trajectory. Results are displayed to enable a validation of the mesh size, and to be able to evaluate potential interference due to the boundary conditions.

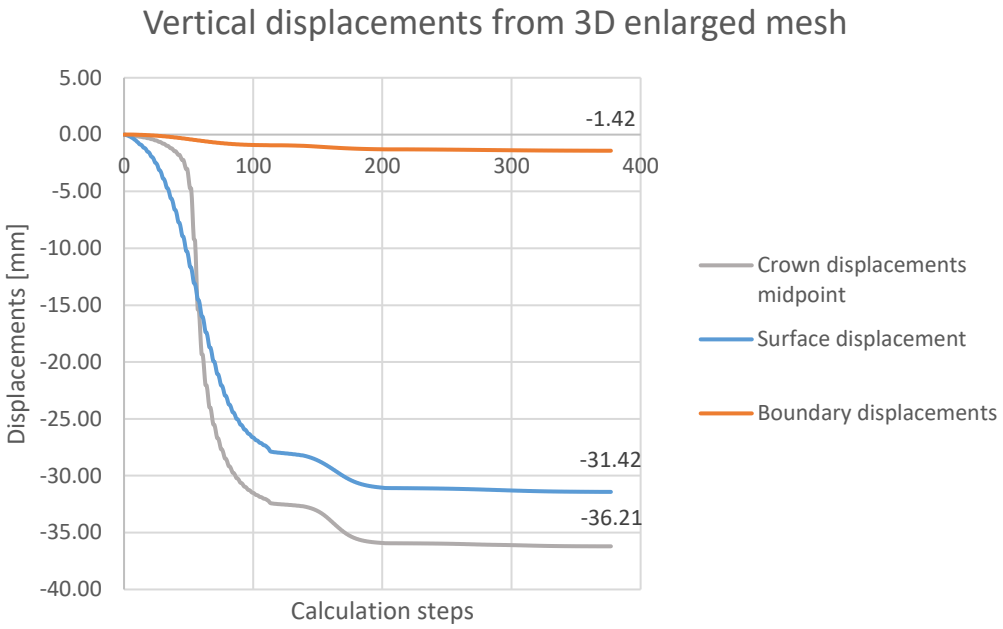

Figure 8.2: Vertical displacements from 3D enlarged mesh.

After the top heading- and complete excavation, the axial force acting on the primary lining at the middle of the trajectory is shown in Figure 8.3. These axial forces can be used for comparison and verification of the 2D analysis.

1: Top heading fully excavated

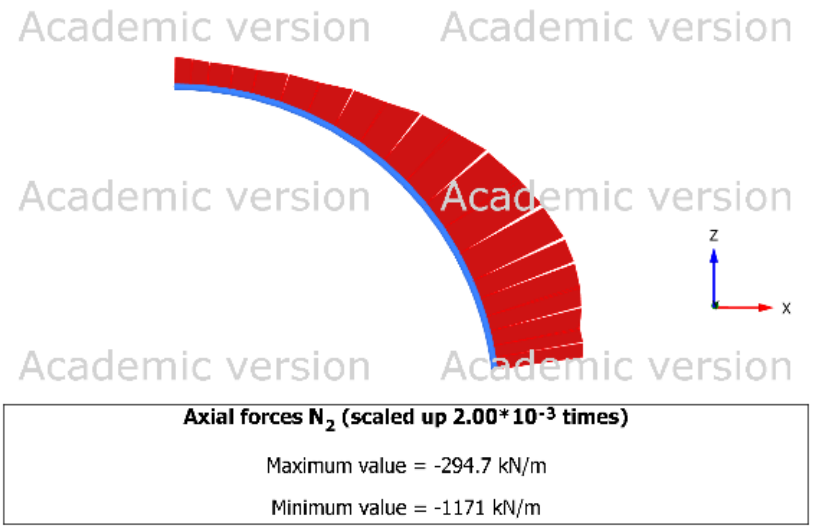

2: Primary lining fully installed

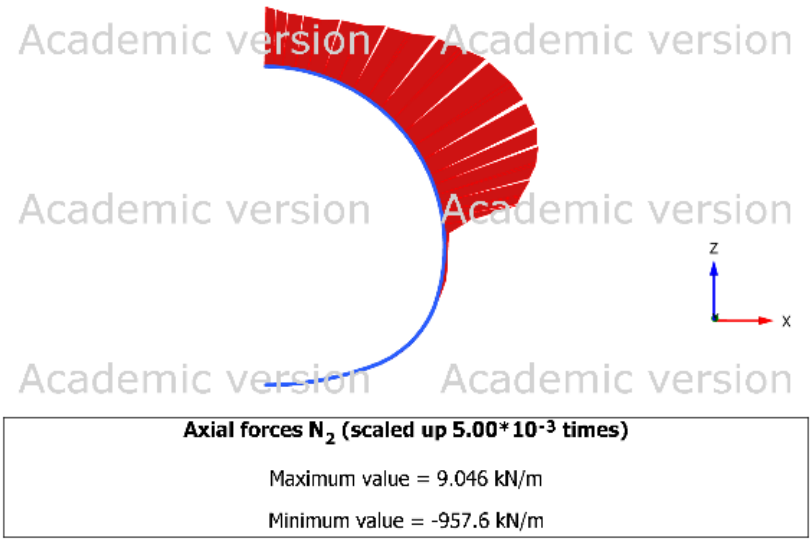

Figure 8.3: Axial force distribution for the primary lining in 3D.

8.1.2 Discussion

The preliminary analysis shows a relatively large difference of displacements happening ahead of the excavation face with an improved core as opposed to an analysis without an improved advancing core. The improved advancing core due to jet grout columns, reduce the pre-convergence by 34.3% compared to neglecting the jet grout columns. The difference in values for the Plate lining 1 and Plate lining 3 are shown in Table 8.1.

Table 8.1: Pre-convergence crown displacements difference.

Analysis	Crown displacements [mm]
Plate lining 1	14.2
Plate lining 3	9.33
Difference	-34.3%

The total crown displacements at the middle of modelled trajectory are for all the 3D analyses within 35-36 mm. It is therefore considered reasonable that that these are the most accurately developed displacements for the model. The higher total displacements shown at the start of the modelled tunnel advancement are likely caused by lack of arching effect, since the first excavation starts from the initial stage. In a full-scale model, deformation would already have happened at this point due to the previous tunnel excavation. For this reason, the crown vertical displacements at the midpoint of the model are considered most accurate.

Since the numerical model neglects lattice girders, wire mesh, elephant foot and applies a hypotethical modulus of elasticity, it is likely to produce higher deformations than in-situ measurements. At the time of this study, the measured displacements from the project are averaging below 10 mm for both surface and crown displacements after excavation, as shown in chapter 4.8. Since the excavation process is not completed, the fully developed displacements cannot yet be determined. No information on the pre-convergence of the cavity is given. The measured displacements could indicate a stronger homogenous nature of the jet grout ring than the characteristic values applied in the analysis. This assumption is strengthened since no significant water ingress was experienced during excavation. It is assumed that higher water ingress would be observed if large deficiencies existed in the jet grout ring.

The jet grout columns are simulated through a homogenized improved ground. If modelled as individual full-strength jet grout columns with real centre-distance, a different pre-convergence could occur. Modelling the columns directly was attempted. With this method the meshing process produced very small triangular elements. It is assumed that these long and small elements can lead to numerical issues, even with a densely refined mesh. Due to the curvature of the columns that intersected with a curved tunnel boundary, a meshing problem occurred. Several attempts were made, but it was eventually concluded that a full modelling of the columns was not feasible. Access to higher computational capacity may provide opportunities for further investigation of this specific problem.

To avoid a convergence failure due to instability at the face of the excavation, a displacement surface was used for the face. The effect of not allowing any displacements in the tunnel direction, could produce some differences compared to an in-situ situation. The method is however an effective approach and can reduce the instability issue of collapse that would otherwise occur in the numerical model. Alternatively, the 50 mm sprayed concrete at the face could be modelled with higher computational costs.

In any case, the difference of pre-convergence shown in Table 8.1 is important in terms of finding design stress states in plane strain models. With a smaller pre-convergence the modelled deconfinement prior to lining installation will be lower, which will assumingly cause higher stresses to develop in the sprayed primary lining. Without accounting for the improved advancing core when using the convergence-confinement method, the primary lining may be designed for lower stresses than what could theoretically occur.

8.2 Jet grout ring capacity

8.2.1 Results

The results of the jet grout ring analysis show the difference between the constitutive models for the jet grout. All non-reduced configurations reached a stable convergence. Figure 8.4 shows total crown displacements of the excavation stage for each jet grout constitutive model. Negative displacements indicate movements towards the cavity. The linear-elastic model with same parameters as JG2 shows identical values to the Mohr-Coulomb model for all extracted results and the lines are therefore overlapping.

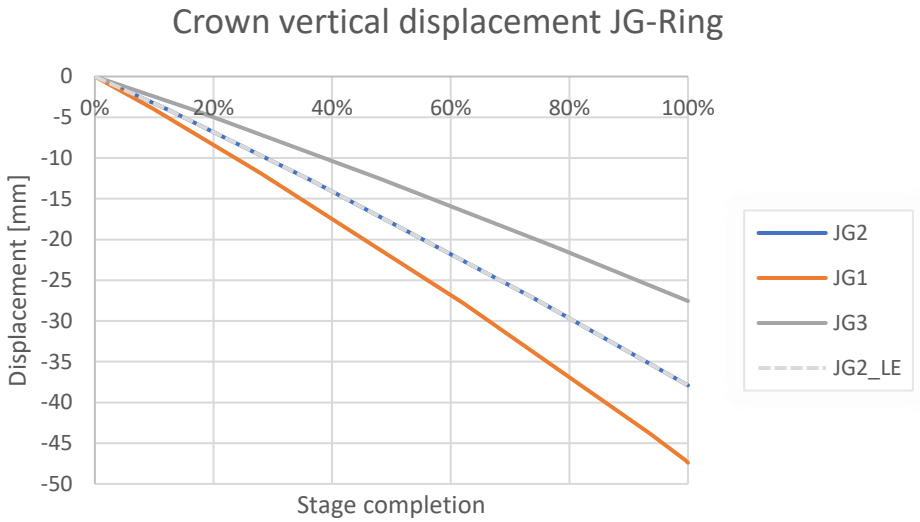

Figure 8.4: Crown displacements of straight excavation of jet grout ring.

Table 8.2 shows the difference in crown displacements between the models from the analysis. JG2 represents the characteristic values of jet grout and serves as reference for the other models.

Table 8.2: Crown vertical displacements from straight excavation with jet grout ring.

Jet grout model	Vertical displacement [mm]	Difference
JG2	-37.91	0 %
JG1	-47.40	25 %
JG3	-27.55	-27 %

In addition to crown displacements, the horizontal displacement of the wall is extracted for each configuration. The location of the node separates the bench and top heading at jet grout intrados. The diagram shows horizontal displacements with regards to the calculation progress in Plaxis, ΣMStage.

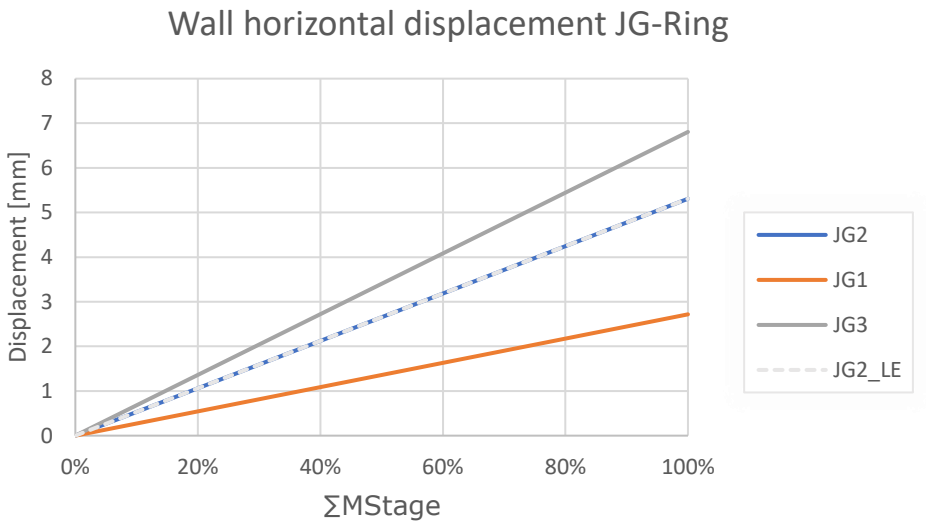

Figure 8.5: Wall displacements from straight excavation with jet grout ring.

Table 8.3 shows the different displacement between the models following this method. JG2 represents the characteristic values of jet grout and serves as reference for the other models. The horizontal displacements are acting towards the boundaries of the model, away from the centreline.

Table 8.3: Horizontal wall displacements from straight excavation with jet grout ring.

Jet grout model	Hor. displacement [mm]	Percentage difference
JG2	5.31	0 %
JG1	6.81	28 %
JG3	2.72	-49 %

In addition to displacements, structural forces in the ring are extracted using *Structural Forces in Volume Plates*. The values are displayed using an approximate orientation of each integrated point located relatively to the centre of the cavity. With this, 0° represents the lowest point of the invert and 180° symbolizing the crown. A visualization of this is showed in the diagrams.

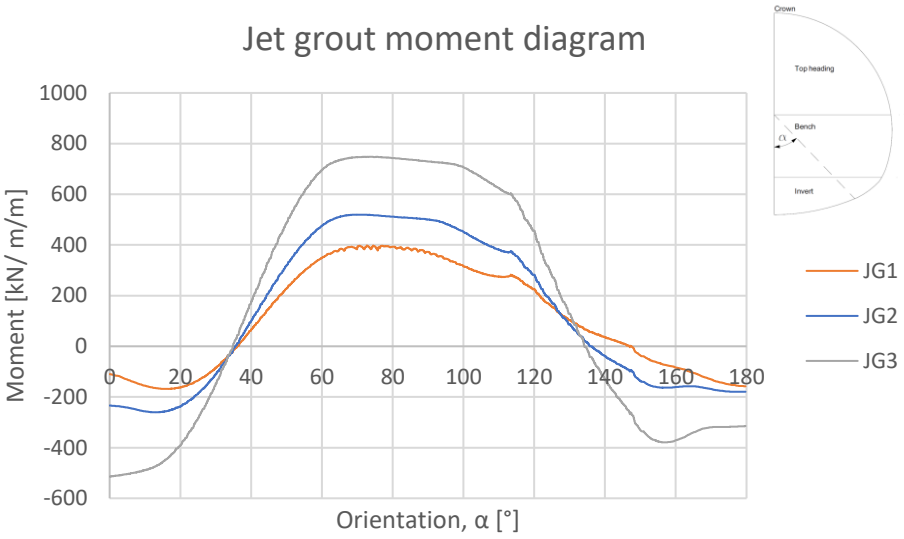

Figure 8.6: Jet grout moment distribution from straight excavation of jet grout ring.

The moment diagram of each model can be seen in Figure 8.6. The moment curves show a similar moment distribution. The Linear-Elastic model is disregarded since it gives the same values as JG2. The thrust diagram is shown in Figure 8.7. The graphical representation from both models show higher thrust forces for a stiffer structure, which directly shows a higher stress concentration in the volume.

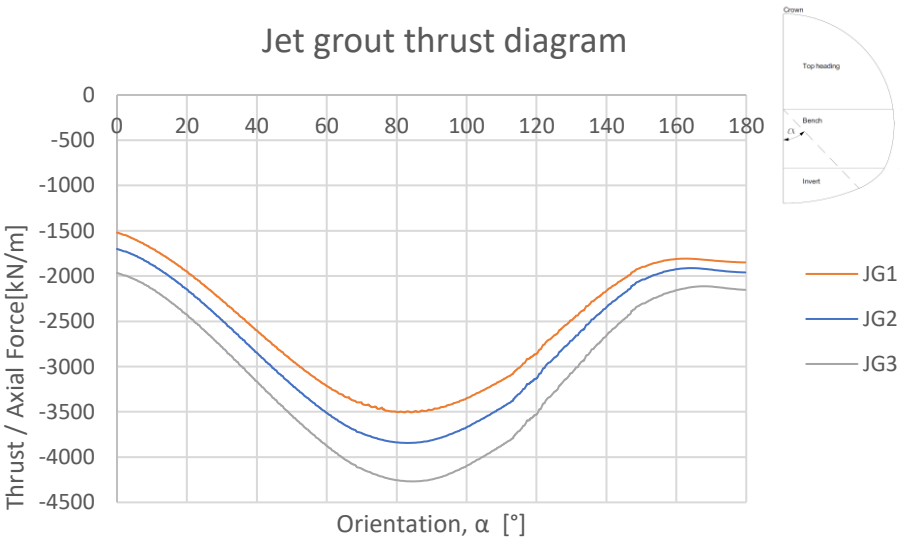

Figure 8.7: Jet grout thrust distribution from straight excavation of jet grout ring

The analysis with reduced JG1 material models both failed to converge. Based on the red failure points in Figure 8.8, a local failure occurred in the ring causing the soil body to collapse. The same failure mechanism happened for the 40% reduced model, which is not shown here.

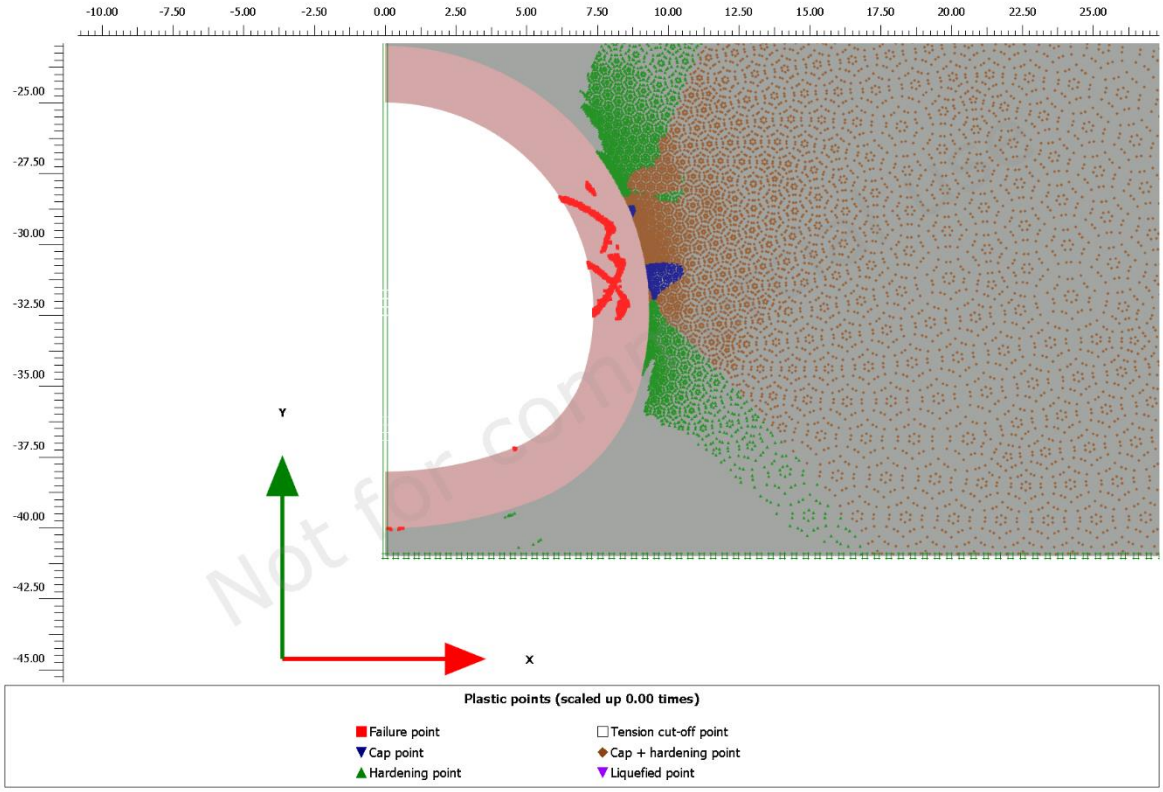

Figure 8.8: Developed plastic points for a 60% reduced cohesion of the JG1 model.

8.2.2 Discussion

Based on the results from the jet grout ring analysis, it can be shown that all constitutive models are theoretically capable of withstanding the full overburden pressure and hydrostatic pressure caused by a full excavation step. The calculations performed in this study does however neglect geometrical imperfections, water ingress and loads such as surcharges and fire. Therefore, the analysis performed here is not enough to verify a safe situation with solely a jet grout ring in the long term.

The crown displacements are higher for the design values of jet grout compared to the characteristic and average values. Results showed 27% reduction in crown displacements between average and characteristic values. The horizontal displacement in the wall increases with a stiffer jet grout model. The horizontal displacements difference was larger than for the vertical crown displacements. This behaviour indicates that increased internal forces resulted in an increased wall displacement.

The moment diagram in Figure 8.6 and thrust diagram from Figure 8.7 are found using *Structural Forces in Volume Plates.* It is important to address that with usage of this tool that integrates stress point, the forces used in design should be compared to other calculation methods. However, in this study the differences in forces are more relevant than actual design, and for this reason other calculation methods are not performed. Simple testing with a "dummy plate" approach have been conducted and reasonable agreements was achieved. The diagrams show that the stiffest jet grout model yields the highest axial force and moments. The result is expected and considered related to the displacements of the jet grout models. Since the stiffness ratio between the ground and the jet grout ring is higher, more of the overburden stress is taken by the jet grout ring.

JG1 – design values

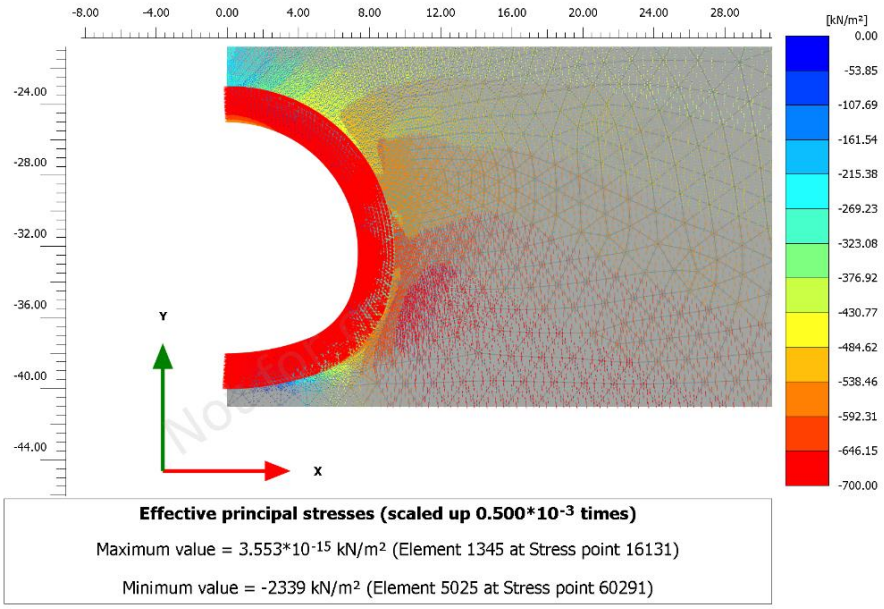

JG3 – Average values

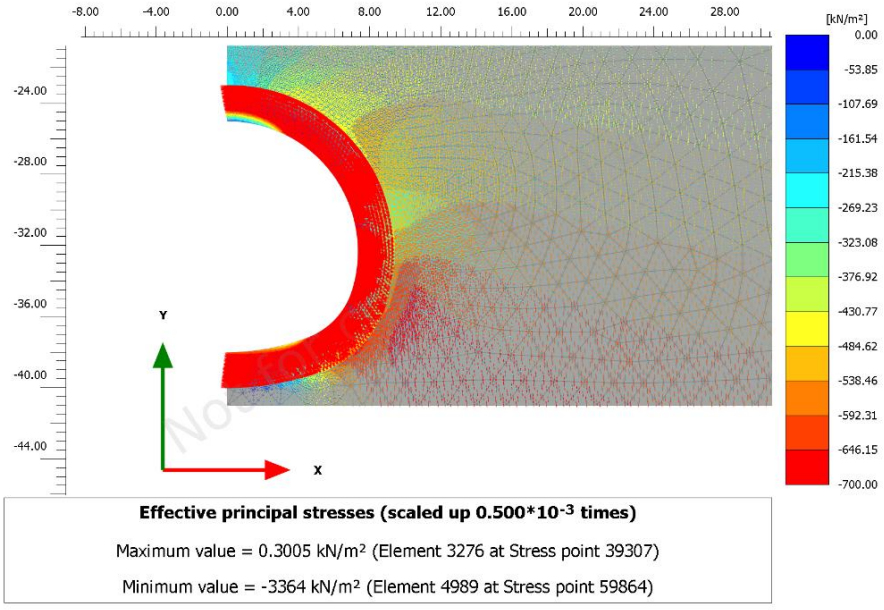

Figure 8.9: Principal effective stress after excavation.

Results from the design value and average value jet grout models are displayed in terms of effective principal stress in Figure 8.9. To be able to evaluate the differences between both constitutive models, the same colouring scale is used for both cases. The model with softer jet ground show higher effective principal stresses around the tunnel extrados. As previously mentioned, this proves that a larger portion of the overburden stress is shared with the ground compared to the stiffer jet grout ring.

The higher stress induced on the stiffer jet grout ring is important to consider for future design of jet grouted support structure. If a degradation of the jet grouted support is simulated to design the permanent structure, it is expected that the stiffer jet grout parameters could transfer higher stresses to the permanent structural system. Future design of similar permanent structures with a degradation method should be simulated with the stiffer material in construction phases. It seems reasonable that design in terms of the deformations should be modelled with a softer jet grout model.

The cohesion of the material model for jet grout used in analysis are based on equations derived from triaxial tests and is likely to differ from the actual in-situ state. Tests performed on the jet grout samples also showed large variations. In addition, the jet grout thickness is modelled at given minimum thickness. The jet grout ring would most likely have an irregular geometry which could be accounted for through probabilistic modelling, which have not been covered in this study.

The hydrostatic load, caused by the groundwater level is expected to yield higher stresses in jet grout ring than the real situation. The actual hydrostatic pressure acting on the ring will depend on the degree of permeability of the jet grout ring, and it is likely that a seeping behaviour occurs through the ring. Due to low water ingress in the excavation process, it’s likely that some water pressure has built up on the extrados of the jet grout ring. This indicates that the jet grout ring serves its purpose in terms of short-term watertightness during excavation.

Analysis performed with reduced cohesion of the jet grout material shows that the design value model does not have a large capacity in terms of shear strength. The reduction performed is not relevant to a realistic situation since primary lining is quickly applied. The parameter study highlights how large stresses in the jet grout wall area, combined with lowered shear strength, yields a failure. Since the real excavation situation is sequential and quickly supported with sprayed concrete, the failure mode observed is not considered realistic.

8.3 Straight excavation method

8.3.1 Results

The straight excavation method was performed with three different configurations shown in Table 7.2. Moment distribution for SE1, where a full excavation with a wished-in-place secondary lining was modelled, is shown in Figure 8.10. The axial force distribution shows an even distribution of compressive axial force throughout the secondary lining. The moment distribution shows an especially large bending moment in the invert.

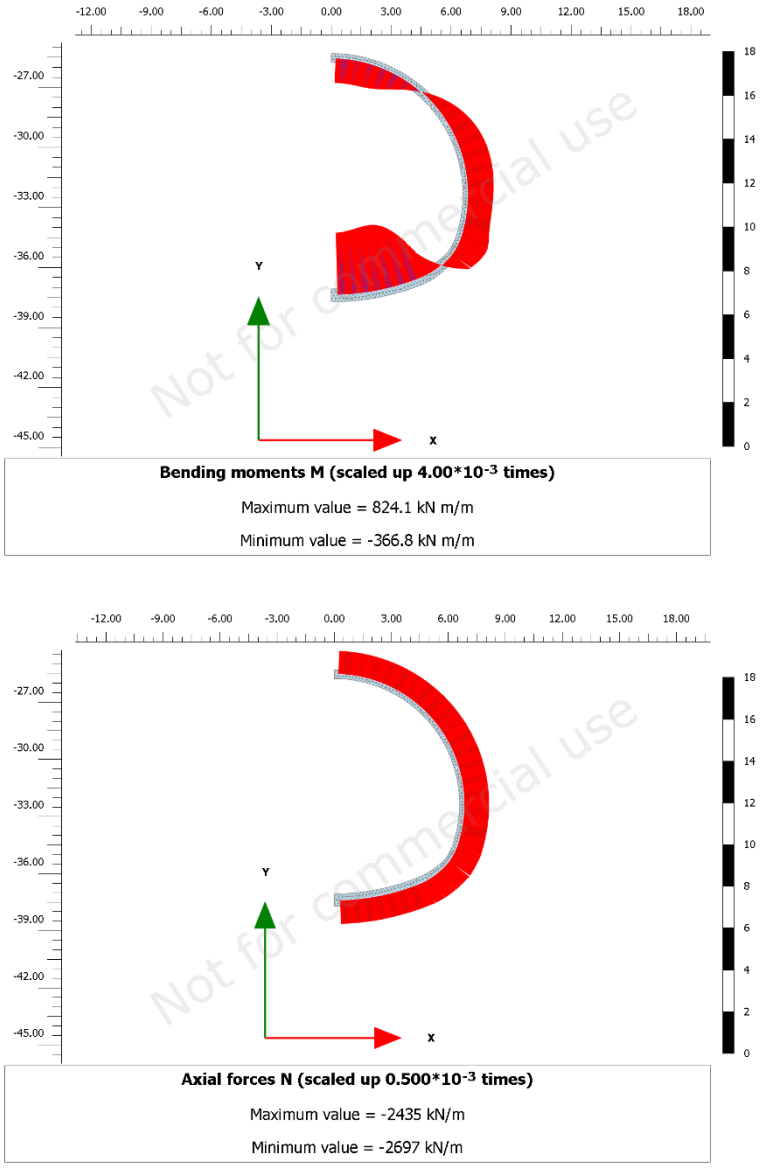

Figure 8.10: Moment and axial force distribution for SE1.

The shear stress acting in the interface can be used to verify the slip surface. The distribution of shear stresses for SE1 can be seen in Figure 8.11.

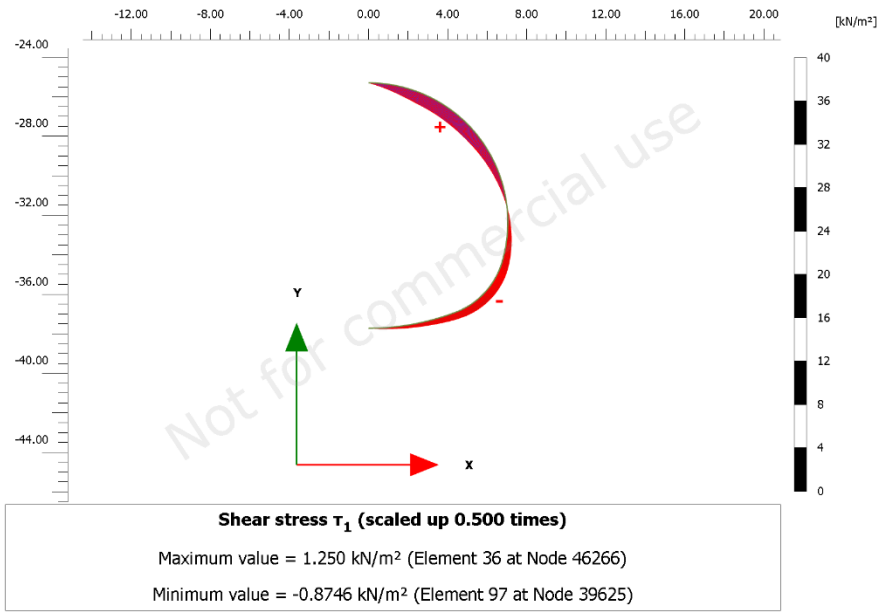

Figure 8.11: Shear stress for interface in SE1.

The three different analyses show different axial force- and moment distributions. The moment distribution for the secondary lining is shown in Figure 8.12. The different configurations are given in the legend. The distributions are similar with slight differences in values.

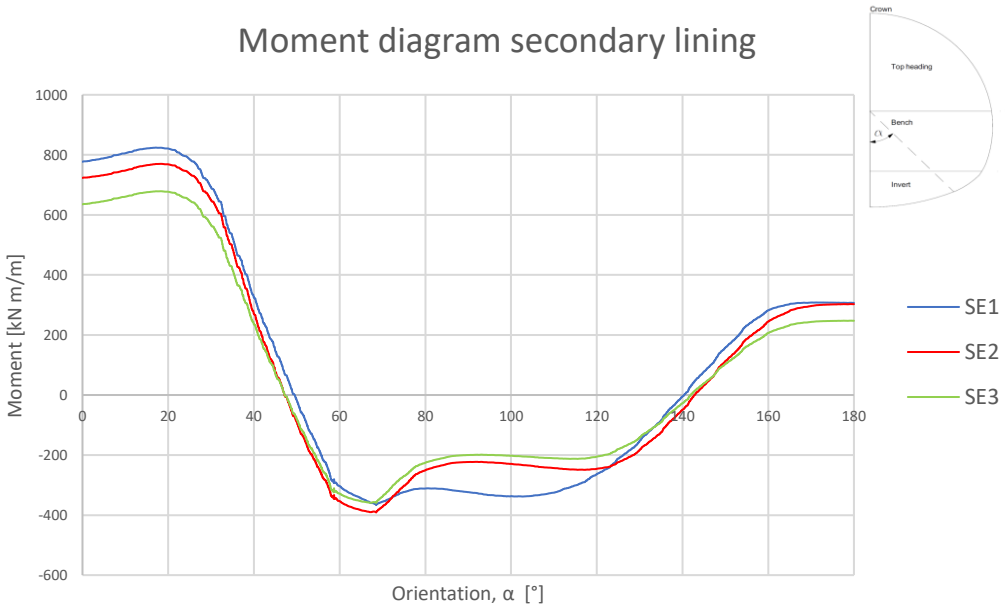

Figure 8.12: Moment distribution in secondary lining for SE method.

The thrust distribution is shown in Figure 8.13. The figures show differences in thrust distributions between the straight excavation configurations. SE1 and SE2 have a similar distribution with SE3 resulting in lower thrust forces because it is shared between linings. SE3 show a different thrust distribution over the orientation.

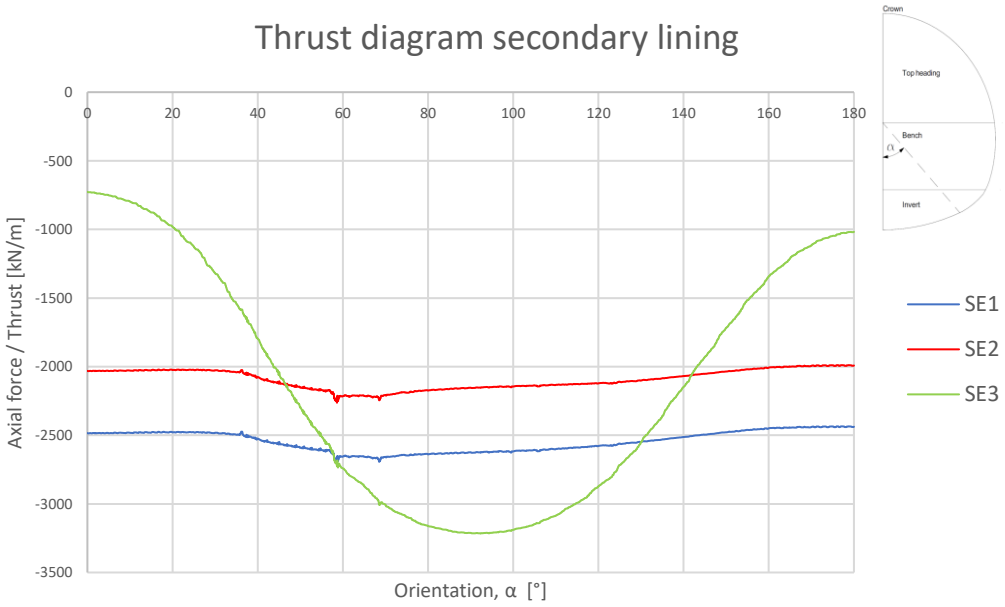

Figure 8.13: Thrust distribution in secondary lining for SE.

The differences in the thrust diagram for the secondary lining can be investigated by looking into the thrust diagram in Figure 8.14 for the primary lining for case SE2 and SE3.

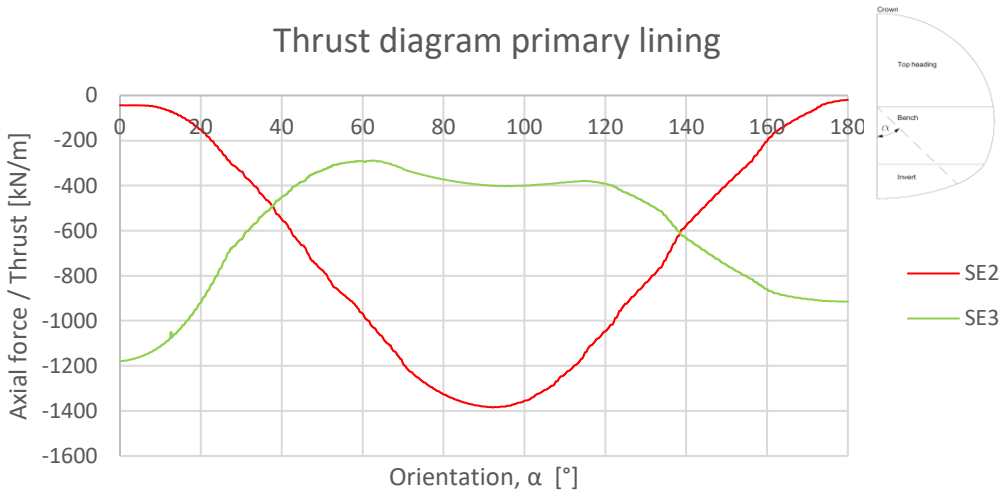

Figure 8.14: Thrust distribution in primary lining for SE2/3.

Figure 8.14 shows a larger axial force in the invert and top heading part of the primary lining for SE3 compared to SE2. When comparing Figure 8.13 and Figure 8.14 the load sharing between the configurations is different due to the shear stresses at the interface.

SE2

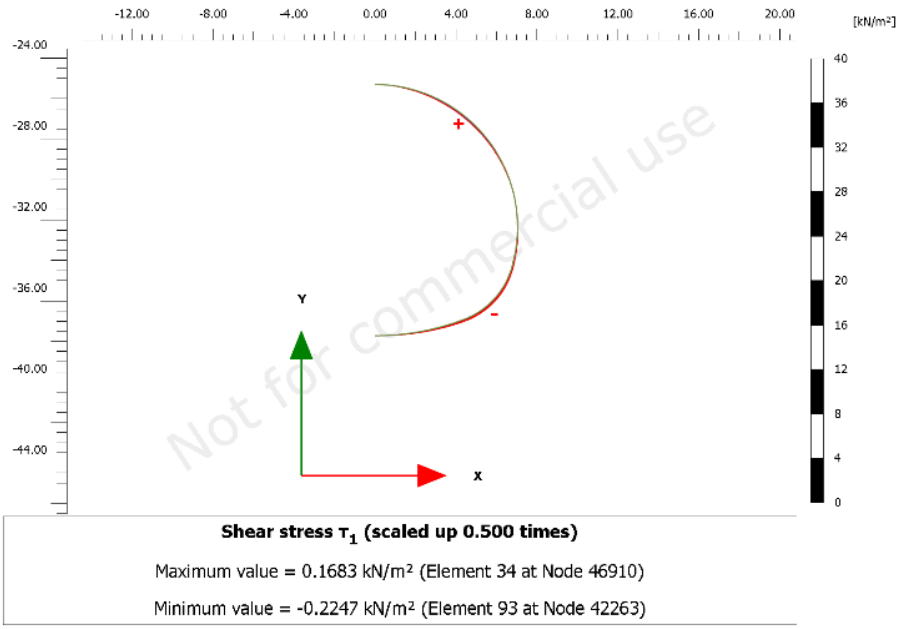

SE3

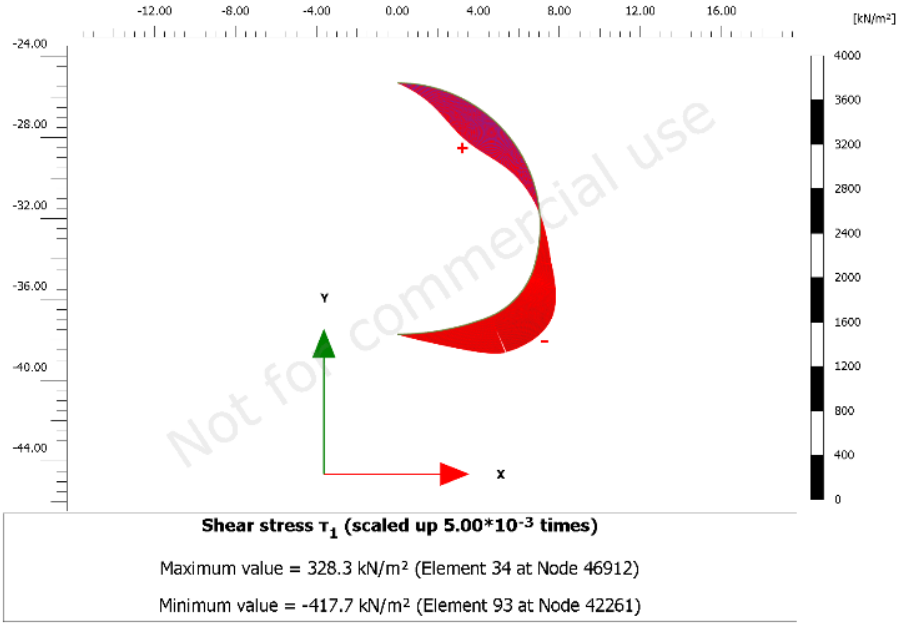

Figure 8.15: Shear stress distribution at membrane for SE2 and SE3.

Figure 8.15 show how the shear stresses are distributed in the modelled membrane between the two lining configurations.

8.3.2 Discussion

The analysis with straight excavation method shows relatively high values for internal forces. Shear stresses in the interface for SE1 from Figure 8.11 confirms that the modelled slip surface experiences low shear stresses. This shows that it can approximate the behaviour of a theoretical frictionless surface. A model with a reduced friction surface that accounts for moraine-lining interaction could have been modelled but is assessed to not describe the actual behaviour. The differences between internal forces in SE1 and SE2 show that most of the stresses from a straight excavation are taken by the secondary lining, which is expected due to the stiffness ratio between the linings.

The composite behaviour observed in SE3 shows lower moments compared to SE1 and SE2, and lower axial force in the invert and top heading. In the bench a higher axial force is observed. In terms of design using a moment-thrust diagram, this is likely to give a more optimized design for the invert and heading. However, the moment combined with the axial thrust in the bench would give a more conservative design. Since design often inherits the worst combination of moment and thrust, no immediate benefits can be shown on the secondary lining design.

8.4 Convergence-confinement method

8.4.1 Displacements

Results

The crown displacements from the 2D CCM is shown in Figure 8.16, which can be compared to the vertical displacements in Figure 8.2. The displacements are considered fully developed at the construction stage when the primary lining is fully installed. With this assumption it is possible to compare the displacements with the preliminary three-dimensional analysis. Surface displacements are smaller than the crown displacements. To verify the boundary conditions, the boundary displacement acting on the surface 60 meters from the centreline is also included in the graph.

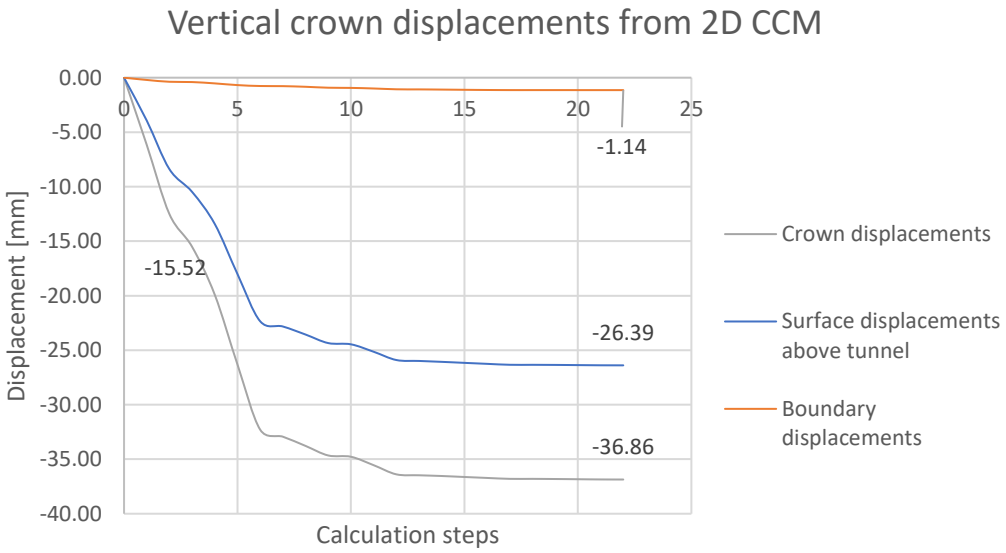

Figure 8.16: Vertical displacements from 2D convergence-confinement analysis.

Discussion

Vertical displacements for the convergence-confinement method compared with the preliminary 3D analysis with enlarged mesh are shown in Table 8.4. The unsupported crown displacements are similar, which is expected since the deconfinement parameter was calibrated from the preliminary 3D analysis. The total crown displacement also shows similar values. Since the displacements are relatively small, being measured in millimetres, the 2D model show comparatively good results. This shows that it is possible to calibrate the 2D model with data from a preliminary 3D model. In terms of stresses, similar crown displacements could indicate that similar stresses will be generated in the linings for both 2D and 3D analysis.

Table 8.4: Comparison of 3D analysis and calibrated 2D analysis.

Position	2D CCM [mm]	3D [mm]	Difference
Unsupported crown displacement	15.52	15.45	-0.45 %
Crown displacement	36.86	36.21	-1.76 %
Surface displacement	26.39	31.42	19.06 %
Boundary displacement	1.14	1.42	24.56 %

In terms of calibrating the stress release, a more thorough method could be performed by looking into the displacement of several points in the intrados of the tunnel. Differentiation of stress release on several points in the tunnel would most likely give more accurate results. The assumption of similar deconfinement parameters of the top heading, bench and lining is also an approximation that could be more accurately performed. The calibration of deconfinement parameter performed in this study was efficient and gave good results in terms of crown displacements. Based on this the method can be applied efficiently in preliminary design. The preliminary analysis with volume lining, however, was not equally efficient as with a plate lining.

The surface displacement above the centreline and at the model boundary differs more between the two approaches. Displacements at surface level from centreline to the vertical boundary are larger in the three-dimensional model. These observations are only relatable to other tunnelling projects with similar ground properties and construction processes. The boundary displacement should in numerical analysis for projects be relatively small compared to the maximum displacements, since this could interfere with results. Generally, the displacements in this study are small and it is not assumed that the boundary displacement are interfering with the internal forces in the linings. The larger surface displacements show that the 3D analysis is the most conservative for settlement calculation in this case.

8.4.2 Sequential excavation

Results

The axial forces obtained during the staged excavation with top heading, bench and invert performed with the convergence-confinement method are shown in Figure 8.17. The axial force distribution in the jet grout ring is shown to the left and axial force distribution in the primary lining to the right.

Top lining activated

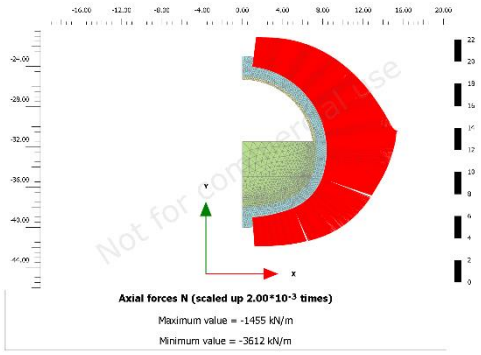

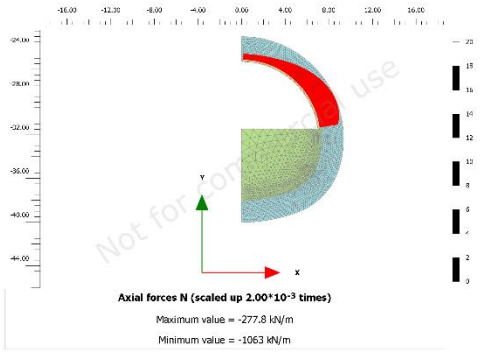

Full primary lining activated

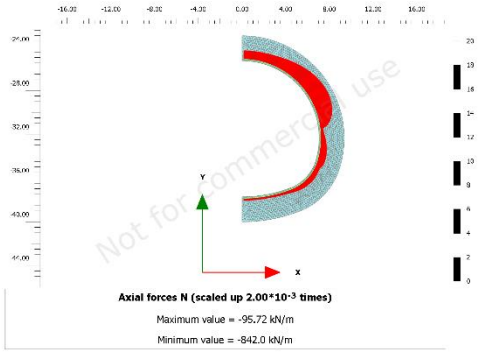

Secondary lining activation

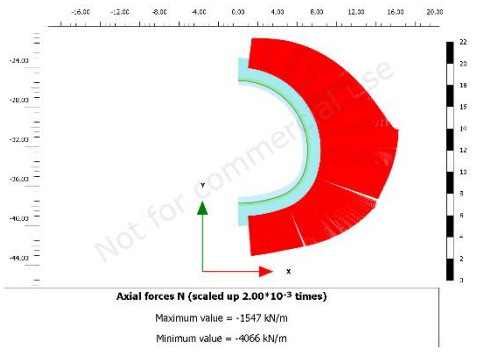

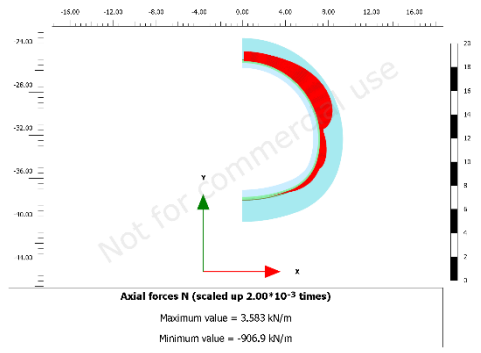

Figure 8.17: Axial force distribution in temporary supports from sequential excavation.

The axial forces acting in the primary lining are largest during the excavation of the top heading. Due to relatively large displacements during the top heading excavation, the stresses are shared between the primary lining and the jet grout ring. This can be seen from the slight notch in the axial force distribution for the jet grout heading part. With deactivation of the bench some of the axial forces in the top of the primary lining are decreased due to the stresses between the lining footing and the improved ground within the cavity. For the subsequent excavation of the bench and invert, the change in axial force is smaller.

The forces acting in the secondary lining after the wished-in-place installation are shown in Figure 8.18 for the configurations with a slip surface. Comparatively to the axial forces in Figure 8.17, relatively small axial forces are acting in the secondary lining. Due to small stress changes in the primary lining and jet grout ring, these forces are mostly integrated from stresses due to self-weight and the groundwater pressure. The largest axial forces in the secondary lining for short-term is a tensile axial force.

1: Groundwater acting on the extrados of the secondary lining.

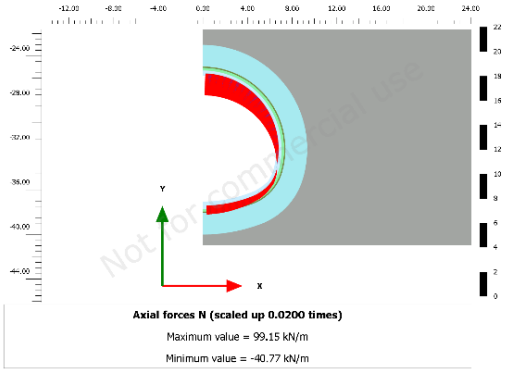

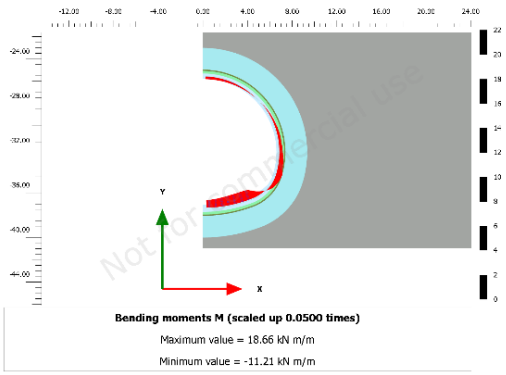

2: Groundwater acting on the extrados of the jet grout ring.

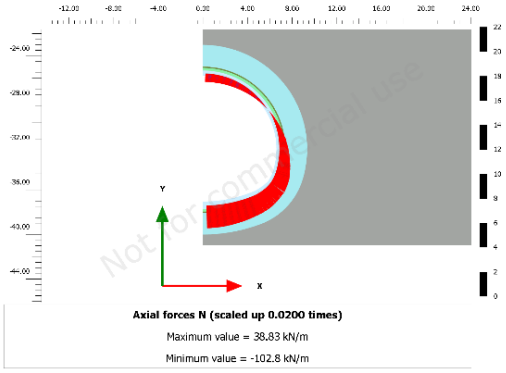

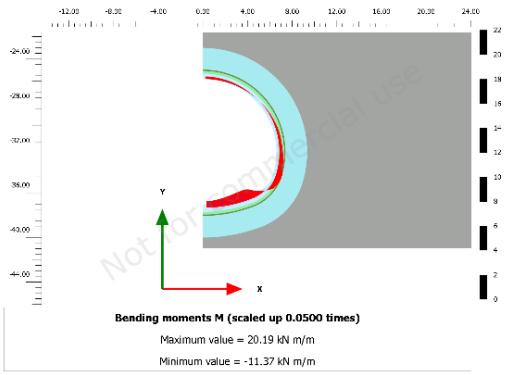

Figure 8.18: Short-term axial force and moment distribution in the secondary lining.

Discussion

Results from the sequential excavation shows that most of the stresses in the temporary supports are occurring from excavation of the top heading. Figure 8.17 shows that with stress-release, most of the stresses are accumulated in the jet grout ring, and later shared between the primary lining and the jet grout ring. The primary lining has an uneven distribution of axial forces, where most are acting on the top lining. At the point of installation, the secondary lining experiences small internal forces compared to the jet grout ring and the primary lining. At short-term the stresses in the secondary lining are generated by self-weight and modelled groundwater pressure. The primary lining would have to form cracks before the groundwater pressure is acting fully on the secondary lining.

Table 8.5: 3D vs calibrated 2D thrust during excavation.

Excavation stage in Plaxis	Preliminary 3D thrust force		Calibrated 2D thrust force	
	N_{max} [kN/m]	N_{min} [kN/m]	N_{max} [kN/m]	N_{min} [kN/m]
Top lining installation	-1171.0	-294.7	-1063.0	-277.8
Full primary lining	-957.6	9.0	-906.9	3.6

Comparison of the axial forces from the preliminary 3D analysis and the 2D analysis is shown in Table 8.5. 3D analysis gives slightly higher maximum axial force in the top heading after complete excavation of the heading. After a complete installation of the primary lining, the axial forces are similar. This shows that also for axial forces the calibrated 2D-model will provide suitable results. Due to the primary lining being modelled in two different ways that are not geometrically equivalent, identical results are not expected. The relatively similar results strengthen the verification of mesh quality with volume lining in the 2D analysis. With the 3D analysis using plate linings, the forces are relatively easy to extract. If a preliminary 3D analysis is used to calibrate a 2D analysis, the design forces for primary lining may just as well be extracted directly from the 3D-model.

The methodology of NATM with controlling the deformation with temporary supports does not yield large stresses at short-term for the secondary lining. At short-term the temporary supports offer a large relaxation. Creep behaviour, loads, degradation of concrete and ground consolidation are the main considerations to evaluate the internal forces in long-term.

8.4.3 Degradation of temporary supports

Results

The degradation of jet grout was modelled with a Mohr-Coulomb model, a user-defined model, and switching the jet grout material model back to moraine properties in one step. The resulting distribution of thrust forces in the secondary lining from the degradation of the jet grout ring, is shown in Figure 8.19. The blue line refers to the point of analysis where the secondary lining was wished-in-place and forms a reference for stress transferred during degradation. The legend shows what model and which reduction factor that is used according to Table 5.10. For example, *DSL_JG_MC0.5* corresponds to the double shell lining and the jet grout is degraded with the Plaxis Mohr-Coulomb model with a reduction factor of 0.5.

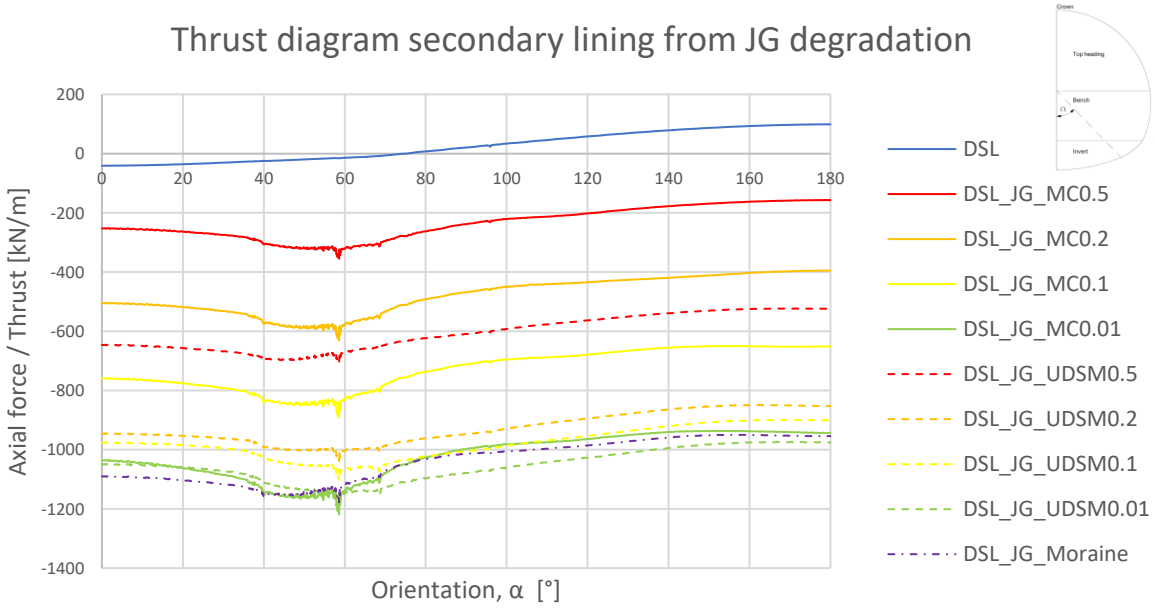

Figure 8.19: Thrust distribution in secondary lining from jet grout degradation.

The figure shows that the user-defined model has faster stress transfer to the secondary lining than the Mohr-Coulomb model with the same reduction. After complete degradation the thrust force is relatively similar for all types of degradation. The uneven distribution in the primary lining, observed from the sequential excavation, is more evenly distributed in the secondary lining.

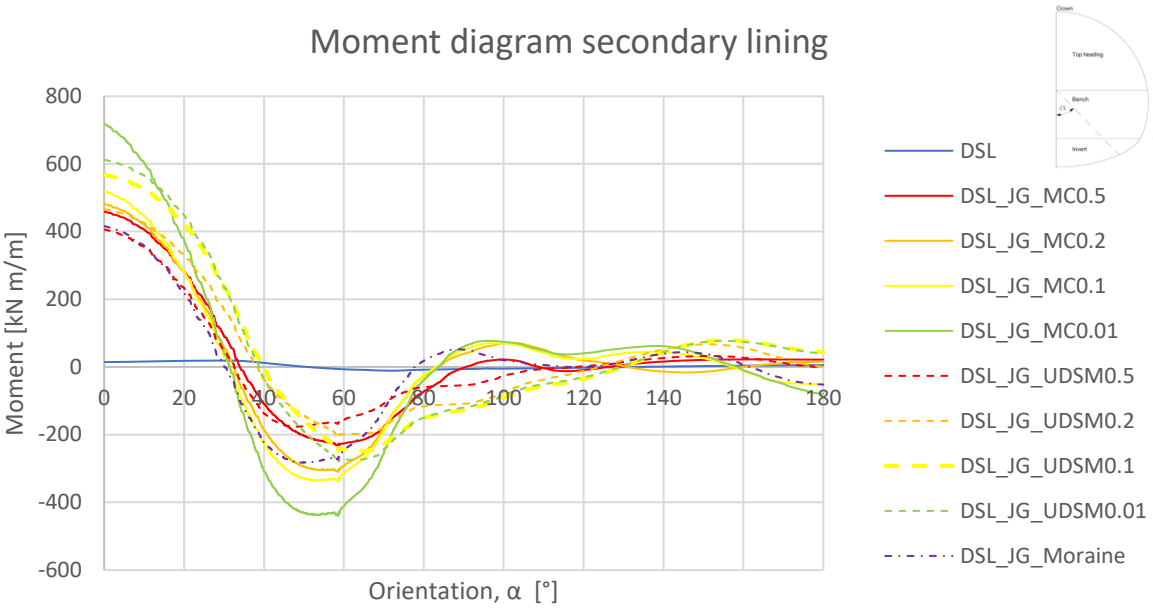

Figure 8.20: Moment distribution in secondary lining from jet grout degradation.

The moment distribution in the secondary lining, during jet grout degradation, is shown in Figure 8.20. Degradation with the Mohr-Coulomb model generally induces the highest final bending moments in the secondary lining. Modelling back to the moraine HS-model generally shows the lowest moments of the complete degradations. The distribution is relatively similar for all models, but the UDSM gives negative bending moments around the bench to heading transition.

To evaluate the stresses acting in the ground after degradation of the jet grout ring, a coloured plot of the effective principal stresses is extracted from different excavation phases in Figure 8.21. The scaling is set to the same values for all three plots to be able to evaluate the stresses in the volume with degraded jet grout. Significantly higher principal stresses in jet grout volume are observed in the converge-confinement method compared to the straight excavation method.

SE1 configuration.

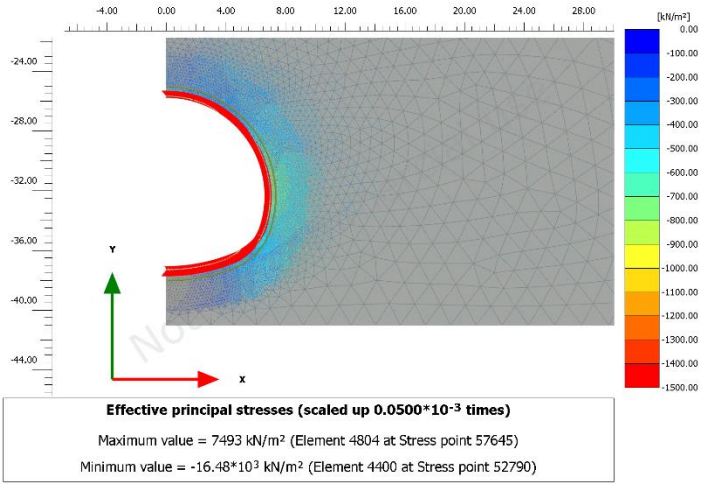

DSL configuration.

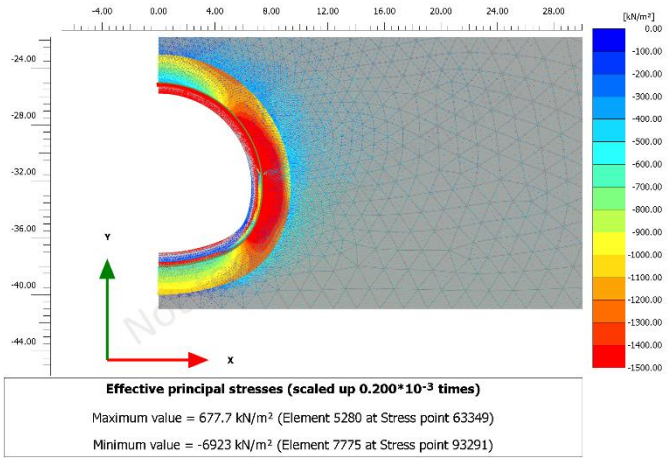

DSL configuration with MC degraded jet grout.

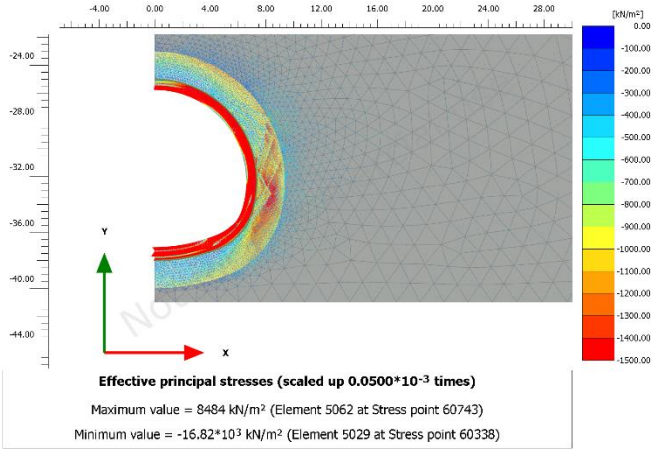

Figure 8.21: Coloured plot with principal effective stresses for different configurations.

The degradation of sprayed concrete was modelled stepwise with a user-defined model or considered degraded back to moraine properties with unit weight of sprayed concrete. Results are displayed mainly to evaluate the contribution from the jet grout ring. The stepwise degradation process with UDSM on sprayed concrete, *DSL_JG0.01_SC0.01,* was performed from the excavation phase with a completely degraded jet grout ring with Mohr-Coulomb model. Axial forces from a complete degradation of sprayed concrete and different reduction factors of the jet grout ring are shown in Figure 8.22.

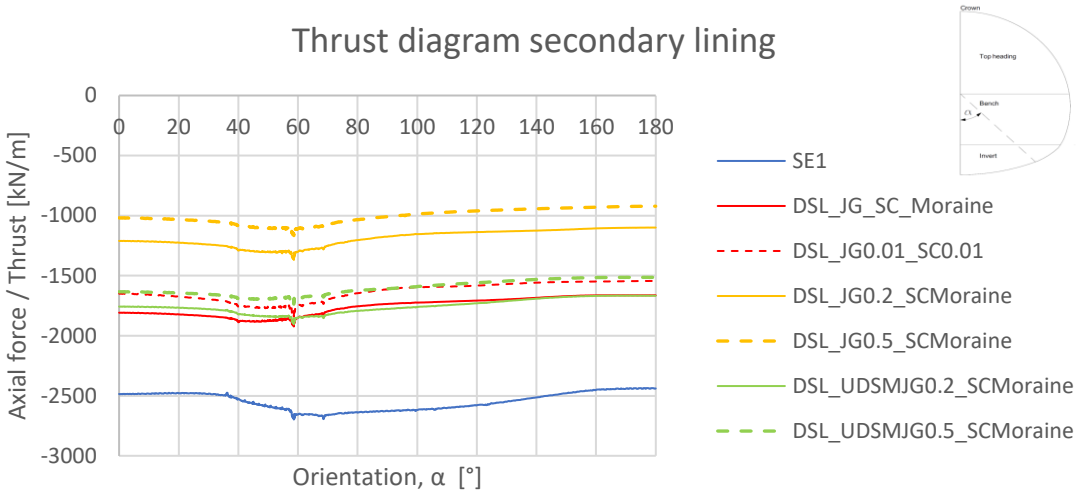

Figure 8.22: Thrust diagram for secondary lining with degraded temporary supports

As seen from the diagram, the partial contribution of jet grout with a user-defined model transfers stress quickly, while partial contribution of jet grout with Mohr-Coulomb model transfers stress slower. This has a significant effect on the thrust forces. The thrust forces are for all methods in the calibrated 2D analysis lower than the straight excavation method without any temporary supports. Degradation with UDSM, and back to moraine properties, yields higher axial forces after complete degradation. Moment distribution results from the same modelled phases are shown in Figure 8.23. No significant differences in distribution are observed for the degraded models.

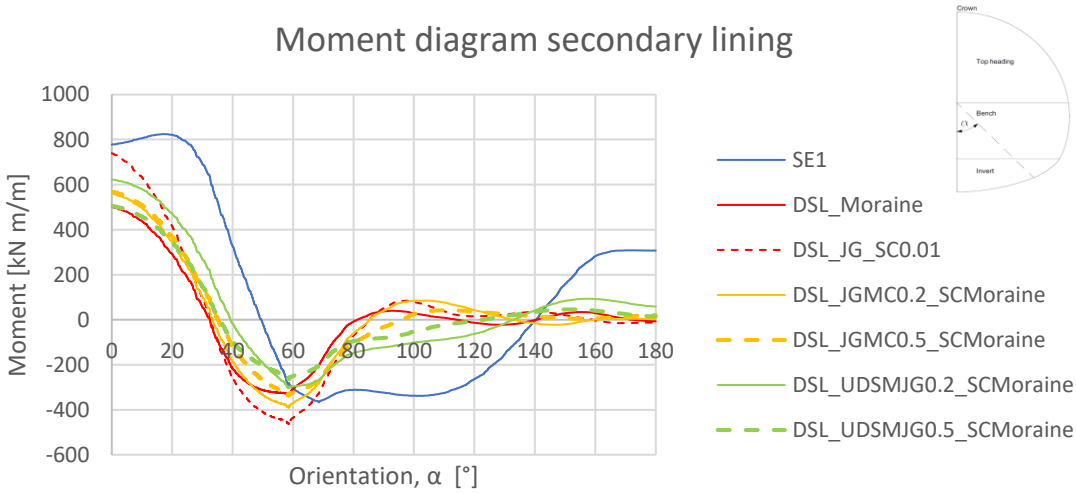

Figure 8.23: Moment diagram for secondary lining with degraded temporary supports.

Discussion

Results from the jet grout degradation show that axial forces in the secondary lining are similar for the three different approaches at complete degradation. This is an indication that the degradation methods have transferred most of the stresses. Degradation of the Mohr-Coulomb model will as discussed induce stress transfer due to plastic behaviour after material yielding. The user-defined soil model, that considers both elastic and plastic change in stress state, transfers stresses at a faster rate with the same reduction factor. These results show that when using a degradation method that considers stress transfer due to reduced elastic stiffness and plastic behaviour, the stress transfer is significantly different from solely modelling stress transfer from plastic behaviour.

If stepwise degradation should be applied to projects in the future, the responsible engineer should be aware of how the stresses are transferred. An approach with complete degradation of elastic stiffness is considered conservative because it is unlikely that the improved jet grout material will be degraded to such an extent. When applying the user-defined model, the initial stress state is not known to the program, which could produce some inaccuracy. Important considerations for this study are that all three of the degradation processes performed in this study are just approximation used to transfer stress.

Figure 8.22 shows the forces acting on the secondary lining from complete degradation of sprayed concrete and variable degradation of the jet grout ring. From this it can be shown that a partial contribution of the jet grout ring, modelled with degradation from plastic material behaviour, would give a significant reduction of axial forces in the secondary lining. The moment distribution is not affected to the same degree. This shows that a partial contribution of jet grout would enable design with reduced thickness of the secondary lining. A reduced thickness would provide substantial cost and environmental savings in large projects.

The axial- and moment forces have been compared with results from the corresponding cross-section in the permanent design reports for the project. The distributions and magnitude are similar, which gives a verification of this degradation method. A direct comparison is not considered relevant, since the design report uses a beam-spring model and several assumptions that are not equivalent with those used in this case study.

The plots in Figure 8.21 clearly illustrates that an arching effect is produced with the jet grout ring. This show that the methodology of the NATM with using the ground as a support arch is achieved with the jet grout arch.

Literature suggests that ground improved in a soil-cement process with no steel reinforcements will degrade only slightly until residual values are formed. The provisional consideration of the jet grout support in tunnels is, as mentioned in literature, due to problems with verifying the structural integrity. New technology and instruments that can verify the jet grout structure exists and could support more cost-effective considerations. If constructors and clients gain confidence in the structural capabilities of ground improved with jet grout columns, significant savings are possible through full or partial contribution of temporary supports. With a potential standardization of tunnel design methods, it will be possible to compare methods and gain even more confidence in new approaches.

8.4.4 Effect of membrane properties

Results

In order to evaluate the effect of the membrane interface parameters, results from four different phases are compared. With the stepwise degradation of jet grout with Mohr-Coulomb model, the linings are experiencing increased stresses. Due to these transferred stresses, an evaluation of the differences in internal forces between a double shell lining and a composite shell lining can be made. The composite shell lining can possibly enable a shared groundwater pressure between the linings. The shear stresses at the interface need to be verified, to evaluate if the slip conditions and bonded conditions are occurring.

Bonded interface

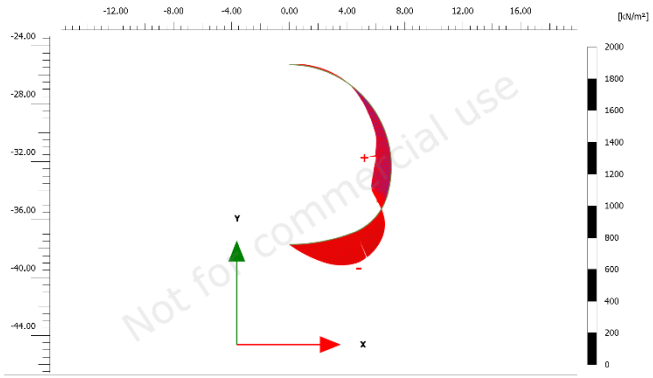

Shear stress τ_1 (scaled up 0.0100 times)

Maximum value = 145.7 kN/m² (Element 1 at Node 48342)

Minimum value = -203.7 kN/m² (Element 130 at Node 48471)

Slip interface

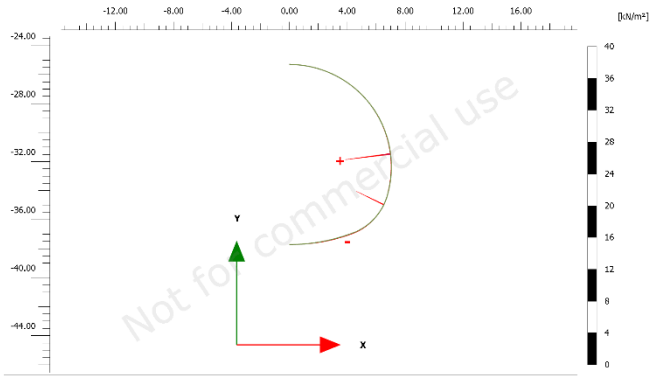

Shear stress τ_1 (scaled up 0.500 times)

Maximum value = 6.306 kN/m² (Element 1 at Node 48342)

Minimum value = -0.08849 kN/m² (Element 129 at Node 49131)

Figure 8.24: Interface shear stresses on CSL and DSL with a MC degraded JG-ring.

Figure 8.24 show how the composite shell with a bonded interface has significantly higher shear stresses at the interface compared to the slip surface. The slip surface has low shear stresses in general, with some shear spikes at the transitions from bench to invert and bench to heading.

The moment diagram for the primary lining is displayed in Figure 8.25 for the different configurations. The moment distributions are similar. There is a difference between the configurations where the jet grout ring is degraded directly to moraine, compared to a stepwise Mohr-Coulomb reduction. The UDSM degraded jet grout ring is not considered in the membrane study.

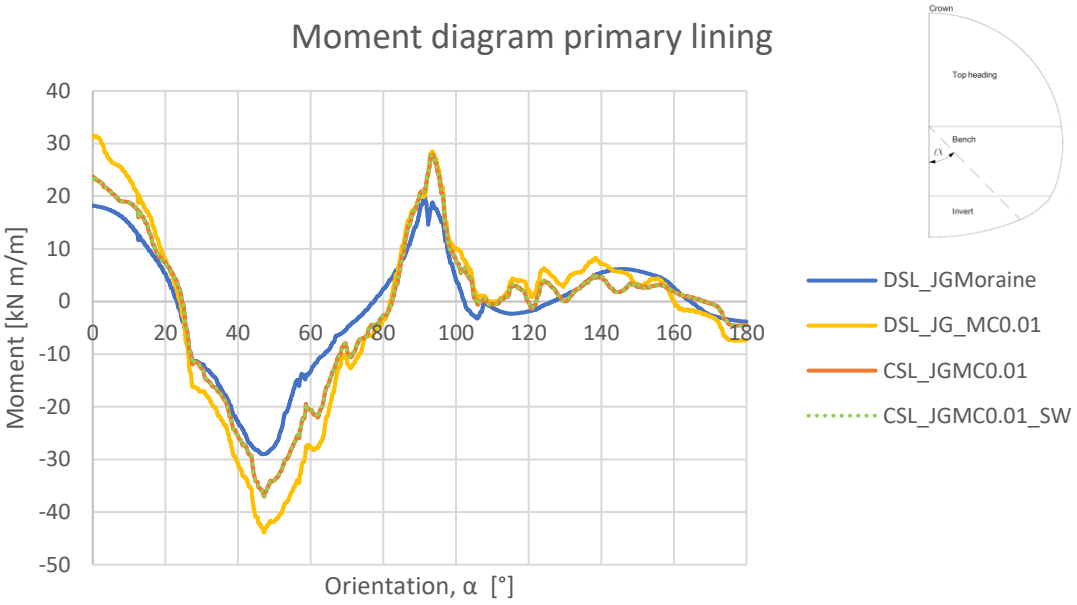

Figure 8.25: Primary lining moment diagram for varying interfaces.

In Figure 8.26 the corresponding moment diagram acting in the secondary lining is compared. This graph shows a notable difference between the two types of degradation processes for jet grout in the DSL configuration. The CSL configurations show that moment forces are approximately unaffected if the groundwater pressure is shared between the linings or acting directly to the secondary lining.

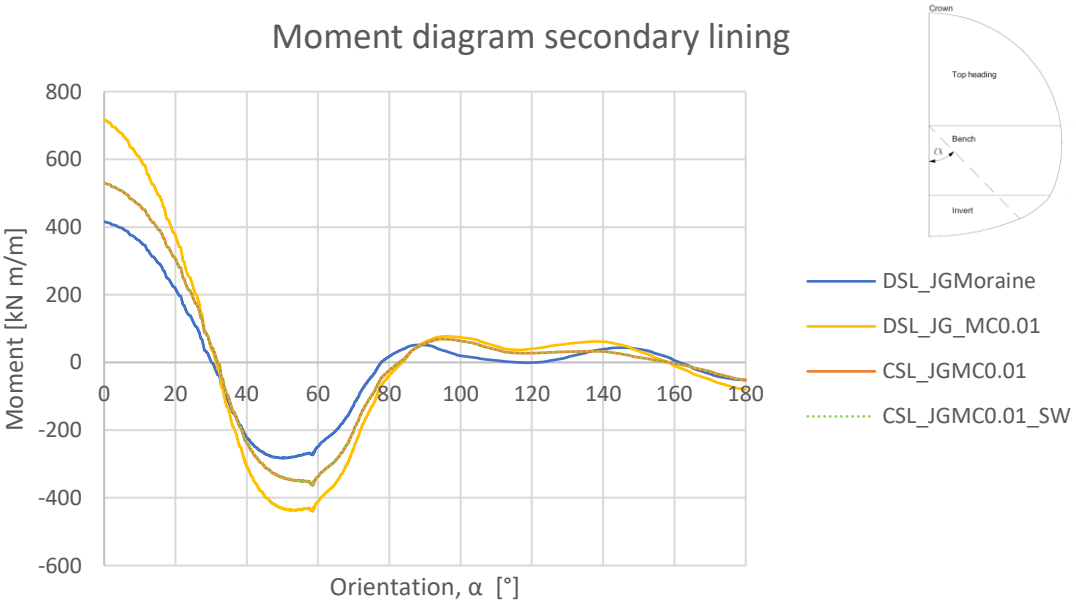

Figure 8.26: Secondary lining moment diagram for varying interfaces.

The thrust diagram for the primary lining is showed in Figure 8.27. The distributions of axial forces between the CSL and the DSL configurations differs from the heading/bench transition to the invert.

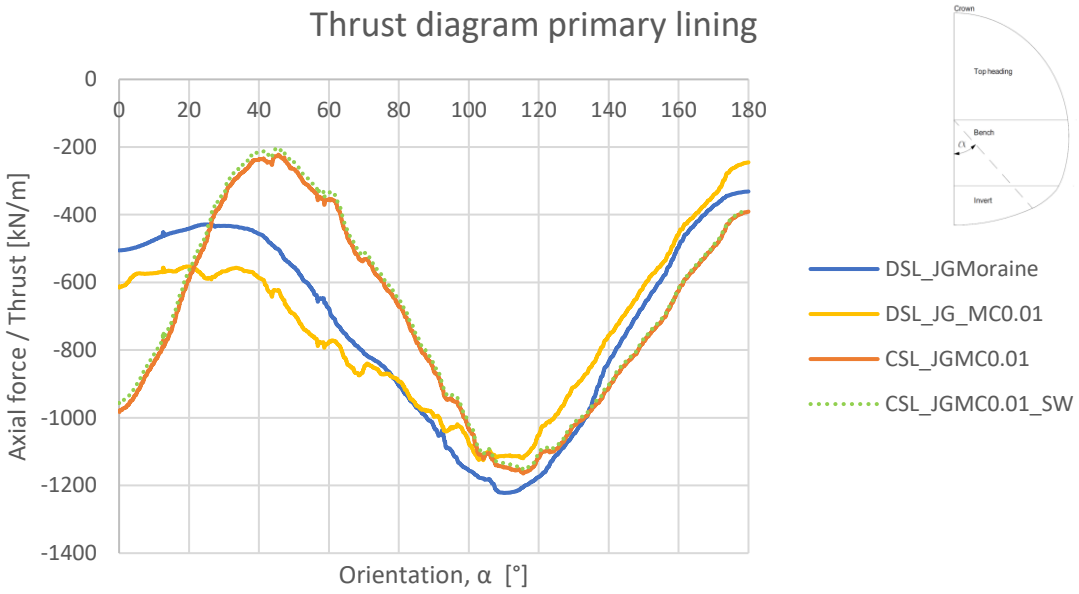

Figure 8.27: Primary lining thrust diagram for varying interfaces.

The same type of difference can be observed in the thrust diagram for the secondary lining in Figure 8.28. In the secondary lining the thrust force is lower for the CSL configurations in the invert and heading section. However, the transition between invert and bench shows a significantly higher axial force. At an orientation angle of 60° the moment of the composite configuration from Figure 8.26 also show a relatively high value.

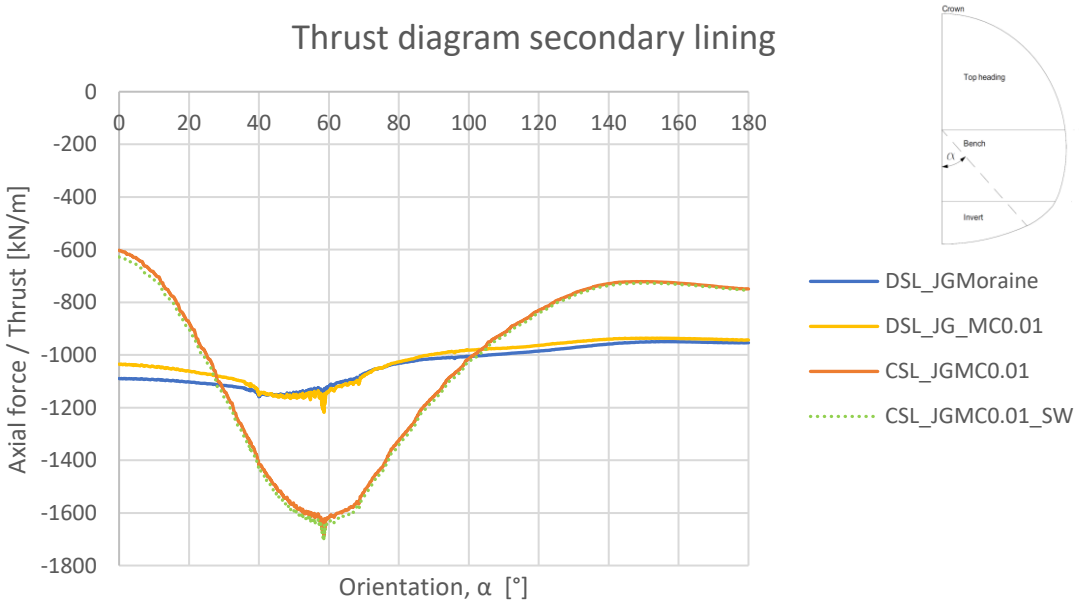

Figure 8.28: Secondary lining thrust diagram for varying interfaces.

Discussion

Results for the double shell lining and composite shell lining were extracted from phases with a completely degraded jet grout ring. The interface stresses shows that the slip condition, verified with small shear stresses, was achieved. The shear spikes that occur at the transitions between bench and heading/invert is assumed to come from a numerical issue. The staggered excavation and the curved tunnel geometry where curves with different radius intersects, is likely contributing to this issue. As seen with the straight excavation method in Figure 8.11, the spikes are not occurring for the full-face excavation in one step. The resulting shear spikes are assumed not to alter the results in the internal forces to a large degree.

Moment diagram for the secondary lining shows slightly higher moments for the DSL configuration with MC degraded jet grout. This is comparable to the CSL configuration since the same degradation process is used. The axial force distribution in the secondary lining shows a higher axial force concentration at the transition from invert and bench for the CSL. For this case study, the structural composite behaviour due to the chosen bonded membrane, does not show internal forces that would be significantly beneficial to the secondary lining design. This conclusion was also reached in chapter 8.3 for the straight excavation method. Similar conclusions have previously been reached by others.

The composite shell configuration with shared groundwater pressure does not yield result in large differences compared to modelling the groundwater directly on the secondary lining. Due to the bonded membrane the load produced by the groundwater pressure is already shared between the linings. The small differences observed are likely occurring because the groundwater pressure is acting on a different geometrical location. Compared to the DSL configuration in short-term, the results from a slip surface show a relatively larger difference with groundwater pressure acting on the secondary lining compared to acting on both linings.

8.5 Limitations of analysis

The case studied features a complex construction, and the numerical analyses performed consider multiple simplifications to find reasonable results. Use of a numerical finite element program offers the capabilities of modelling these complex situations. During this study multiple numerical issues was encountered. Some of these problems were bugs in the version of the numerical program, which caused the calculation to fail or yield unrealistic results, which lead to a time-consuming process of troubleshooting. Examples of using the wrong input parameters caused by large quantity of material models and structural elements was also experienced.

Based on these issues, engineering experience and critical assessment is considered the most important part of designing a complex underground structure such as a soil tunnel. Simplified design methods may provide just as relevant results as trying to model a complex numerical model, because of the potential for errors. However, performing a preliminary three-dimensional analysis can provide a quick and easy way to get good results, considering the complex situation. Simplification should be performed with special attention to avoid meshing difficulties. A preliminary numerical analysis can empower the engineer with confidence to not be overly conservative in lining design. The method will be an approximation, so conservatism with results is still important.

As discussed in the preliminary analysis, the current crown displacements measured in the project are lower than results from the numerical analysis performed. This gives an indication that some conditions are more favourable than modelled. It is important to consider that the parameters used are approximations to an in-situ situation. Examples of conditions that could be more favourable, or unfavourable than modelled, are:

- Modelled geometry.
- Groundwater depth.
- Higher cohesion of the moraine.
- Stiffer jet grout material.
- Variations in jet grout ring thickness.
- Higher early-age strength of sprayed concrete.

The modelled geometry was chosen conservatively, and this does have an impact in displacements. It is expected that the temporary supports can take the stresses from overburden pressure. However, with the relatively small displacements measured, a back-calculation would potentially yield higher forces in the temporary supports. If the temporary supports are considered with no structural contribution in the long-term, the internal forces calculated with numerical analysis, could be closer to the straight excavation method than the results from this case study. Such considerations are not covered by this study but is presented for further work on the subject matter.

9 Conclusion

The main objective of this thesis is to evaluate the potential relaxation from the temporary support system on the secondary lining of a soil tunnel using Plaxis finite element program. In addition, the interaction between the primary and secondary lining was investigated with sheet- and sprayed membrane properties. Key factors of the numerical analysis have been discussed, and an attempt to approximate the realistic construction method have been performed with Plaxis 2D and 3D. Based on the research questions, the following conclusions can be drawn with the described limitations:

- With the sequential excavation method, the temporary supports have been shown to completely stabilize the excavation. Therefore, the short-term internal forces in the secondary lining are mostly generated from self-weight and modelled groundwater pressure. In long-term, the secondary lining should, according to the project, be designed based on the criteria of no contribution from the temporary supports. Realistically, the jet grout ring is considered unlikely to fully degrade, and with this assumption the secondary lining will not experience the full overburden pressure. Because of the arching effect provided by the temporary supports, a portion of the stresses have been shown by the analysis to be redistributed to the surrounding soil after the degradation. This proves that the arching stresses from the temporary supports will provide relaxation on the secondary lining.
- Modelling with partial degradation of the jet grout ring, show a potential reduction of designing axial forces in the secondary lining. This can enable a reduced lining thickness, which would reduce costs and emissions. With new technology it could be possible to verify the structural capability of the jet grout structure to a certain degree. Verified structural capability would enable a design consideration with partly- or full contribution of the jet grout. The primary lining for this project, with steel reinforcement, is prone to corrosion and structural degradation. Using another sprayed concrete technology, like fibre-reinforced sprayed concrete, is more likely to enable long-term contribution in the design.
- Methods with partial degradation of temporary supports used in this thesis show a stress transfer to the secondary lining. The three methods in this thesis all showed relatively similar internal forces in the secondary lining for complete degradation. The material models used to perform the degradation have different rates of stress transfer. A potential use of this method should state which approach is used and what the effect will be. With support in literature this method can provide a design alternative to other methods such as a beam-spring model. The work in this thesis does not include other modelling options, and no direct comparisons are made.

- The structural capabilities of the jet grout structure show that, with the derived material models, it can theoretically handle the stresses from a one-step excavation. Design to account for surcharges, fire, freeze-thaw processes and watertightness have been neglected. Uncertainties in terms of homogeneity and material variance are only accounted for with a statistical approach for parameter determination. Current experiences from the project could indicate a relatively homogenous structure due to low water ingress and small deformations. This proves the jet grout rings feasibility for non-cohesive soils with groundwater.
- Analysis with different properties for the membrane interaction between linings show a different axial force distribution in the linings. The moment distribution is similar between a double shell lining and a composite shell lining. Axial forces are lower for the composite shell lining in the invert lining and top lining but show a higher axial force for the bench lining. From these results, no direct benefit to design is achieved with a bonded membrane in the specific configuration. The groundwater pressure was shown to be shared between the linings, which have been shown by other studies to potentially reduce the design thickness of the secondary lining.
- The method with a preliminary three-dimensional model provides a relatively quick and easy way to calibrate a two-dimensional model. In terms of efficiency, large simplifications and modelling with plate linings reduced the potential issues and gave an efficient approach. Modelling small and slender structures with volume elements in a three-dimensional model could be time consuming and demands a very refined mesh. If a preliminary three-dimensional model is used, the design forces of the temporary supports may just as well be extracted directly.

10 Further work

In terms of soil tunnelling there is much knowledge to be gained about the design and construction. To face the growing demand of the construction industry to become more sustainable, new technology and increased knowledge could reduce the emissions. Hopefully, with a standardization of tunnel design it will be possible to find more optimized solutions. Further work on the topics discussed in this thesis could include:

- Investigation on different ways to verify the structural integrity of a jet grout structure in tunnelling. Existing methods such as downhole and cross-hole seismic tomography have shown good results but is expensive and time consuming. If the structure can be verified as homogenous and the strength parameters can be estimated, the industry could be provided with confidence to include jet grouting for long-term structural capabilities in soil tunnelling. Special emphasis should be put on the cost- and time consumption of the verification process.
- Evaluating the different design methods for soil tunnelling in terms of material- and cost optimization. Due to the many different methods present in literature, a comparison should be made. For environmental aspects, verifying a safe excavation with material savings would be a step in the right direction. Engineering companies would benefit from a study on time efficiency of the different methods. It could be interesting to compare results from a method of degradation in the continuous finite element method with a beam-spring model, to see if the subgrade reaction modulus produces similar results to a continuous interaction.
- Performing a back-calculation of the case study, after the displacement monitoring is completed, and comparing it with results from this thesis to investigate the actual structural parameters of the jet grout ring and the linings. Full three-dimensional modelling would also be relevant to investigate results of a realistic layering model.
- The composite shell lining configuration investigated in this study showed no direct benefits to lining design for this case study. However, due to the relatively low observed water ingress from the jet grout ring, other configurations and applications should be investigated. An example would be to apply the spray-on waterproofing membrane directly to the jet grout ring, and then apply a permanent sprayed concrete lining. If sufficient bond is achieved in the membrane, this approach could reduce costs and emissions from the secondary lining. Additional benefits would be the potentially efficient and secure installation procedure with sprayed membrane and direct application of permanent sprayed concrete.
- The assumed corrosion of the temporary lining, encased by the jet grout ring and secondary lining, would likely cause a material expansion. In the assumption that this happens, it would be reasonable to also consider the stresses occurring from the possible expansion. The potential additional forces from the assumed material behaviour should be investigated.

References

Aldrian, W., Thomas, A. and Holter, K. (2021) *Permanent Sprayed Concrete - an international update*.

Athanasopoulo, A. *et al.* (2019) Standardisation needs for the design of underground structures, *European Commission-JRC Technical Reports*.

Backer, L. and Hæstad, N. (2020) *UDK 02 Kulvert og Løsmassetunnel - tekniske utfordringer og gjennomføring av totalentreprise*. Unpublished paper presented at Tunneldagene i Drammen. Drammen.

Balmer, G. G. (1958) *Shear strength and elastic properties of soil-cement mixtures under triaxial loading*.

BaneNOR (2018) Upcoming projects.

BaneNOR (2019) *Teknisk designbasis for InterCity-strekningene* Bane Nor.

BaneNOR (2022) *Drammen-Kobbervikdalen*. Available at: https://arcg.is/1DHyrz (Accessed: 29.03 2022).

Barla, M. and Bzowka, J. (2013) Comparing numerical alternatives to model jet grouting in tunnels, *Electronic Journal of Geotechnical Engineering*, 18, pp. 2997-3008.

Barpi, F., Barbero, M. and Peila, D. (2011) Numerical modelling of ground-tunnel support interaction using bedded-beam-spring model with fuzzy parameters, *Gospodarka Surowcami Mineralnymi*, 27.

Bentley (2021a) *Plaxis 2D - Scientific Manual*.

Bentley (2021b) *Plaxis 3D - Reference Manual*. Bentley.

Bentley (2021c) *Plaxis 2D - Reference Manual*. Bentley.

Bloodworth, A. and Su, J. (2018) Numerical analysis and capacity evaluation of composite sprayed concrete lined tunnels, *Underground Space*, 3(2), pp. 87-108. doi: 10.1016/j.undsp.2017.12.001.

Bobet, A. (2001) Analytical Solutions for Shallow Tunnels in Saturated Ground, *Journal of Engineering Mechanics-asce - J ENG MECH-ASCE*, 127. doi: 10.1061/(ASCE)0733-9399(2001)127:12(1258).

Broere, W. (2016) Urban underground space: Solving the problems of today's cities, *Tunnelling and Underground Space Technology*, 55, pp. 245-248. doi: 10.1016/j.tust.2015.11.012.

BTS (2004) *Tunnel lining design guide*. Thomas Telford.

Bull, W. B. (1977) The alluvial-fan environment, *Progress in Physical Geography: Earth and Environment*, 1(2), pp. 222-270. doi: 10.1177/030913337700100202.

Burke, G. K. (2004) Jet grouting systems: advantages and disadvantages *GeoSupport 2004: Drilled Shafts, Micropiling, Deep Mixing, Remedial Methods, and Specialty Foundation Systems.* pp. 875-886.

Carter, J., Booker, J. and Yeung, S. (1986) Cavity expansion in cohesive frictional soil, *Géotechnique*, 36, pp. 349-358. doi: 10.1680/geot.1986.36.3.349.

Carter, J., Miura, N. and Zhu, H. (2009) Improved Prediction of Lateral Deformations due to Installation of Soil-Cement Columns, *Journal of Geotechnical and Geoenvironmental Engineering - J GEOTECH GEOENVIRON ENG*, 135. doi: 10.1061/(ASCE)GT.1943-5606.0000155.

CEN (2012) Sprayed concrete - Part 1 *Definitions, specifications and*

conformity: Standard Norge.

CEN (2016) Eurocode: Basis of structural design: Standard Norge.

CEN (2019) Utførelse av spesielle geotekniske arbeider *Jetinjisering*: Standard Norge. (Accessed: 07.04.2022).

CEN (2021) Eurokode 2 - Prosjektering av betongkonstruksjoner *Del 1-1: Almenne regler og regler for bygninger*: Standard Norge.

Chadwick, P. (1959) The quasi-static expansion of a spherical cavity in metals and ideal soils, *The Quarterly Journal of Mechanics and Applied Mathematics*, 12(1), pp. 52-71.

Cordon, W. A. (1962) Resistance of soil-cement exposed to sulfates, *Highway Research Board Bulletin*, (309).

Coulter, S. and Martin, C. D. (2006) Effect of jet-grouting on surface settlements above the Aeschertunnel, Switzerland, *Tunnelling and Underground Space Technology*, 21(5), pp. 542-553. doi: 10.1016/j.tust.2005.07.005.

Covil, C. S. and Skinner, A. E. (1994) Jet grouting—a review of some of the operating parameters that form the basis of the jet grouting process *Grouting in the ground.* pp. 605-629.

Croce, P., Flora, A. and Modoni, G. (2014) *Jet grouting: technology, design and control*. CRC Press.

Dimmock, R., Haig, B. and Su, J. (2011) SPRAY APPLIED WATERPROOFING MEMBRANES: KEY SUCCESS FACTORS AND DEVELOPMENT OF EFFICIENT SPRAYED CONCRETE TUNNEL LININGS, *Sixth International Symposium on Sprayed Concrete, Tromso, Norway*. pp. 110-124.

Duddeck, H. and Erdmann, J. (1985) Structural design models for tunnels in soft soil, *Underground Space;(United States)*, 9.

Duddeck, H. (1988) Guidelines for the design of tunnels, *Tunnelling and Underground Space Technology*, 3(3), pp. 237-249.

Eggestad, Å. (1998) Byggegrop for reparasjon av Eidsvolltunnelen, *Fjellsprengningsdagen 1998*, *Oslo*. Norsk jord- og fjellteknisk forbund.

Erdmann, J. (1983) Comparison of plane and development of 3-dimensional analyses for tunnelling, *Institut für Statik Technische Universität Braunschweig*.

Flora, A. *et al.* (2012) Mechanical analysis of jet grouted supporting structures *Geotechnical Aspects of Underground Construction in Soft Ground.* CRC Press, pp. 837-846.

Fries, T. (2000) Ausfahrtstun nel Ristet - Erfahrungen aus dem Lockergesteinsvortrieb *Spezielle geotechnische Lo¨sungen bei der Umfahrung*

Zu¨ich West. vol. 140 of Mitteilun-gen der Schweizerischen

Gesellschaft fur Boden- und Felsmechanik,. Societe Suisse de M

ecanique des Sols et des Roches, 140, pp. 34-38.

Galan, I. *et al.* (2019) Durability of shotcrete for underground support– Review and update, *Construction and Building Materials*, 202, pp. 465-493. doi: https://doi.org/10.1016/j.conbuildmat.2018.12.151.

Galler, R. *et al.* (2009) The New Guideline NATM – The Austrian Practice of Conventional Tunnelling, *BHM. Berg- und hüttenmännische Monatshefte*, 154(10), pp. 441-449. doi: 10.1007/s00501-009-0503-9.

Galli, G., Grimaldi, A. and Leonardi, A. (2004) Three-dimensional modelling of tunnel excavation and lining, *Computers and Geotechnics*, 31(3), pp. 171-183. doi: https://doi.org/10.1016/j.compgeo.2004.02.003.

Hasan, M. F. and Canakci, H. (2022) Assessing the Effect of Seawater and Magnesium Sulfate on the Durability and Strength Properties of Cement-Stabilized Full-Scale Soilcrete Column Constructed in Clayey Soil, *Arabian Journal for Science and Engineering*. doi: 10.1007/s13369-022-06740-6.

Heuer, R. E. (1974) Important ground parameters in soft ground tunneling, *Subsurface exploration for underground excavation and heavy construction*. ASCE, pp. 41-55.

Holter, K. *et al.* (2014) *Testing of sprayed waterproofing membranes for single shell sprayed concrete tunnel linings in hard rock*.

Holter, K. G. (2016) Performance of EVA-Based membranes for SCL in hard rock, *Rock Mechanics and Rock Engineering*, 49(4), pp. 1329-1358.

Hung, J. *et al.* (2009) *Technical Manual for Design and Construction of Road Tunnels - Civil Elements*. AASHTO.

Höser, S. *et al.* (2018) Untersammelsdorf Tunnel - Challenges and special measures during tunnelling in lacustrine clay, *Geomechanics and Tunnelling*, 11(5), pp. 450-461. doi: 10.1002/geot.201800039.

ILF (2018) Brenner Base Tunnel - Lot Eisackquerung (pp. 5).

ILF (2020a) *Temporary Support Design Report*. (UDK 02 Kulvert og løsmassetunnel - Løsmassetunnel).

ILF (2020b) *Excavation and support - Support Class "SC 2"*. (UDK 02 Kulvert og løsmassetunnel - Løsmassetunnel).

ILF (2020c) *Temporary support measures - General overview 1 of 2*. (UDK 02 Kulvert og løsmassetunnel - Løsmassetunnel).

ILF (2020d) *Temporary Support Design Report*. (UDK 02 Kulvert og løsmassetunnel - Løsmassetunnel).

ILF (2020e) *Temporary support measures - General overview 2 of 2*. (UDK 02 Kulvert og løsmassetunnel - Løsmassetunnel).

ILF (2020f) *Permanent Support Design Report*. (UDK02 Kulvert og Løsmassetunnel).

ILF (2021a) *Soil tunnel - Permanent support - Section Type 1 - Geometric Definition*. (UDK 02 Kulvert og løsmassetunnel - Km 53,603 - 54,431).

ILF (2021b) *Soil tunnel - Permanent Support - General overview*. (UDK 02 Kulvert og Løsmassetunnel).

Jernbaneverket (2016) Slik bygges jernbanetunneler.

John, M. and Mattle, B. (2003) Factors of shotcrete lining design, *Tunnels & Tunnelling International*, 35(10).

Johnson, R. P., Swallow, F. E. and Psomas, S. (2016) Structural properties and durability of a sprayed waterproofing membrane for tunnels, *Tunnelling and Underground Space Technology*, 60, pp. 41-48. doi: https://doi.org/10.1016/j.tust.2016.07.013.

Jorstad, F. A. (1968) Leirskred i Norge.

Kartverket (2022) *Norgeskart*. Available at: www.norgeskart.no.

Kielbassa, S. and Duddeck, H. (1991) Stress-strain fields at the tunnelling face?Three-dimensional analysis for two-dimensional technical approach, *Rock Mechanics and Rock Engineering*, 24(3), pp. 115-132. doi: 10.1007/bf01042857.

Langåker, M. Ø. (2014) *Joberget tunnel-Analysis of stability and support design for tunneling in soil*, Institutt for geologi og bergteknikk.

Lier, K. E. (2017) Jetpeling, utførelse under krevende forhold, in Mathisen, L. (ed.) *Teknologidagene 2017*, *Trondheim*. docplayer: Jetgrunn, pp. 73.

Lignola, G. P., Flora, A. and Manfredi, G. (2008) Simple Method for the Design of Jet Grouted Umbrellas in Tunneling, *Journal of Geotechnical and Geoenvironmental Engineering*, 134, pp. 1778-1790. doi: 10.1061/(ASCE)1090-0241(2008)134:12(1778).

Lorenz, S. and Galler, R. (2015) Investigation of the interaction between sheet membranes, geotextile and sprayed concrete in tunnelling.

Lunardi, P. (1997) Ground improvement by means of jet-grouting, *Proceedings of the Institution of Civil Engineers-Ground Improvement*, 1(2), pp. 65-85.

Lunardi, P. (2008) *Design and construction of tunnels: Analysis of Controlled Deformations in Rock and Soils (ADECO-RS)*. Springer Science & Business Media.

Marcher, T., John, M. and Ristic, M. (2011) Determination of load-sharing effects in sprayed concrete tunnel linings, *Underground Construction*, pp. 8.

Mitchell, J. K. (1976) The properties of cement-stabilized soils, *Proceeding of residential workshop on materials and methods for low cost road, rail, and reclamation works*. pp. 404.

Mork, G. (2022) Mail correspondance on the progress of the project, 08.04.22.

Muir Wood, A. (2000) *Tunnelling: Management by design*. Taylor & Francis.

Ngan Vu, M., Broere, W. and Bosch, J. W. (2017) Structural Analysis for Shallow Tunnels in Soft Soils, *International Journal of Geomechanics*, 17(8), pp. 04017038. doi: 10.1061/(asce)gm.1943-5622.0000866.

NGI (2020) *Faction report of soil conditions*. (UDK02 Kulvert og Løsmassetunnel - Geoteknikk/Løsmassetunnel).

NIRAS (2020) *Plan og profil - Km 53.603- 54.431*.

Norconsult (2017) *Soil tunnel report*.

Norconsult (2019a) *Fagrapport Geoteknikk - Åpen byggegrop UDK 02*.

Norconsult (2019b) *Geoteknisk datarapport UDK 02*.

Ochmański, M., Modoni, G. and Bzówka, J. (2015) Numerical analysis of tunnelling with jet-grouted canopy, *Soils and Foundations*, 55(5), pp. 929-942. doi: https://doi.org/10.1016/j.sandf.2015.08.002.

Oke, J., Vlachopoulos, N. and Diederichs, M. (2018) Improvement to the Convergence-Confinement Method: Inclusion of Support Installation Proximity and Stiffness, *Rock Mechanics and Rock Engineering*, 51(5), pp. 1495-1519. doi: 10.1007/s00603-018-1418-0.

Palla, R. and Leitner, S. (2009) Application of jet grouting on the various contracts in the Lower Inn Valley, *Geomechanik und Tunnelbau*, 2(6), pp. 693-708. doi: 10.1002/geot.200900059.

Panet, M. *et al.* (2001) The convergence–confinement method, *Press ENPC*.

Panet, M. and Sulem, J. (2022) *CONVERGENCE-CONFINEMENT METHOD FOR TUNNEL DESIGN*. Springer.

Peck, R. B. (1969) Deep excavations and tunneling in soft ground, *Proc. 7th ICSMFE, 1969*, pp. 225-290.

Pelizza, S. and Peila, D. (1993) Soil and rock reinforcements in tunnelling, *Tunnelling and Underground Space Technology*, 8(3), pp. 357-372. doi: 10.1016/0886-7798(93)90020-v.

Pichler, C. *et al.* (2004) Optimization of jet-grouted support in NATM tunnelling, *International Journal for Numerical and Analytical Methods in Geomechanics*, 28(78), pp. 781-796. doi: 10.1002/nag.366.

Pillai, A. *et al.* (2017) Sprayed concrete composite tunnel lining–load sharing between the primary and secondary lining, and its benefit in reducing the structural thickness of the lining, *Proceedings of the World tunnel congress*.

Pinto, F. *et al.* (2013) Ground Heave Due to Jet Grouting Near an Existing Structure.

Pöttler, R. (1985) Ideeller Elastizit~tsmodul zur Absch~tzung

der Spritzbetonbeanspruchung bei Felshohlraumbauten. *Felsbau 3.* pp. 136-139.

Pöttler, R. (1990) Time-dependent rock—Shotcrete interaction a numerical shortcut, *Computers and Geotechnics*, 9(3), pp. 149-169. doi: https://doi.org/10.1016/0266-352X(90)90011-J.

Ritchie, H. and Roser, M. (2018) Urbanization, *Our world in data*.

Ryan Gratias, C. A. and Willis, D. (2014) The Next Level: Why Deeper Is Better for TBMs in Mining, *North American Tunneling: 2014 Proceedings*.

Rygh, J. A. (1992) Norwegian tunnelling in general, *Tunnel and Underground Space*, 2(1), pp. 123-151.

Sagaseta, C. (1987) Analysis of undrained soil deformation due to ground loss, *Géotechnique*, 37(3), pp. 301-320. doi: 10.1680/geot.1987.37.3.301.

Sauer, G., Dietmaier, P. and Bauer, E. (1990) Design of tunnel concrete lining using capacity limit curves (CLC), 65, pp. 29-33.

Schikora, K. and Fink, T. (1982) Berechnungsmethoden moderner, bergmännischer Bauweisen beim U-Bahn-Bau, *Bauingenieur*, 57, pp. 193-198.

Schutz, R. (2010) *Numerical modelling of shotcrete for tunnelling*, Imperial College London.

Semprich, S., Scheid, Y. and Gattermann, J. (2003) Compressed air tunnelling - determination of air requirement. Springer Vienna, pp. 249-301.

Shihata, S. A. and Baghdadi, Z. A. (2001) Long-term strength and durability of soil cement, *Journal of materials in civil engineering*, 13(3), pp. 161-165.

Sloot, M. v. d. (2019) *Tunnel advancement script for Plaxis 3D*. Available at: https://communities.bentley.com/products/geotech-analysis/w/plaxis-soilvision-wiki/45448/tunnel-advancement-script-for-plaxis-3d (2022).

Stella, C., Ceppi, G. and D'Appolonia, E. (1990) Temporary tunnel support using jet-grouted cylinders, *Journal of construction engineering and management*, 116(1), pp. 35-53.

Su, J., Bloodworth, A. and Haig, B. (2013) Experimental investigations into the interface properties of composite concrete lined structures, *Proceedings of world tunnel congress, Geneva. Taylor & Francis, London*.

Su, J. and Thomas, A. (2015) Design of sprayed concrete linings in soft ground—a Crossrail perspective, *Crossrail Project: Infrastructure design and construction*, 1, pp. 123-136.

Su, J. and Bloodworth, A. (2016) Interface parameters of composite sprayed concrete linings in soft ground with spray-applied waterproofing, *Tunnelling and Underground Space Technology*, 59, pp. 170-182.

Su, J. and Bloodworth, A. (2018) Numerical calibration of mechanical behaviour of composite shell tunnel linings, *Tunnelling and Underground Space Technology*, 76, pp. 107-120. doi: 10.1016/j.tust.2018.03.011.

Su, J. and Bloodworth, A. (2019) Simulating composite behaviour in SCL tunnels with sprayed waterproofing membrane interface: A state-of-the-art review, *Engineering Structures*, 191, pp. 698-710. doi: 10.1016/j.engstruct.2019.04.067.

Swoboda, G. (1979) Finite element analysis of the new Austrian tunneling method (NATM). Available at: https://eurekamag.com/research/018/929/018929207.php.

Thomas, A. (2008) *Sprayed concrete lined tunnels*. CRC Press.

Thomas, A. (2021) The design of the Crossrail tunnels in UK, *Geomechanics and Tunnelling*, 14(4), pp. 340-346. doi: 10.1002/geot.202100014.

Trevi (2021a) *Jet Grouting Compartment 1 Final Report*.

Trevi (2021b) *Jet Grouting Compartment 2 Final Report*.

Trevi (2021c) *Jet Grouting Compartment 3 Final Report*.

Trevi (2021d) *Jet Grouting Compartment 4 Final Report*.

Trevi (2021e) *Jet Grouting Compartment 7 Final Report*.

Trevi (2021f) *Jet Grouting Compartment 8 Final Report*.

Trevi (2021g) *Jet Grouting Compartment 9 Final Report*.

Trevi (2021h) *Jet Grouting Compartment 10 Final Report*.

Trevi (2021i) *Jet Grouting Compartment 11 Final Report*.

Trevi (2021j) *Jet Grouting Compartment 12 Final Report*.

Trevi (2021k) *Jet Grouting Compartment 6 Final Report*.

Trevi (2021l) *Jet Grouting Compartment 5 Final Report*.

Trunda, V. and Hilar, M. (2020) NATM TUNNELS – CONSIDERATION OF THE PARTLY DAMAGED PRIMARY LINING IMPACT FOR THE SECONDARY LINING EVALUATION, *Acta Polytechnica*, 60, pp. 145-150. doi: 10.14311/AP.2020.60.0145.

Tyrens (1985) *VA-Tunnel Örby, Stockholm*. Available at: http://www.jetgrunn.no/images/jetgrunn/pdfs/p46.pdf.

UN (2019) World population prospects 2019, *Vol (ST/ESA/SE. A/424) Department of Economic and Social Affairs: Population Division*.

USACE (1997) Engineering and Design: Tunnels and Shafts in Rock, *US Army Corps of Engineers*.

Usman, M. *et al.* (2011) Three Dimensional Load Analysis of Tunnel Linings Including Weathering Processes of the Shotcrete, *BHM Berg- und Hüttenmännische Monatshefte*, 156(12), pp. 487-491. doi: 10.1007/s00501-011-0043-y.

Usman, M. and Galler, R. (2013) Long-term deterioration of lining in tunnels, *International Journal of Rock Mechanics and Mining Sciences*, 64, pp. 84-89. doi: https://doi.org/10.1016/j.ijrmms.2013.08.028.

Vegdirektoratet (2014) *Håndbok V221 - Grunnforsterkning, fyllinger og skråninger* Statens Vegvesen.

Vegdirektoratet, S. V. (2015) Håndbok N500 Vegtunneler: Høringsutgave 2015: Statens vegvesen.

Vegvesen, S. and Vegdirektoratet (2006) Vegtunneler: normaler [Håndbok 021]: Statens vegvesen.

Veidekke (2022) UDK 02 - Løsmassetunnel Monitoring TM 150 - 240.

Vesić, A. S. (1972) Expansion of cavities in infinite soil mass, *Journal of the soil Mechanics and Foundations Division*, 98(3), pp. 265-290.

Vlachopoulos, N. and Diederichs, M. S. (2009) Improved Longitudinal Displacement Profiles for Convergence Confinement Analysis of Deep Tunnels, *Rock Mechanics and Rock Engineering*, 42(2), pp. 131-146. doi: 10.1007/s00603-009-0176-4.

Vlachopoulos, N. and Diederichs, M. S. (2014) Appropriate Uses and Practical Limitations of 2D Numerical Analysis of Tunnels and Tunnel Support Response, *Geotechnical and Geological Engineering*, 32(2), pp. 469-488. doi: 10.1007/s10706-014-9727-x.

Wallis, S. (2008) *Design considerations on approach to Brenner Baseline high-speed rail connection in Austria*. Available at: https://www.tunneltalk.com/Austria-Design-considerations-for-high-speed-rail.php (Accessed: 17.02.2022).

Wang, Z.-F., Bian, X. and Wang, Y.-Q. (2017) Numerical approach to predict ground displacement caused by installing a horizontal jet grout column, *Marine Georesources & Geotechnology*, 35(7), pp. 970-977. doi: 10.1080/1064119X.2016.1273288.

Wong, I. and Poh, T. (2000) Effects of Jet Grouting on Adjacent Ground and Structures, *Journal of Geotechnical and Geoenvironmental Engineering - J GEOTECH GEOENVIRON ENG*, 126. doi: 10.1061/(ASCE)1090-0241(2000)126:3(247).

Yahya, S. and Abdullah, R. (2014) A Review on Methods of Predicting Tunneling Induced Ground Settlements, *Electronic Journal of Geotechnical Engineering*, 19, pp. 5813-5826.

Zienkiewicz, O. C., Taylor, R. L. and Zhu, J. Z. (2005) *The finite element method: its basis and fundamentals*. Elsevier.

Ziller, L. and Cont, M. (2018) Evaluation of long-term ground load on conventional tunnel linings.

Zumsteg, R. and Langmaack, L. (2017) Mechanized Tunneling in Soft Soils: Choice of Excavation Mode and Application of Soil-Conditioning Additives in Glacial Deposits, *Engineering*, 3(6), pp. 863-870. doi: 10.1016/j.eng.2017.11.006.

Aagaard, B. and Gylland, A. S. (2017) E39 Joberget løsmassetunnel-Rørskjerm: Erfaringsrapport.

Aagaard, B. G., Asgeir S; Schubert, Peter; Løne, B (2016) The Joberg tunnel. Successful tunnelling in moraine., pp. 10. Available at: https://ic-group.org/fileadmin/Magazin_PDFs/WTC_2017/Aagaard_Gylland_Schubert_Lone_The_Joberg_tunnel__successful_tunneling_in_moraine..pdf.

Appendix

A Material models in Plaxis

Plaxis 2D supports multiple material models to simulate the behaviour of soil and other continua. Information on the material models used are extracted from the Plaxis 2D Reference Manual. Formulas and information covered in this chapter are directly derived from the manual. The material models for Plaxis 2- and 3D only varies in terms of the additional dimension from the out-of-plane axis. An important parameter in the different models is the drainage type. Models can be drained, undrained or non-porous depending on the engineer's input and allowances on the different models given by the program. Material models suitable for the case study are shown below. The applied models are later described in detail.

- Linear Elastic model [LE]
- Mohr-Coulomb model [MC]
- Hardening Soil model [HS]
- Hardening Soil model with small-strain stiffness [HSsmall]
- Concrete model [Concrete]

Reference used in the appendix:

Bentley (2021a) *Plaxis 2D - Material Models Manual*. Bentley.

A.1 Linear Elastic model

The Linear Elastic model (LE) is commonly used to simulate structural behaviour that have higher strength properties than soil. It is not capable of modelling non-linear plastic behaviour. Depending on choice of drainage type, a few parameters are used to describe this model as shown in the Appendix Table A-1.

Appendix Table A-1: Parameters in the Linear-Elastic Model

Parameter	Description	Formula	Unit
E’	Effective Young’s modulus		kN/m^2
v'	Effective Poisson’s ratio		[-]
G	Shear modulus*	$G = \frac{E'}{2(1+v')}$	kN/m^2
E_{oed}	Oedometer modulus*	$E_{oed} = \frac{E'(1-v)}{(1+v')(1-2v')}$	kN/m^2
*	Selecting these parameters automatically changes E’ and v’. If not entered the values are calculated using the formulas.		
E'_{inc}	Incremental stiffness increase	$Default: 0$	[kN/m^3]
y_{ref}	Reference level		[m]

Using advanced properties, it is possible to vary young modulus by depth using an incremental increase in stiffness per unit of depth E'_{inc} with an additional parameter y_{ref} which is a reference to the y-coordinate system. The reference level effectively decides when the increase is enabled.

A.2 Mohr-Coulomb model

The Mohr-Coulomb model is a linear-elastic perfectly plastic model with a Mohr-Coulomb failure criteria used to simulate soil. The model features the two stiffness parameters from LE and an additional three strength parameters. MC enables quick engineering checks with low computational costs and the parameters are obtainable through basic soil tests. Parameters in the model are given in Appendix Table A-2.

Appendix Table A-2: Parameters in the Mohr-Coulomb model.

Parameter	Description	Formula	Unit
E'	Effective Young's modulus		[kN/m^2]
c'	Effective Poisson's ratio		[-]
G	Shear modulus*	$G = \frac{E'}{2(1+v')}$	[kN/m^2]
E_{oed}	Oedometer modulus*	$E_{oed} = \frac{E'(1-v)}{(1+v')(1-2v')}$	[kN/m^2]
c'_{ref}	Effective cohesion		[kN/m^2]
φ'	Effective friction angle		[°]
ψ	Dilatancy angle		[°]
V_s	Shear wave velocity	$V_s = \sqrt{\frac{G}{\rho}}, \quad where\ \rho = \frac{\nu}{g}$	[m/s]
V_p	Compression wave velocity	$V_p = \sqrt{\frac{E}{\rho}}, \quad where\ \rho = \frac{\nu}{g}$	[m/s]
E'_{inc}	Incremental stiffness increase	$Default: 0$	[kN/m^3]
c'_{inc}	Incremental cohesion increase	$Default: 0$	[kN/m^3]
y_{ref}	Reference level		[m]

Equivalent to the linear elastic model, an increase in stiffness with depth can be simulated with an incremental young's modulus E'_{inc} by a reference y-coordinate y_{ref}. The reference coordinate is also relevant when a potential incremental increase in effective cohesion c'_{inc} is enabled. The model comes with an option to allow *Tension cut-off* which is relevant when tensile stresses are relevant. This model is commonly used to directly describe interface properties between modelled structural elements. The Mohr-Coulomb model also allows for parameters that alter velocities of wave propagation in the medium.

A.3 Hardening Soil model

The Hardening Soil model is a hyperbolic elastoplastic model formulated on shear hardening plasticity framework. The model involves compression hardening to simulate irreversible soil compaction. According to the reference manual it is used to simulate cohesionless soil as well as softer types of soil like clay and silts. The parameters of the HS-model are shown in Appendix Table A-3.

Appendix Table A-3: Parameters in the Hardening Soil model.

Parameter	Description	Formula	Unit
E_{50}^{ref}	Secant stiffness in standard drained triaxial test		[kN/m^2]
E_{oed}^{ref}	Tangent stiffness for primary oedometer loading		[kN/m^2]
E_{ur}^{ref}	Unloading/reloading stiffness.	$Default: E_{ur}^{ref} = 3E_{50}^{ref}$	[kN/m^2]
m	Power for stress-level dependency of stiffness		[-]
C_c	Compression index		[-]
C_s	Swelling index or reloading index		[-]
e_{init}	Initial void ratio		[-]
v_{ur}	Poisson's ratio for unloading-reloading	$Default: 0.2$	[-]
p^{ref}	Reference stress for stiffness	$Default: p^{ref} = 100\ kN/m^2$	[kN/m^2]
K_0^{nc}	K_0-value for normal consolidation	$Default: K_0^{nc} = 1 - \sin(\varphi)$	[-]
c'_{ref}	Effective cohesion		[kN/m^2]
φ'	Effective friction angle		[°]
ψ	Dilatancy angle		[°]
c'_{inc}	Incremental cohesion increase	$Default: 0$	[kN/m^3]
y_{ref}	Reference level		[m]
R_f	Failure ratio q_f/q_a	$Default: 0.9$	

Additions in HSsmall

$\gamma_{0.7}$	Shear strain at which $G_s = 0.722G_0$	[-]
G_0^{ref}	Reference shear modulus at very small strains ($\varepsilon<10^{-6}$)	[kN/m2]

Tension cut-off is an optional parameter, equivalent to the setup in the MC-model, allowing for tensile strength. If use of a HSsmall model is opted, for additional parameters become available. This HSS is used to model reactions from small strains to large strains and is an extension of the HS-model. The input parameters are recalculated by the program during analysis to be dependent on the stress state. Equation 8 show how the stiffness moduli is dependent on the stress state. This type of dependency is also featured for unloading-reloading stiffness and oedometer stiffness.

$$E_{50} = E_{50}^{ref}\left(\frac{\sigma_3' + a}{p_{ref} + a}\right)^m \tag{8}$$

In the formula *a* is attraction and E_{50} is elastic modulus at 50% secant modulus.

A.4 Interfaces

To represent soil-structure interaction Plaxis use interfaces between boundaries of different materials. Absence of an interface will tie the structure and soil together, preventing slipping or gapping. For material models the alternative to "consider gap closure" makes sure contact is re-established between structure and soil before compressive stresses can develop. The interface connects the nodes between the materials as two elastic-perfectly plastic springs and can have defined properties to simulate the real interaction.

Roughness of the interaction is simulated using a strength reduction factor, R_{inter}, which varies from 0.001 to 1. A rigid connection with a factor of 1 is default. The strength reduction factor relates the strength and stiffness of the adjacent material or specific interface material. Formulas defining the relationship of the strength of interfaces are shown below. This involves friction angle, cohesion and tensile strength. For undrained behaviour the cohesion becomes the undrained strength and is related in the same manner.

$$tan\varphi_{inter} = R_{inter} * tan\varphi_{soil}$$

$$c_{inter} = R_{inter} * c_{soil}$$

$$\sigma_n < \sigma_{t,i} = R_{inter}\sigma_{t,soil}$$

Regarding the stiffness of the interface springs, the shear and normal stiffness are by default calculated by the program from the relevant material stiffness. It is possibly to set the interface to a custom interface material which allows for control over the parameters. The shear and normal stiffness, K_s and K_n, can then be directly applied. This will override the program from internally deriving the parameters. These values are a relationship between modulus of elasticity and shear in terms of material thickness. By default, the interface stiffness is related as shown below.

$$E_{oed,i} = 2G_i \frac{1 - v_i}{1 - 2v_i}$$

$$G_i = R_{inter}^2 G_{soil} \leq G_{soil}$$

$$v_i = 0.45$$

If the interface is elastic, then relative movement to the plane and perpendicular can occur. This relates directly to slipping and gapping. The magnitudes of such displacement are as shown below.

$$Elastic\ gap\ displacement: \frac{\sigma_n}{K_n} = \frac{\sigma_n t_i}{E_{oed,i}}$$

$$Elastic\ slip\ displacement: \frac{t}{K_s} = \frac{\tau t_i}{G_i}$$

A.5 User-defined soil model

The user-defined soil model (UDSM) is a feature in Plaxis that enables the user to implement other constitutive models, than those already available in the program. A programming language can be used to compile the program into a Dynamic Link Library, which can be added to a Plaxis program directory. In this way the user can extract previous stress and state variables from Plaxis and update them with new variables. Predefined subroutines are used to simplify the process. The user can call on the established subroutines and modify them according to their needs.

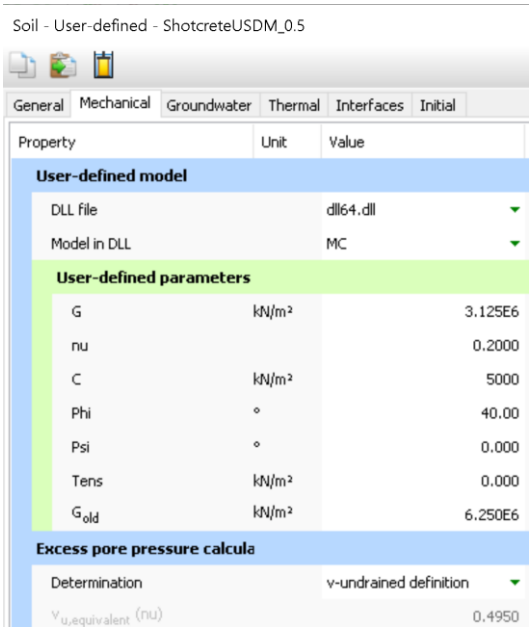

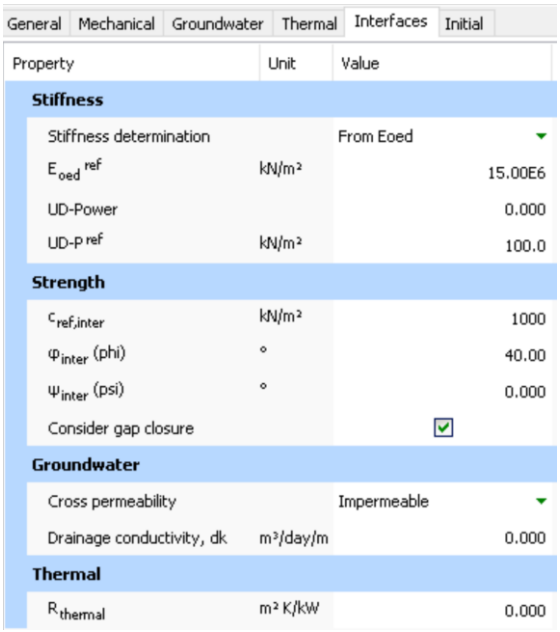

The figures above show the user-defined model applied in the thesis, with values for the shotcrete model with reduction factor of 0.5. An existing Mohr-Coulomb subroutine is used, and the G_{old} parameter was implemented in the subroutine by Gustav Grimstad.

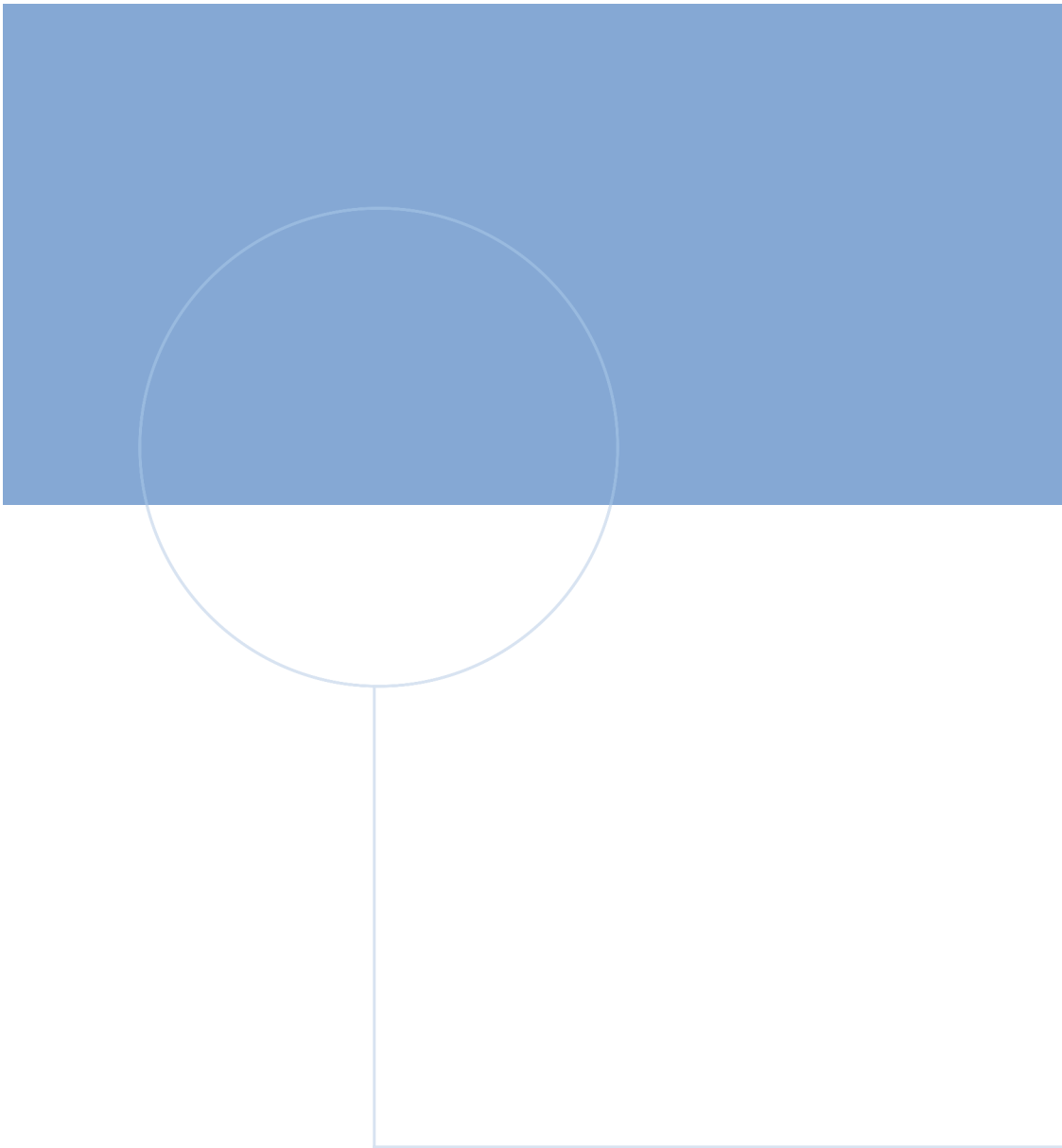

NTNU
Norwegian University of
Science and Technology

Norconsult